Design and testing of a radiant high temperature burner

Design and Testing of a Radiant High Temperature Burner

W.F.J. Sampers

CIP-DATA KONINKLIJKE BIBLIOTHEEK, DEN HAAG

Sampers, W.F.J.

Design and testing of a radiant high temperature burner /

W.F.J. Sampers. - Eindhoven : Institute for Continuing Education, Faculty of Mechanical Engineering. - I11. Final report. - With index, ref.

ISBN 90-5282-293-X

Subject headings: porous radiant burner / thermionic energy conversion

Design and Testing of a Radiant High Temperature Burner

Wil Sampers

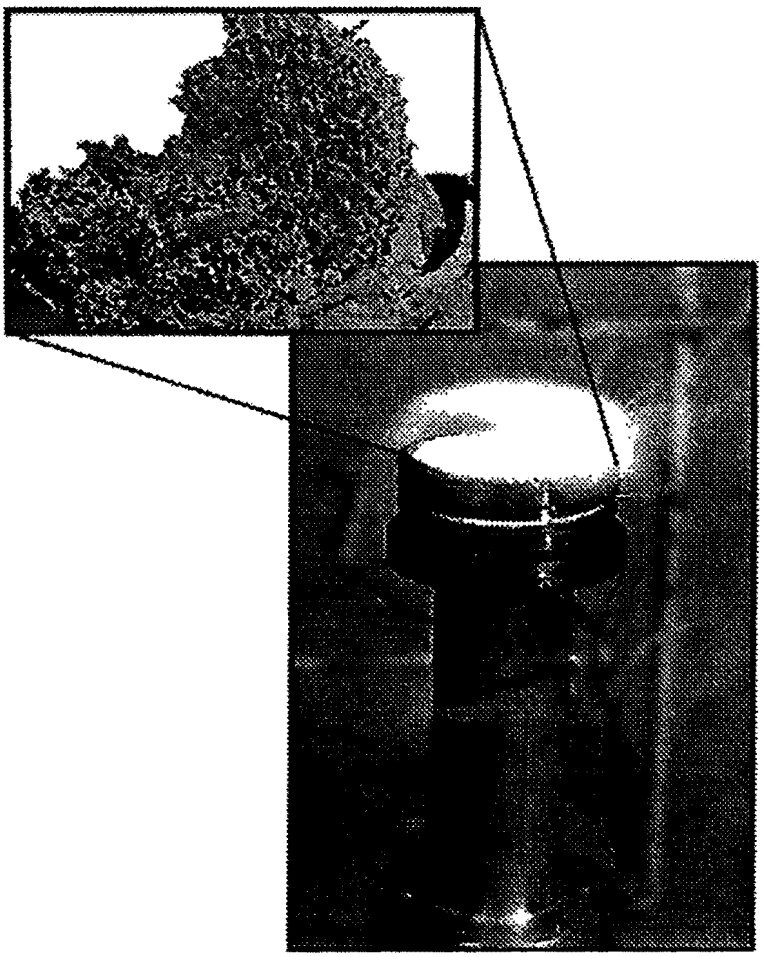

Technische Universiteit Eindhoven

Design and Testing of a Radiant High Temperature Burner

Final Report

W.F.J. Sampers

Institute for Continuing Education
Faculty of Mechanical Engineering
November 1993

report WOC-WET 93.028

Supervisors:
ir. G. Janssen (Gemco Furnaces b.v.)
prof. dr. ir. A.A. van Steenhoven (TUE)
ing. J.M.W.M. Schoonen (TUE)

Abstract

Since 1978 a thermionic energy converter (TEC) for terrestrial applications is being developed within the research-project High Temperature Constructions. Basically the TEC is a diode, which converts heat directly into electricity. The TEC imposes large demands on its heat-source: it must deliver a heat-flux of 1.5 kW (340 kW m^{-2}) at a temperature of 1723 K. The heat-source has to be a burner fuelled by natural gas. The TEC and burner will form a complete unit, which can be used for heating of (green)houses.

The purpose of this project is to design and build a test-furnace for the TEC. For the heat-source, the concept of a porous radiant burner is chosen. The porous body is made of partially stabilized zirconia. Much attention is paid to the stabilization of the combustion in the ceramic, so that flash-back can not occur. Further the burner is able to withstand severe thermal cycling. On top of the burner a simple but effective furnace can be placed. This furnace can be used to test the TEC.

The performance of the burner is monitored experimentally. The highest temperature reached is 1965 K at an input power of 9.5 kW. If the TEC will be placed in the furnace, it will receive 0.35 kW under these circumstances. For the objective of 1.5 kW, the burner temperature needs to be increased to 2273 K. To increase the burner temperature, the combustion air can be enriched with oxygen. The materials used in the construction performed satisfactory, but they suffered from thermal shock and corrosion. New materials must be sought or the thermal shock must be less severe.

For the future the design must be combined with preheating of the combustion air, leading to a burner coupling high temperature with uniform heating. Apart from heating the TEC, the design can be adapted to fields where similar features are needed like environmental applications.

Contents

Figures

Tables

Nomenclature

a	fit parameter	—
a	airfactor	—
A	surface	m^2
A	constant for thermal shock	—
b	fit parameter	—
c	fit parameter	—
c_p	specific heat content	$J\ kg^{-1}\ K^{-1}$
C	constant	—
C	shapefactor for thermal shock	m^{-1}
C_1	constant in Planck's law $3.7415\ 10^{-16}$	$W\ m^2$
C_2	constant in Planck's law $1.4388\ 10^{-2}$	m K
d	fit parameter	—
D	diameter	m
e	fit parameter	—
E	Hooke's modulus	Pa
E	emissive power	$W\ m^{-3}$
f	fit parameter	—
F	viewfactor	—
g	acceleration due to gravity 9.81	$m\ s^{-2}$
G	factor in Gebhart's zone model	—
Gr	Grashof number $\rho^2\ g\ \alpha\ (T-T_\infty)\ L^3\ /\ \mu^2$	—
h	heat transfer coefficient	$W\ m^{-2}\ K^{-1}$
H	enthalpy	$J\ kg^{-1}$
H_i	combustion enthalpy	$J\ kg^{-1}$
k	heat conductivity	$W\ m^{-1}\ K^{-1}$
L	length	m
n	number	—
Nu	Nusselt number $h\ L\ /\ k$	—
p	pressure	Pa
P	power	W
Pr	Prandtl number $c_p\ \mu\ /\ k$	—
r	radius	m
R	first thermal shock parameter	K
R'	second thermal shock parameter	$J\ m^{-1}\ s^{-1}$
Re	Reynolds number $\rho\ L\ u/\mu$	—

S_f	sizing factor	—
Q	heat flux	W
t	time	s
T	temperature	K
u	velocity	$m\ s^{-1}$
U	thermovoltage of a thermocouple	V
z	height	m
z	fit variable	K
α	coefficient of thermal expansion	K^{-1}
β	Biot number h L / k	—
δ	thickness	m
Δ	difference	
Δ	error	
ε	emissivity	—
ε	strain	—
η	efficiency	—
ϕ_v	volume flow	$m^3\ s^{-1}$
ϕ_m	mass flow	$kg\ s^{-1}$
Φ	material property	
μ	dynamic viscosity	$N\ s\ m^{-2}$
ν	poisson's ratio	—
ρ	reflectivity	—
ρ	density	$kg\ m^{-3}$
σ	constant of Stefan-Boltzmann 5.67 10^{-8}	$W\ m^{-2}\ K^{-4}$
σ	stress	Pa
σ_f	modulus of rupture, stress at fracture	Pa
τ	transmittance	—

indices

1, 2, 3,	
4, 5	zone numbers
b	black
c	convection
crit	critical
casing	the casing of the furnace
flue	flue gasses
i	number of insulation layer

in	inside of the furnace wall
in	inlet
ins	insulation
m	maximum
m	measurement
out	outside of the furnace wall
out	outlet
rad	radiation
r	reference junction
surr	surroundings
tc	thermocouple
ε	emissivity corrected
λ	at constant wavelength

Except where otherwise stated, the measures in drawings are in mm.

Except where otherwise stated, the measure of 1 m^3 means 1 m^3 of the product or substance concerned at an absolute pressure of 1.01325 bar and an absolute temperature of 273.15 K.

1 Introduction

1.1 History of the Project

Within the research-project High Temperature Constructions of the Eindhoven University of Technology since 1978 a combustion heated Thermionic Energy Converter (TEC) is being developed. This research is conducted in cooperation with the Production Technology group, the Faculty of Chemical Engineering and some commercial companies.

Basically the TEC is a diode of which one of the two electrodes, the emitter will emit electrons thermionically, when heated to sufficient high temperature (1723 K) [Veltkamp & van Kemenade, 1993]. The other electrode, the collector, is cooled (873 K) and catches the electrons emitted. In this way heat is directly converted into electricity. The TEC will have a current density of 100 Am^{-2} and a low potential difference of 0.5 V.

After the development of TECs for space applications in the 1960's, the TEC is now being developed for terrestrial applications. Its advantages are the absence of moving parts and its capability to be used to top conventional heat consuming processes. In such processes fuel has to be burned more efficiently and at higher temperatures to heat the TEC. The heat produced by the TEC at the collector side and heat available in the flue gasses can be used to drive the process. In this way a higher overall efficiency can be realised.

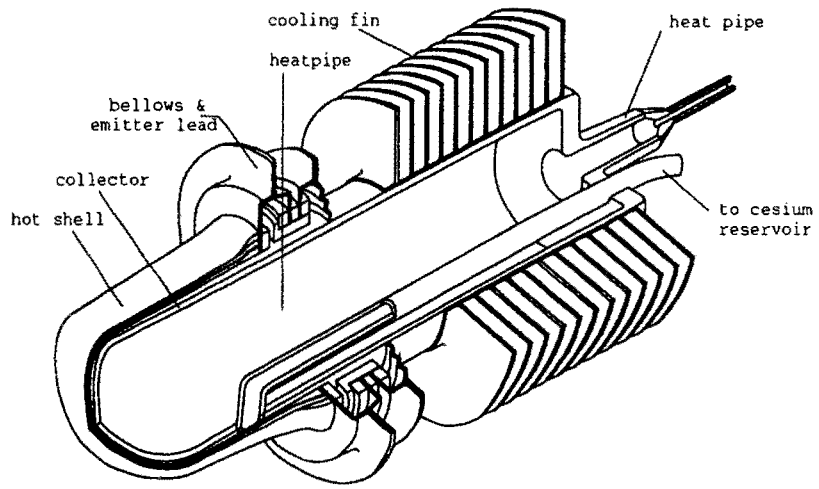

Figure 1.1. The EUT thermionic energy converter.

1.2 Problem Definition

The problem at hand is to design and build a test-furnace for the TEC. In the near future it needs to be tested in a furnace reaching such temperature that it will be able to drive the TEC. In the furnace it must be possible to measure the temperature of the hot-shell, being the part of the TEC inside the furnace. The bellows of the TEC (see figure 1.1) must remain below 537 K, because they are brazed with copper.

It is preferable that the TEC can be tested in all positions. The most difficult position is pointed downwards because the heat-pipe has to work against gravity.

Because a commercial heater using the TEC is one goal of the research, the findings derived from designing a laboratory heater should be applicable to commercial heater design. This implies that the laboratory heater must be fuelled with natural gas. After some modifications it then should be usable in a home environment.

1.3 List of Demands

Demands:

— The hot-shell must be heated to 1723.15 K (1450 °C).
— The TEC must be heated with a power of 1500 Watt, e.g. 340 kW/m^{-2} on its maximum diameter of 75 mm.
— The TEC must be heated by the combustion of natural gas.
— It must be possible to measure the temperature of the hot-shell.
— The TEC must be tested pointed downwards.
— The insulation near the bellows of the TEC must be cooler than 573.15 K (300 °C).
— The design must allow enough space for the cooling of the TEC.
— The design must be safe.

Wishes:

— The TEC can be tested in more than one position.
— TECs of different forms and sizes can be tested.
— Natural gas is burned only with air, no additional oxygen feed is needed.
— The temperature of the emitter can be varied from 1673 to 1873 K.
— The heat flux to the TEC can be varied from 1250 to 1750 Watt.
— The furnace has a short start-up time.
— The NO_x production is lower than 40 ppm.

1.4 Set-Up and Goal of the Project

The project was split into two parts. The first part concentrates on the heat-source or burner. Its result will be a working pilot burner which can be used to heat a TEC. The second part concentrates on the casing of the combustion chamber or furnace. Its design has to be practical and usable.

This report describes the first part of the project: the development of a laboratory burner which, combined with a simple casing, can be used to test the TEC. Therefore in chapter 2 orienting questions will be answered. Based on the initial list of demands in section 1.3 the performance required of the burner is calculated. In combination with the literature study a detailed list of demands for the laboratory burner is formulated.

Chapter 3 describes the actual design of the burner and its specifications. Chapter 4 discusses experimental results obtained from the test-rig. Finally chapter 5 discusses the conclusions and chapter 6 the recommendations.

Throughout the report, the absolute temperature in Kelvin is used. Therefore degrees Celsius are often transformed to Kelvin. Then the ".15" is omitted in the text for readability.

2 Orienting Design Study

Before we can start designing a burner and furnace, a number of orienting questions have to be answered. Amongst these questions are:

Can the required combustion temperature be reached using natural gas ?

Can the TEC be heated by a convective jet ?

Can the TEC be heated by radiant exchange ?

What is the influence of an insulating furnace ?

What principles of burners are known, which one can do the job ?

The answers result in a list of criteria. These criteria are used in chapter 3 to evaluate and choose a concept for the burner.

2.1 Combustion Temperature

The fuel to be used is natural gas, as stated in the list of demands. The adiabatic flame temperature of natural gas with air varies in literature from 2230 K [de Goey, 1990], 2273 K [Gasunie, 1980] to 2293 K [Gasunie, 1988]. This temperature is reached, when the combustion enthalpy is only used to heat the reaction products. This implies that the flame does not loose energy to a heat sink. In practice the temperature in the flame zone is lower.

The adiabatic flame temperature can be raised in two ways: using pure oxygen to enrich the air and preheating the mixture. Using pure oxygen implies that no ballast nitrogen is heated to the combustion temperature. The adiabatic flame temperature of methane with pure oxygen is 3010 — 3053 K [Gaydon & Wolfhard, 1979].

Preheating the mixture has the effect, that the combustion enthalpy is added to the enthalpy of the preheated gasses. In this way the flame temperature is raised. The procedure to calculate the adiabatic flame temperature is described in appendix A.

Figure 2.1 shows the dependence of the flame temperature on the temperature of the initial air. For the calculations, methane is "kept" at room temperature. This implies that heat is needed to heat methane from room temperature to combustion temperature. The reason for preheating the combustion air and methane separately is the low auto-ignition temperature of a methane-air mixture. The auto-ignition temperature is 903 K [Gasunie, 1988]. So the mixture ignites spontaneously when preheated above 903 K.

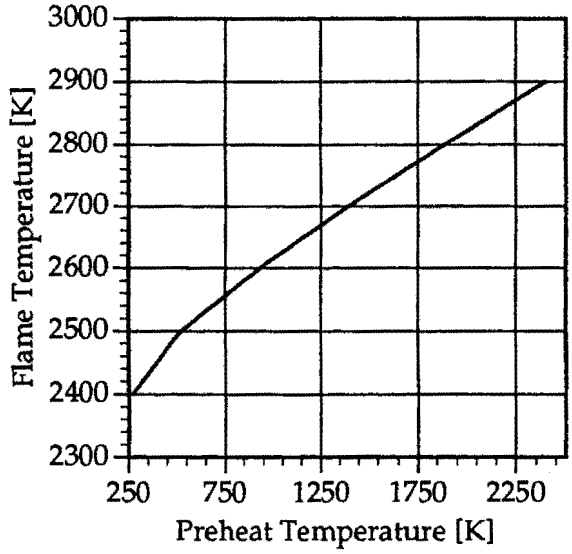

Figure 2.1 The flame temperature as function of the preheat temperature of the air.

The flame temperature can also be increased by enriching the air with pure oxygen. This implies that the methane flow and oxygen flows are kept constant but the nitrogen flow is decreased. The mixture stays stochiometric. Figure 2.2 shows the dependence of the flame temperature on the percentage oxygen in the air (20% being normal air and 100% pure oxygen).

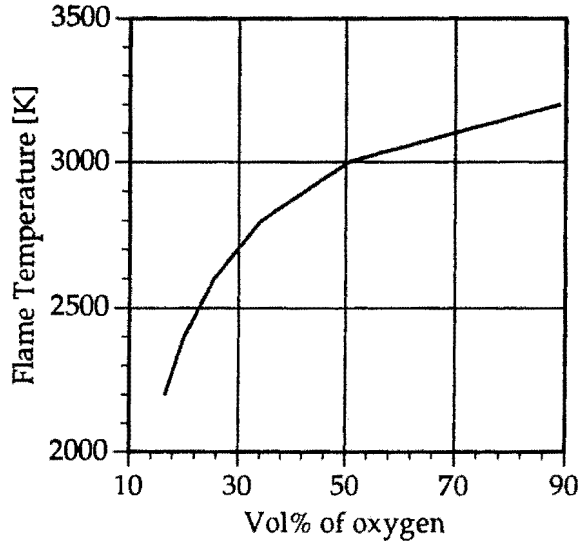

Figure 2.2 Adiabatic flame temperature as function of the amount of oxygen in the air (air temperature is 293 K).

The calculated values in figure 2.1 & 2.2 are not completely consistent with the literature data presented earlier. The reason is that all reactions taking place during combustion are modelled by only six chemical equations. Especially at high temperatures when more dissociative reactions become important, errors can occur.

2.2 Heat Transfer by Normal Jets

The direct impingement of turbulent jets on a surface leads to high localized heat transfer rates (figure 2.3). A major disadvantage, however, is that the heat flux can be highly non uniform and dependent of the distance from the axis of the jet.

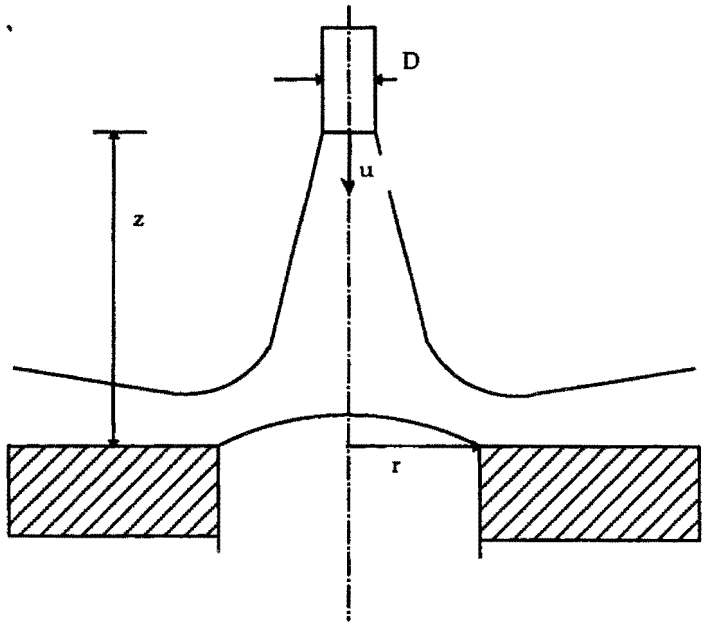

Figure 2.3 Impinging jet normal to the surface.

The basic heat transfer mode of a jet is convection. However dissociative effects can augment the heat transfer for burners placed on a small distance of the surface. The different radicals in the flue gasses recombine on the surface, thus liberating their formation enthalpy.

The following figure 2.4 can be constructed for a jet without dissociative heat transfer (appendix B). The parameters are the flux to the TEC Q=1500 Watt, TEC-Temperature 1723 K, jet-diameter D=7.6 mm, radius r=38 mm (for the TEC) and distance z=46 mm.

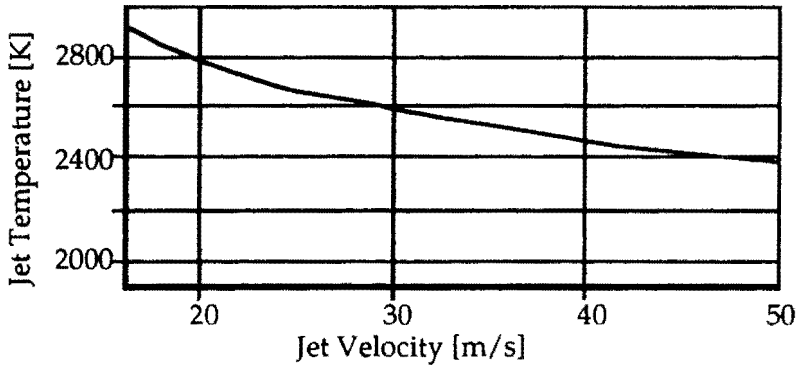

Figure 2.4 Temperature of the jet as function of the jet-velocity.

On the TEC-surface, recombination of the reaction-products may strongly enhance the heat transfer. Recombination may increase the heat transfer coefficient with 100 % [Chen & McGrath, 1969]. Chen & McGrath based this estimation on thermochemical calculations for an oxygen/propane flame, transferring heat to a sphere.

In principle this solution is feasible to heat the TEC. Its main disadvantages are the expected non-uniform heat flux and the high velocities required.

2.3 Model of a Furnace in order to Estimate the Temperature and Power of a Radiant Burner

Radiation is another way to heat the TEC. The TEC can be placed in a furnace and heated by a radiating body. The radiating body itself can reach the required temperature in several ways: ohmic heating, microwaves or combustion. In our case combustion must be used.

Different heat transfer modes are present in the furnace; forced and natural convection, conduction and radiation. In most cases, forced convection and radiation are dominant. At the high temperatures, we are considering, radiation alone is the main mode. It transfers 80-90% of the heat.

Evaluating the equations ruling this type of heat transfer problems, analytical solving will only be possible for very simple cases. On the other hand, exact computational fluid dynamics modelling gives the possibility to solve radiation, combined with convective heat transfer problems.

To start, a zone-method is used to evaluate the geometry of the furnace heated by a radiative burner. Afterwards the radiation exchange between TEC and a radiative burner is estimated, when the TEC is placed above the burner in free atmosphere without a furnace.

2.3.1 Evaluation of the Furnace by means of Gebhart's Zone Method

A principal choice is made for a cylindrical furnace of all possible geometries. This choice is based on the findings of Seuren [1991]. In this cylinder, the burner and the TEC are placed in the two ends planes of the cylinder. The outlet is in the wall of the cylinder itself. The cylinder is divided into five zones for evaluation by a zone method (figure 2.5):

zone 1. the burner,
zone 2. the TEC,
zone 3. the insulating ring around the burner,
zone 4. the insulating ring around the TEC,
zone 5. the insulating body of the cylinder.

The main assumption is that a zone has a constant temperature. Further assumptions are:

— the influence of the convective laminar jet of flue gasses and gas radiation are neglected compared to the solid body radiation inside the furnace [Seuren, 1991],

— the emissivity and heat conductivities of the insulating walls are constant,
— the emissivity of the TEC is constant (ε=0.9 based on a SiC-coating with a rough surface),
— the TEC can be considered as a flat disc,
— the influence of the outlet is neglected,
— all surfaces are gray,
— conduction through the insulation is one dimensional.

The radiation within the enclosure is solved by Gebhart's zone method as described in appendix C. Gebhart's zone method requires the viewfactors of the system. These are derived using the standard case of two parallel discs having the same axis and some viewfactor algebra (see appendix C.1).

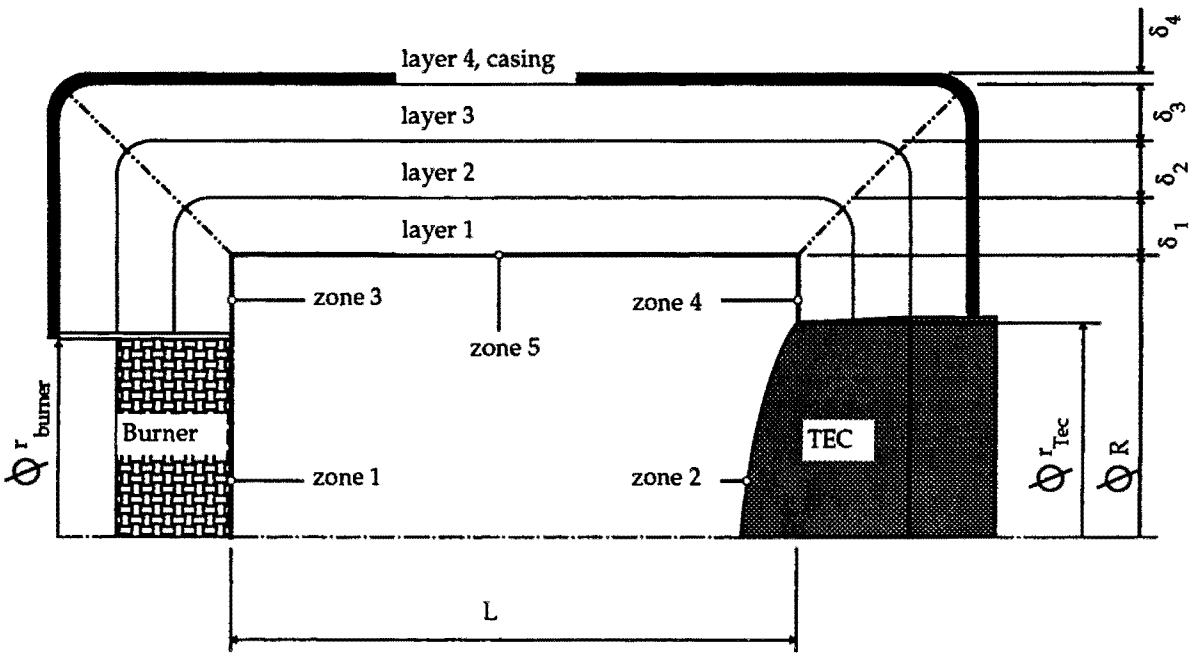

Figure 2.5 The furnace divided in five zones and the four insulation layers.

The radius of the burner is set to 35 mm. The reason for this choice was the availability of commercial cellular ceramics. The radius of the TEC is 38 mm. The boundary conditions are the demanded temperature and power of the TEC, 1723 K and 1500 Watt (zone 2). The other boundary conditions are the insulation losses through the two rings (zone 3&4) and through the body (zone 5). The insulation loss is found by solving the heat balance of the insulation: conduction through the insulation equals the loss to the surroundings on the casing of the furnace.

The algorithm is described in more detail in appendix C.3.

2.3.2 *Results of the Zone Method*

With help of the model described in the preceding paragraph the influence of length, radius, and insulation is evaluated. In total four designs

for the insulation are used. The first design is an adiabatic wall, the other three (ins I, ins II, ins III) are listed in the following table.

The insulation is build from four layers. The first layer of all variants is a zircar cylinder. The second layer is formed of durablanket, being able to withstand 1873 K. The third layer is Wacker WDS, a superisolator (maximum service temperature 1100 K). The fourth layer is a steel casing of 1 mm. The calculations were started with insulation variant I. In insulation II the Wacker WDS is replaced by durablanket to see the effect of a worse insulation package. In insulation variant III the thickness of the Wacker WDS is doubled, compared to I. In this way the insulation is improved.

	layer 1, inside	layer 2	layer 3	layer 4, casing
	δ [m] k [W m^{-1} K^{-1}]	δ [m] k [W m^{-1} K^{-1}]	δ [m] k [W m^{-1} K^{-1}]	δ [m] k [W m^{-1} K^{-1}]
Ins I	0.025 0.3 Zircar	0.05 0.25 Durablanket	0.05 0.025 Wacker WDS	0.001 42 Steel
Ins II	0.025 0.3 Zircar	0.025 0.25 Durablanket	0.05 0.25 Durablanket	0.001 42 Steel
Ins III	0.025 0.3 Zircar	0.025 0.25 Durablanket	0.10 0.025 Wacker WDS	0.001 42 Steel

Table 2.1 Composition of the three insulation variants, the layers are indicated in figure 2.5.

Optimizing the furnace geometry the most important parameter appears to be the burner temperature. Refrained by material limits the burner temperature has to stay as low as possible, otherwise it will be impossible to materialize the burner.

Concluding optimalisation becomes a rather simple exercise: the optimum furnace is the furnace where, within the geometrical limits, the temperature of the burner, required to deliver a heat flux at the TEC of 1500 W, is the lowest. The statement "within the geometrical limits" is ruled by other considerations like the space needed for a temperature measurement of the hot-shell, or the space needed for the TEC.

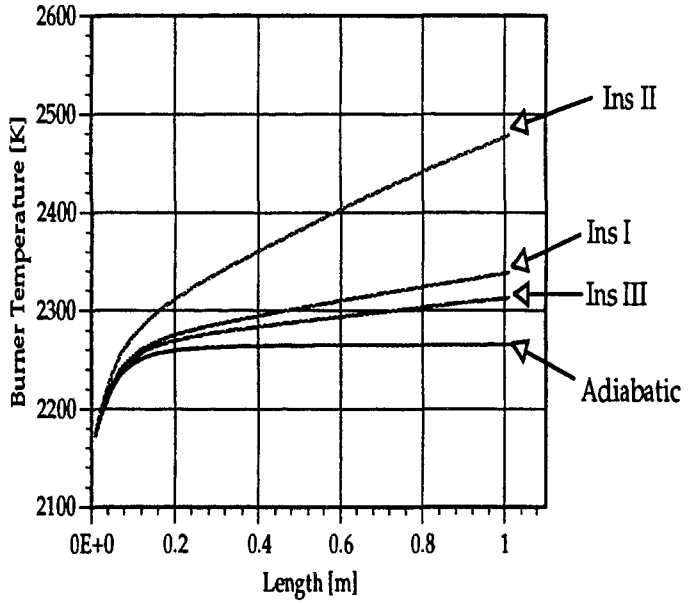

Figure 2.6 The required temperature of the burner as function of the furnace length, with a constant inner furnace radius of 0.05 m.

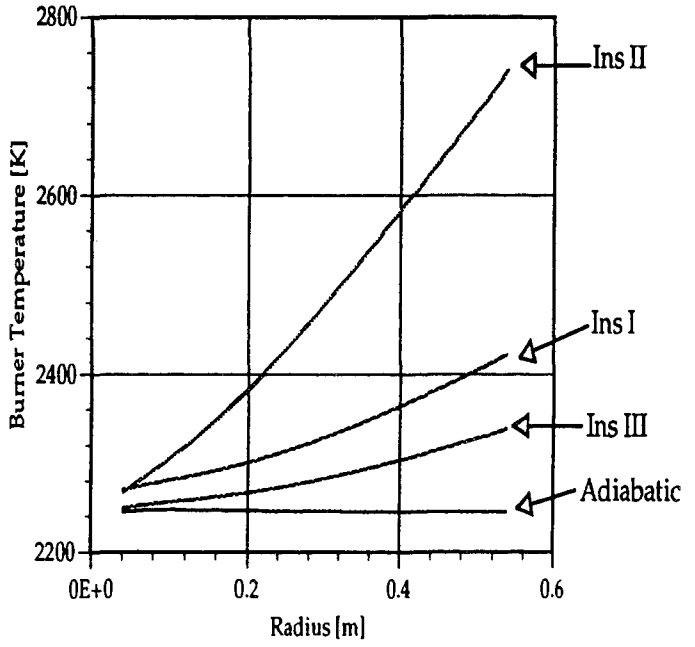

Figure 2.7 The required temperature of the burner as function of the inner furnace radius, with a constant furnace length of 0.1 m.

In the figures 2.6 & 2.7 the importance of the insulation is clearly shown. Besides when the furnace becomes longer or broader, the outer surface of the furnace increases, so the losses increase. When the length decreases to zero, the solution approaches the analytical solution for two infinite parallel plates. From 0<L<0.2 m the heat loss through rings (zone 3 & 4) has a strong influence. From L=0.2 m this influence decreases when the furnace is well insulated.

To give an impression of the other heat fluxes and temperatures the following table presents the values for the zones at a length of 0.1 meter, a radius of 0.05 m and insulation package I.

Zone	Heat flux [W]	Temperature [K] of the inner furnace wall	Temperature of casing [K]
1, burner	1566	2254	—
2, TEC	-1500	1723	—
3, ring burner	-3	1938	320
4, ring TEC	-2	1979	321
5, body	-61	1947	314

Table 2.2 Temperatures and heat fluxes of the five zones at a length of 0.1 m, radius 0.05m and ins I.

The presented calculations were performed with an emissivity for the zircar of 0.1. An additional numerical experiment is performed, where the emissivity was set to 0.9. The result is a slight decrease in the required burner temperature.

2.3.3 *Estimation of the Temperature and Power of a Burner Heating the TEC Directly*

It would be very advantageous to heat the TEC directly without a furnace. The temperature of the heater can be estimated by a radiant heat exchange balance. The heat balance is worked out in appendix C.4. From the heat balance the relation between the required burner temperature and the distance between burner and TEC can be evaluated.

Figure 2.8 presents the relation between the required burner temperature and the distance. The parameters used are the heat flux at the TEC Q =1500 W, TEC temperature 1723 K, burner radius 35 mm, TEC radius 38 mm, TEC emissivity 0.9 and burner emissivity according to equation (c.22).

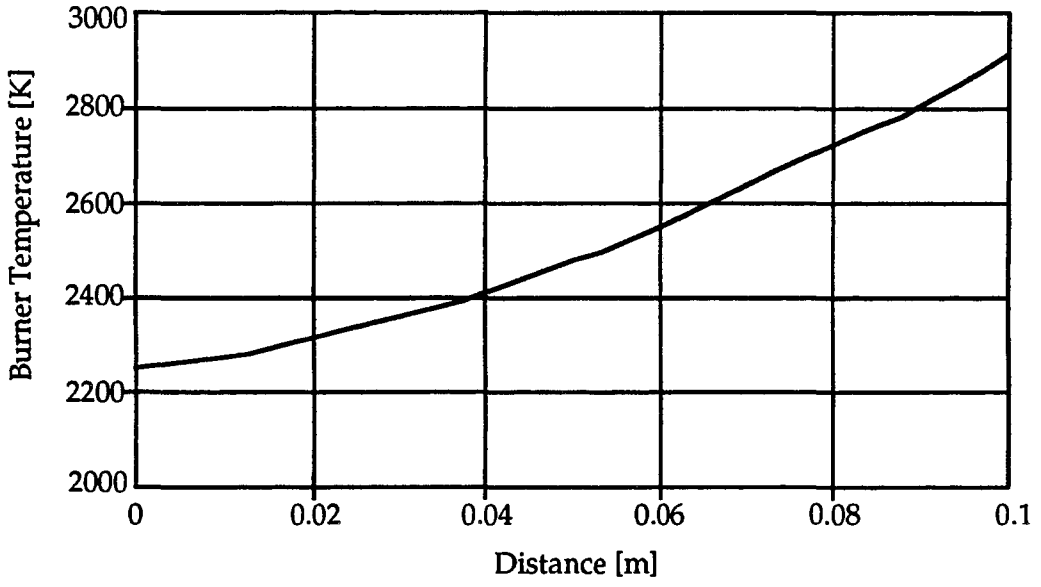

Figure 2.8 The required burner temperature as function of the distance between burner and TEC without furnace.

Evaluating figure 2.8, it is seen that to heat the TEC with a burner temperature of 2273 K, the TEC and burner must stand less than 15 mm apart. In this stage, it becomes interesting to see if the jet of flue gasses can improve the heat transfer to the TEC. On the other hand, it can be interesting to discuss the list of demands anew. If the temperature of the hot shell can be measured, one way or another, it is very advantageous to work without a furnace. The whole test-rig would become less complex.

2.3.4 Concluding Remarks Concerning the Design of a Furnace

First it can be concluded, that it is not practical to heat the TEC with a radiative body without insulating furnace. Without furnace, the distance between TEC and burner has to be very small or the required burner temperature has to be very high. A small distance implies that it is almost impossible to measure the hot-shell temperature (except for thermocouples) and that it is impossible to measure the burner temperature. A high burner temperature leads to unrealistic material demands. The additional heat flux from the jet of flue gasses can influence the heat transfer to the TEC positively, so this effect has to be studied.

Although the model does not take all physical effects into account, it gives sufficient information to design the furnace. Two logical design tendencies present themselves. First, the furnace has to be build as small as possible within the bounds of the list of demands. Second, the insulation of the furnace has to be laid out very effectively.

This implies that measurement holes and the outlet can have a large impact on the performance of the furnace. The actual effects can be evaluated through more accurate CFD modelling.

2.4 Survey of Burners

Many combustors are presented in literature, based on the heating principles discussed in this chapter. Two heat transfer modes are used: convective heat transfer and radiant heat transfer.

Combustion consists of two stages. First the fuel is mixed with oxidizer and second the mixture reacts. Basically the mixing can be done in two ways, premixing or mixing by diffusion. Premixing means that the fuel and oxidizer are completely mixed before the combustion takes place. The combustion process is not slowed down by the mixing. So the reaction takes place fast and the flames are short and hot.

For diffusion mixed flames the oxidizer has to be supplied from the surroundings to the fuel through the reaction zone. This implies that the reaction has to wait for the supply of oxidizer by diffusion. Because diffusion is a rather slow process, these flames will be long and not so hot. The mixing is often enhanced by the introduction of mixing flow patterns like swirls.

A disadvantage of premixed burners is that the mixture can not be preheated due to auto-ignition. This becomes more important at larger burner powers where preheating of the air is often used to increase the efficiency. To preheat the air many concepts are presented in literature. These can be classified into two groups: regenerative and recuperative burners.

The simplest concept of a recuperative burner consists of two or three concentric tubes. Through the inner tube the gas is supplied, through the middle ring the air and through the outer tube the flue gasses are sucked back (see figure 2.9) [Schmid, 1980]. The flue gasses transfer their heat to the combustion air. To enhance the heat transfer fins can be used [God & Ebner-Brunner, 1984]. Nicholson [1983] presents an overview of recuperative techniques including large heat exchangers for gas-turbines, furnaces, etc..

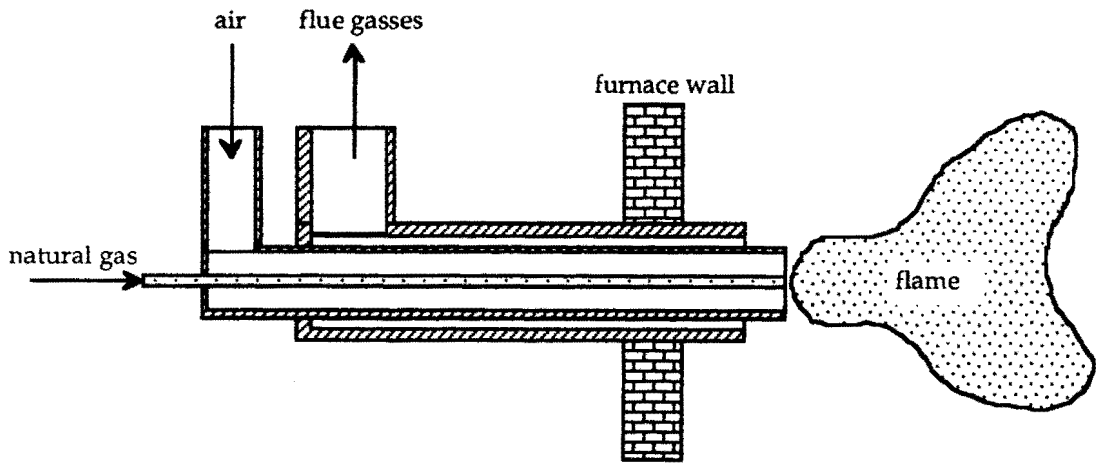

Figure 2.9 Sketch of a recuperative burner.

Webb [1985] presents a burner, incorporating regenerative preheating of the combustion air (figure 2.10). In this concept, two burners are mounted next to each other. The burner mouth is connected to a packed bed

regenerator. When one burner works, the other sucks in the flue gasses and heats its packing. After some time, a valve switches and the other burner takes over. The air it uses is heated by the packing, which was heated by the flue gasses in the previous cycle.

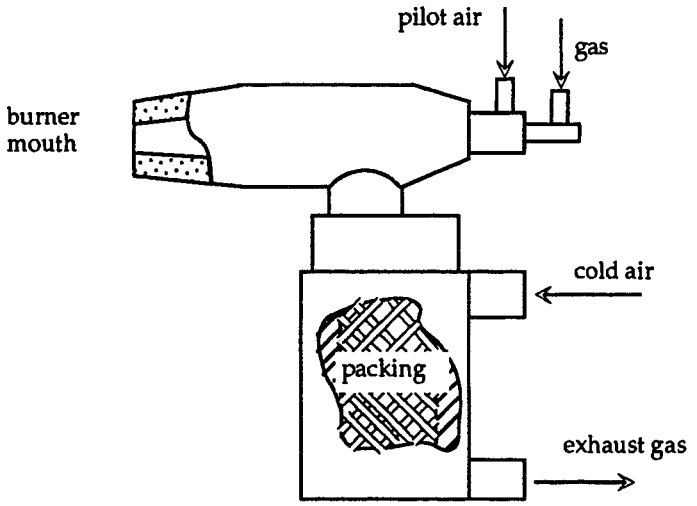

Figure 2.10 Sketch of Webb's regenerative burner.

Otherwise regenerative techniques are mainly used in large structures like a glass melting tank. Again Nicholson [1983] presents a nice overview. Different concepts are the rotary regenerative preheater, static regenerators, the pebble air heater, etc..

High combustion temperatures can also be reached by enriching the combustion air with oxygen. Pure oxygen is in general injected instead of supplied premixed [Levinson, 1986]. Injection leads to a higher luminosity of the flame. Thus the flame transfers more heat by radiation. Some injection methods are shown in figure 2.11.

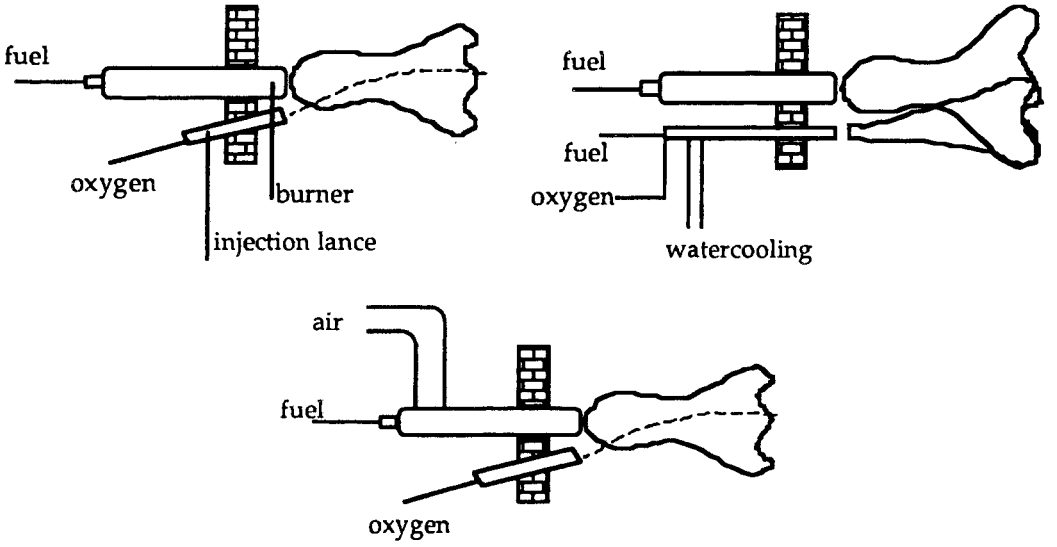

Figure 2.11 Oxygen injection.

Schmid [1980] build two burners, which use oxygen enriched air. The burners reached temperatures up to 2233 K. The first burner consists of three

concentric tubes through which gas, air plus oxygen and coolant water are supplied. The second burner is cooled by the combustion air. In this way the combustion air is preheated by cooling the burner.

Another group of burners are the radiant burners. The principle of a radiant burner is that the combustion enthalpy is transferred to a ceramic or metal body. This body heats the load by means of radiative exchange. The classic design of a radiant burner is shown in figure 2.12a. Figure 2.12b shows a different type of radiant burner. Its mouth and the furnace wall around the mouth is heated by swirling flow gasses [Harbeck, 1985].

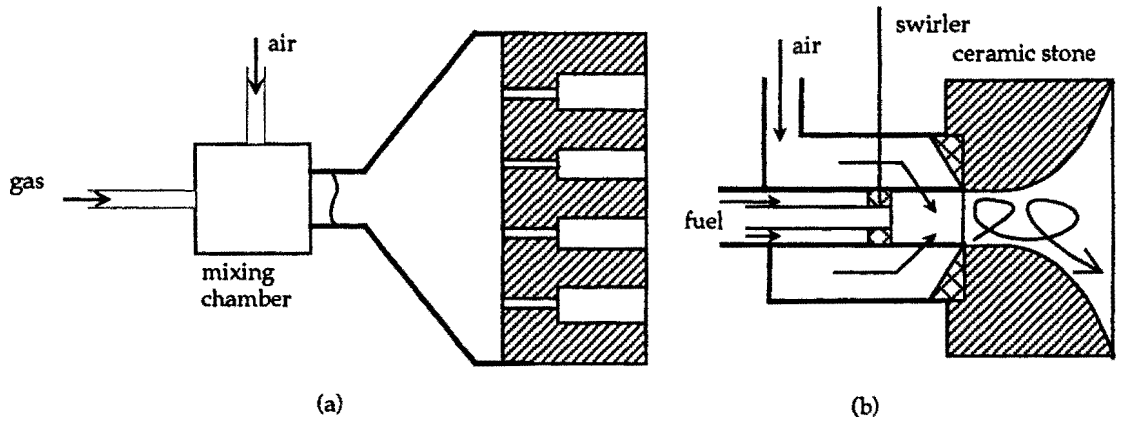

Figure 2.12 (a) Classic radiant burner, (b) STB burner [Harbeck, 1985].

A different approach to radiant burners is the use of porous bodies. One concept of a porous body is the use of fibres woven into a blanket or sheet. In between the fibres, the combustion is located. The combustion heat is transferred efficiently to the fibres due to the high heat-exchange surface. Originally metal fibres were used limited to 1473 K, later ceramic fibres are used. Golombok & Shirvill [1988] published a study estimating the emissivity of fibrous materials.

A recent development is the use of reticulated ceramics or so-called cellular ceramic materials (ccm). Initially ccm's are used to filter liquid metals. In 1982 Echigo published the idea to use the characteristic heat transfer properties of ccm's to diminish heat-losses of furnaces.

A porous radiant burner can adjust to three burning modes. The first is surface combustion, where the combustion takes place within the surface layer of the ccm. This layer is heated up and starts to radiate. The second mode is free flame combustion, where numerous small flames are formed above the surface of the ccm. The ccm remains rather cool. The third mode occurs, when the combustion takes place inside the ccm. By convection the ccm is heated. Inside the ccm the heat is transported by conduction and radiation to the surface layer radiating to the load. The three modes can be realised through careful regulation of the gas mixture velocity.

The basic form of burner of ccm is a flat plate (figure 2.13a). In figure 2.13b another interesting concept, the porous tunnel burner is shown [Coles & Grimm, 1975]. The tunnel leads to a better radiative heat-exchange.

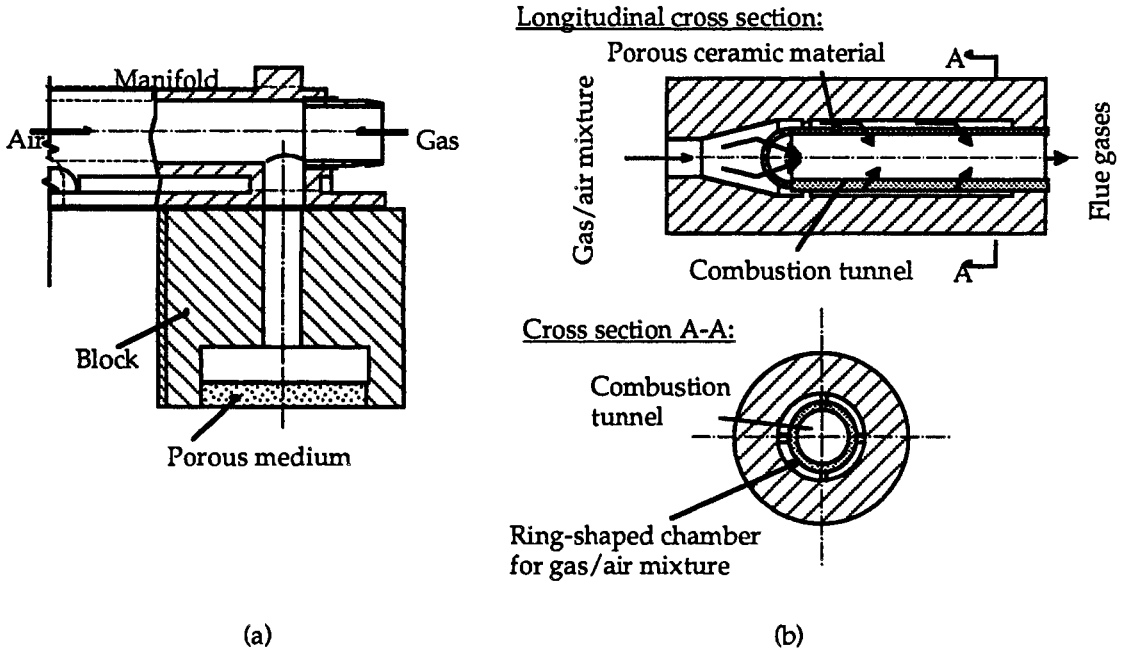

Figure 2.13 (a) Flat porous radiant burner [Pritchard e.a., 1977], (b) Porous tunnel burner [Coles & Grimm, 1975].

Porous radiant burners provide a large work-area from low heating powers to high powers (2 MW/m^2), uniform heating and compact construction. A disadvantage is the severe demand on the material due to the high temperatures and thermal shock.

2.5 Resulting Design Criteria

As mentioned in chapter 1, the task is to design a burner to heat the TEC in a laboratory environment. Therefore the following list of design criteria is formulated based on the list of demands. Besides some additional wishes are given.

A. The temperature of the burner is thus, that the TEC receives a heat flux of 1500 W (340 kW/m^2), while the hot-shell has a temperature of 1723 K. The wish is that the burner temperature and the heat flux can be higher and variable.

B. The burner temperature has to be as low as possible. This wish is based on the limited ability of materials to withstand very high temperatures in an oxidizing atmosphere. The approximate melting temperature of ceramics can vary from 2323 K (Al_2O_3) to 2873 (ZrO_2) and 3073 (UO_2) [Richerson, 1992]. This is the absolute limit. The maximum usage temperature is much lower than the melting temperature; 200 to 600 K is normal. Another failmode is thermal shock. The thermal shock depends on the difference between the burner temperature and the temperature of the surroundings. When this difference becomes smaller, the thermal shock will be less severe.

C. The burner has to be safe.

D. It is convenient, when the burner heats up fast and changes fast to changing working conditions. The demand is that the burner itself is at work temperature within 10 minutes. The wish is faster than 10 minutes.
E. The TEC is designed to work in a combustion atmosphere. With future applications in mind the burner must be fuelled with natural gas. It is practical, when no oxygen is needed to augment the temperature.
F. We like it, when the burner is cheap to produce.
G. The heat flux to the TEC has to be as constant as possible. Therefore the wish is that hot-spots are avoided.
H. The burner is to be used to test a TEC with a hot-shell diameter of 76 mm. The top of the hot-shell is slightly curved. In this context, it is wished that the burner can be used to test larger or smaller TECs.
I. The most difficult position for the TEC to work is pointing down. When the burner is placed opposite to the TEC, it must transfer its heat upward. Wish is that the burner can be placed under all angles.
J. For the laboratory burner no demand for NO_x emission is imposed. The law allows at this moment a maximum emission of 40 ppm.
K. The burner will make noise. Porous radiant burners mounted in central heating systems are known to whistle loudly. In future the burner-TEC combination is placed in a house, so it should be silent.
L. The construction must be simple. Different ideas in the design will be tested, so the burner rig must be modular.

Table 2.3 summarizes the design criteria.

Criteria		Demand	Wish
A	Burner temp. needed for a hot-shell temp. and a heat flux to the TEC of:	1723 K 1500 W	higher variable
B	Burner temp. from material point of view	T_{max}=3000 K	lowest
C	Safety	Laws	-
D	Speed of heating up	<10 min	faster
E	Fuel	natural gas	no oxygen
F	Price	-	cheap
G	Constant heat flux to TEC	-	no hot-spots
H	Capable of testing different geometries of TECs	D=0.076 m	D larger/ smaller
I	Position of burner	vertical, flame up	360° free
J	NO_x production	-	<40 ppm
K	Noise production	laws	-
L	Simple construction	-	modular

Table 2.3 Criteria for the design of the TEC-burner.

Some criteria conflict, for example criteria A and B. A asks a high burner temperature to give flexibility. B asks a low burner temperature to avoid material problems. In this way, more conflicts are found.

A first step to solve the conflicts is to rank these criteria. The criteria are ranked using the ordinal scheme shown in table 2.4. Exceptions are criteria C (Safety) and K (Noise production). They do not have wishes, so are not involved in the choosing process. In this table, the criteria are listed in capital letters on the diagonal staircase. On the crossing of a row and a column (like in a distance table between cities) two criteria are compared. The most important is written on the crossing.

For example consider the bold **h** in table 2.4. On this crossing criterion D (speed of heating up) is compared with H (different TEC geometries). For a laboratory burner, it is more important that it is able to heat different TECs than that it must react fast to changing work-points. So h is noted on the crossing. When the table is filled all appearances of a criterion are counted, including the capital letters. The capitals are counted to prevent the appearance of zero. The last column shows the total.

A	b	a	a	a	g	a	a	a	a	8
	B	b	b	b	b	b	b	b	b	10
		D	d	d	g	**h**	i	d	l	4
			E	e	g	h	i	e	l	3
				F	g	h	i	f	l	2
					G	g	g	g	g	9
						H	h	h	h	7
							I	i	l	5
								J	l	1
									L	6

Table 2.4 Ordinal scheme of the design criteria, on the crossing stands the criterion which is the most important. In the last column the total appearances of a criterion are listed.

Although this process seems to be very objective, it is not. First the ranking is performed with in mind that a laboratory burner is to be designed. For a commercial burner criteria like NO_x-emission and price become more important. Second there are bears and ghosts, speaking metaphorically. I expect that it will be hard to find a material, which can function at more than 2273 K in an oxidizing atmosphere. So I consider this a bear on the road to a working design. Thus criterion B is rated very important. But it can show out that this bear is only a ghost, blown away by the wind easily (or by producers of materials).

The weight-factors for each criterion are equal to the number of times they appear in the ranking in table 2.4.

3 Design of the Burner

In this chapter the way to, and the actual design of the laboratory burner is discussed. First the choice between three concepts is made. Then the chosen concept is developed.

3.1 Choice of the Concept

Based on the findings of chapter 2, three concepts are considered to be viable. These concepts are a turbulent jet burner (see section 2.2), a flat porous radiant burner and a porous tunnel burner (sections 2.3 and 2.4). All three burners can heat the TEC, if the combustion temperature is high enough. In all cases the combustion temperature of a natural gas/air mixture is too low. The combustion temperature has to be increased. As seen in section 2.1, the combustion temperature can be increased by enrichment of the combustion air with oxygen or by preheating the combustion air.

Based on the criteria in section 2.5, the choice between the concepts will be made. The concepts already satisfy the demands. Thus only the wishes decide the final concept in this discriminating process. To choose between the three concepts, the following method is used.

The wish of a criterion is coupled to a performance range. Maximum performance yields 10 points, minimum performance 1 point. In between the score is linearly interpolated. The score (S) is multiplied with the weight factor (WF; presented in table 2.4) resulting in a weighed score (WS). The weighed score is summed up and gives an evaluation of each concept.

I tried to give the score objectively. Therefore an additional technique is used for the choice between the burner concepts.

For the choice between preheating and oxygen enrichment, the two are simply compared. The best gets two points, the other one point.

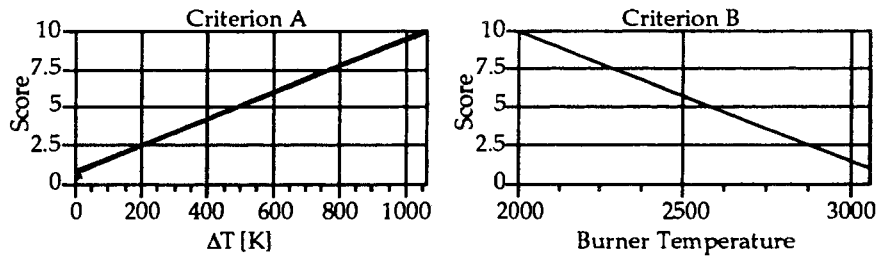

Figure 3.1 Score charts for criterion A, based on the difference between the required burner temperature and the adiabatic flame temperature of natural gas with oxygen, and for criterion B, based on the required burner temperature.

To evaluate criterion A, the difference between the required burner temperature to heat the TEC and the highest adiabatic flame temperature (3053 K for natural gas with pure oxygen) is used. The greater the difference, the higher the flexibility of the burner to produce a higher heat flux to the TEC.

The lowest required temperature of a flat radiant body is 2240 K. The tunnel augments the emissivity (see figure 3.3). When a surface emissivity of 0.5 is assumed, the apparent emissivity of the tunnel becomes 0.8. Thus the tunnel delivers an equal radiant heat flux at a temperature of 2000 K. This value is used as the maximum achievable; a difference of 3053 K - 2000 K yields 10 points. The flat burner has a flexibility of 3053 K - 2240 K, yielding 8 points. For the jetburner, a velocity used in practice is 25 m/s. The required temperature of the jet is 2700 K, yielding 4 points.

The combustion temperature which can be reached with 100 % oxygen is 3053 K. The combustion temperature reached with 100 % preheating is 2900 K. So oxygen enrichment gives more fexibility.

Criterion B uses the burner temperature to find the score. The combustion temperature is the limit to the burner temperature giving a score of 1. The minimum burner temperature is that of a tunnel, 2000 K. The flat burner has a temperature of 2240 K, giving 8 points. The jetburner has a temperature of 2700 K, giving 4 points.

Criterion D favours the jetburner. Ignite the jet and the burner is heated (10 points). The tunnelburner has the highest thermal mass, so it gets 1 point. The flat burner will be in between: 5 points.

Preheating implies the use of a heat exchanger: thus additional time is needed for starting. So oxygen enrichment is preferred.

Criterion E has as wish that no oxygen is used. This has no impact on the choice of the burner concept. But it is clear, that preheating is preferred over oxygen enrichment.

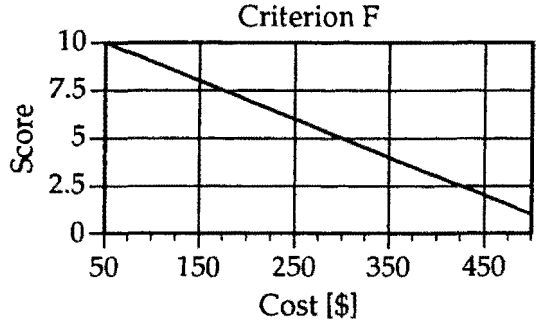

Figure 3.2 Score chart for criterion F, based on the estimated material cost.

Criterion F concerns the material cost of the burner. The score will be based on the estimated cost of the burner module. The rest of the rig is assumed to be similar for the three concepts. For the jetburner we can choose a ceramic nozzle, for example zirconia. The estimated price is $200. With some insulation material the total burner module will cost $225. The flat burner can be build around a ceramic filter, estimated cost $15. With some insulation, the estimated total cost is $50. A porous tunnel will be more expensive, lets say 10 times. The insulation will also be more expensive,

because the form is more complicated. So the total cost of the tunnelburner is $250. The maximum cost "possible" is based on a concept with a porous tunnel ($150) placed in a gastight alumina tube ($250). The maximum cost yielding 1 point is $500.

For preheating again the argument of the heat exchanger applies. So oxygen enrichment is preferred.

Criterion G wishes a constant heat flux density to the TEC. When the radiant burners are uniformly heated, the flux is constant over the hot-shell surface. For the jet the heat transfer is a function of the hot-shell radius. The radiant burners are given 10 points and the jetburner 5 points.

Criterion H demands geometrical flexibility of the burner. The wish is that TECs with different diameters can be tested. Smaller is no problem for all three concepts. Larger diameters give problems for all three burners. In all cases, the temperature has to become higher. So the geometrical flexibility can be coupled to the flexibility in heat transfer of criterion A. The same points are given.

Criterion I wishes that the burner can be rotated in vertical direction. Maximum rotation is 360° for the jetburner (10 points). Minimum rotation is 0° (1 point). The two porous burners can be turned 180° (90° to both sides). When the porous burners are turned more than the lower half of the circle, pieces material (broken apart by thermal shock) fall down. The rotation of 180° yields the mean score: 5.5 points.

Criterion J, the NO_x production, can be coupled to the burner temperature. Roughly the NO_x production increases, when the combustion temperature increases. So the same score as for criterion B is given.

Oxygen enrichment is preferred to preheating in this context. When the air is enriched with oxygen, less to none nitrogen is available to form NO_x.

Criterion L is difficult to evaluate. Again we have to form an impression of the future design. The simplest design is just a nozzle or tube of steel (10 points). A complicated design is for example Webb's regenerative burner (figure 2.10) as reference for 1 point. The jetburner can consist of a ceramic nozzle, which acts as thermal barrier upstream. The nozzle is mounted with a gasket in a stainless steel tube. Its rating is 9 points. The flat burner (figure 2.13) is more complicated, but also consists of two modules. A foam is clamped in insulation material. Its rating is 8 points. The tunnel burner is the most complicated of the three. The gas mixture has to be distributed over the cylinder. And the mounting of the cylinder in a tube is not simple. Its rating is 4 points.

Due to the heat exchanger, preheating leads to a more complicated design. Besides that, the gas and air have to be supplied separately, when the air is preheated above 873 K. Otherwise the mixture will auto-ignite.

Criteria		Flat PRB		Tunnel PRB		Jet Burner		Oxygen		Preheat	
	WF	S	WS	S	WS	S	WS	S	WS	S	WS
A Hot-shell temperature and heat flux	8	8	64	10	80	4	32	2	16	1	8
B Burner temperature	10	8	80	10	100	4	40	-	-	-	-
D Speed of heating up	4	5	20	1	4	10	40	2	8	1	4
E Fuel	3	-	-	-	-	-	-	1	3	2	6
F Price	2	10	20	6	12	6.5	13	2	8	1	4
G Constant heat flux to TEC	9	10	90	10	90	5	45	-	-	-	-
H Different TEC geometries	7	8	56	10	70	4	28	-	-	-	-
I Position of burner	5	5.5	27.5	5.5	27.5	10	50	-	-	-	-
J NO_x production	1	8	8	10	10	4	4	2	2	1	1
L Simple construction	6	8	48	4	24	9	54	2	12	1	6
TOTAL			**414**		**418**		**306**		**49**		**29**

Table 3.1 Discriminating scheme for the three alternatives (WF:weightfactor, S:score, WS:weighed score).

From table 3.1 it is concluded that a radiant burner is the best alternative for a laboratory burner. However, a choice has to be made between a tunnel or a flat burner. Further it follows from table 3.1, that the combustion temperature must be increased by enriching the air with oxygen.

The two remaining alternatives, the tunnel and the flat PRB, use the same heating principle. The main advantage of the tunnel burner is that the tunnel stabilizes the combustion and that the apparent emissivity at the outlet of the mouth will be higher. The TEC could even been placed into the burner. A disadvantage is the high demand on the tunnel material. The form is more complicated than a flat burner and it needs a higher structural strength than the flat burner.

The combustion in the flat burner will not stabilize easily. But its advantage is its simplicity. Further the demands on the porous material are lower. Even cracks could be allowed, when the global structure remains intact.

Because it is expected, that the material of the porous body will cause serious problems, the flat burner is chosen. When the material fails, pieces will break from the body. In case of the tunnel they fall down. In case of the flat burner a broken piece stays on its place, when it is larger than the pores. But the concept has to be compared to the other ones to improve the design. The flat burner did not score best for the following criteria:

1. The lowest burner temperature: the tunnel works at a lower burner temperature for equal heat flux. Due to the cylindrical form the radiant output is higher than the flat burner, when both have the same surface temperature. This improvement can not be implemented in the flat burner. However in the future this enhancement can be used in a next generation of burners. Condition is that a material will be found being able to stand the severe demands.

2. Speed of heating up: the jet-burner will respond fastest to changes in the gas-supply. Also its start-up will be fastest. The difference between the concepts is due to the thermal mass of the porous body. The reaction of the radiant burners is governed by the reaction of the porous body to changes in working-point. Thus the thermal mass of the porous body has to be low.

   A cellular ceramic will be used as radiant body. It combines a high heat exchanging surface to a low thermal mass. So the burner will react fast compared to classical radiant burners, depicted in figure 2.12.
3. Position of the burner: the jet-burner can easily be turned 360°. The porous burner will contain a ceramic foam. Due to thermal stresses cracks will form in the ceramic. Turning the burner will cause parts of the porous body to fall down, thus shortening the life-time of the burner. For the laboratory burner, this will be accepted.

Figure 3.3 shows the final concept and its basic parts. It consists of a gas supply unit where separately natural gas, compressed air and oxygen can be supplied. The gas flows are mixed in a mixing chamber and led through a support-tube to the burner-head. The burner-head is a separate module, which can be exchanged easily to test improvements in the design. Over the burner-head a simple insulation casing can be placed.

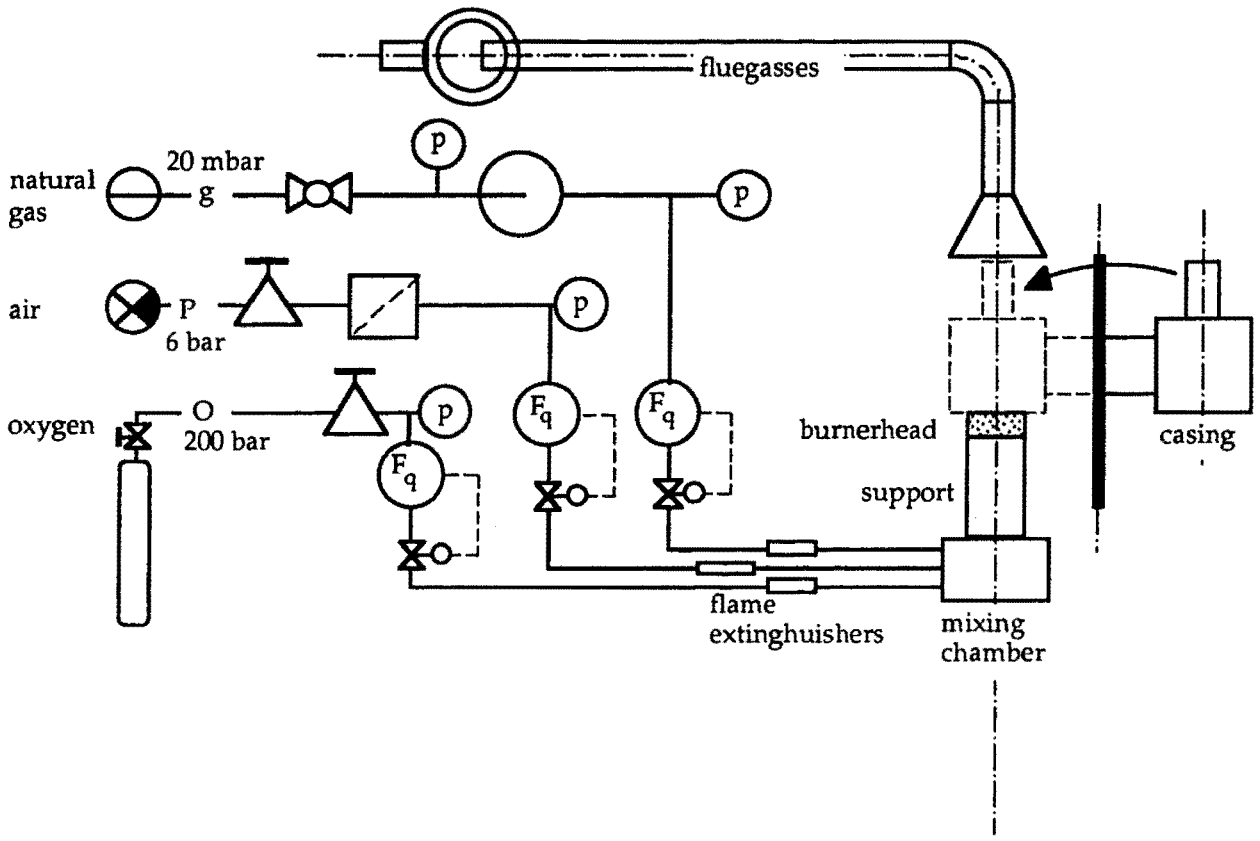

Figure 3.3 Concept of the total burner test-rig.

The test-rig consists of four modules: the burner-head, the gas supply, the furnace and the measurement instrumentation. In the next sections, the construction of the different parts will be discussed.

3.2 The Burner-Head

The burner-head embodies the following functions: stabilization of the combustion, heat transfer from the reacting gasses to the TEC, and insulation of the combustion zone from the surrounding construction. A cellular ceramic material (ccm) is chosen as basic component for the burner-head. This component will be further denoted as the foam.

The main function of the foam is to transfer heat from the reacting gasses to the TEC. Figure 3.4 shows the structure of a foam: pores and struts. In the foam, the high temperature gas transfers convectively its heat to the foam. The convective transfer is efficient due to a high heat exchanging area per volume. Within the foam, heat is transported to the top and bottom by radiation and conduction. The top radiates to the TEC, the bottom heats the rest of the construction and preheats the gas mixture.

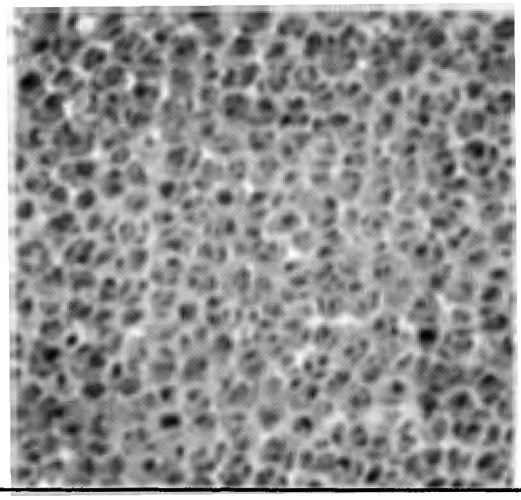

Figure 3.4 Cross-section of a cellular ceramic, the used zirconia (20 ppi).

In general the design variables for a cellular ceramic are:

1. Material composition; the base material will follow from requirements made by the temperature and oxidizing atmosphere.
2. Manufacturing process; this depends mainly on the chosen material. For example zirconia ccm's are produced by coating a polymer substrate with a ceramic slurry. The polymer is fired out of the green body, which is afterwards sintered.
3. Number of pores per linear inch (ppi); this statistic number is specified by the manufacturer. It is expected, that it has a distinct influence on the pressure drop. Further it affects the heat transfer through the foam. Small pores increase the optical thickness, so the temperature difference over the foam will increase. Brooks' measurements [1990] confirm that this effect exists, but it is not very significant.
4. Material relative density; this indicates the strut sizes in the foam and ranges from 5 to 30% of the theoretical density.
5. Thickness and shape; these parameters are important for mechanical strength, fluid flow resistance, optical thickness, edge effects etc.. Some

manufacturers are able to make relative complex forms like cylinders, helixes, and spheres [Brooks, 1990].

3.2.1 *Material Choice*

To fulfil its function, the ccm must:

— be resistant to the reactive oxidizing environment of burning natural gas,
— be capable to withstand 2273 K, while keeping its form,
— have a good thermal shock resistance,
— have a high emissivity,
— have a low heat content and a low heat conductivity to diminish heat losses.

The material is found by discriminating along this list of demands. A first rash overview of standard available ceramic materials yields materials like MgO, BeO, Al_2O_3 and ZrO_2. After comparing these materials, partially stabilized zirconia by magnesia is chosen. One of the main reasons is its resistance to thermal shock. A detailed account of the material selection can be found in Moonen [1993].

The firm Morganite, England supplied the PSZ foams through the firm Profiltra in Almere, The Netherlands. Two porosities were ordered: 10 ppi and 20 ppi. The diameter of the foams is 75 mm and the thickness 25 mm. To start the investigation a diameter near the diameter of the TEC is chosen and the foams were commercially available this way. The material properties are summarized in table 3.2.

The radiative properties of zirconia are not well defined. The spectral emissivity of zirconia is 0.18 - 0.43 at a wavelength of 0.65 μm according to the Mikron Instrument Company and 0.06-0.09 at the same wavelength according to Marmer [1971]. Further Seuren [1991] states that the total emissivity is 0.3 without reference to literature. Bramson [1968] gives the total emissivity of zirconia as function of temperature. The total emissivity varies from 0.16 at 1300 K to 0.7 at 2400 K (see figure C.2). In this investigation the data of Bramson are used.

Radiative properties are defined by the surface of a material. The influence on the properties by the surface has two causes. First the roughness of the surface can cause large differences. Second the material composition is not constant. To stabilize zirconia different additives are used like magnesia, yttria, or alumina in different amounts. The atoms at the surface determine the radiative properties of a material. So when different atoms appear at the surface due to doping, the radiation properties change. Those two effects explain the difference in the literature data.

Chemical composition [%]		SiO_2 [0.4], TiO_2 [0.2], Fe_2O_3 [0.1], Al_2O_3 [0.1], CaO [0.1], MgO [3.0], $ZrO_2 + HfO_2$ [96.2]
Apparent porosity [%]		20
Bulk density [kg m^{-3}]		4580
Specific heat [J kg^{-1} K^{-1}]		550 — 810 (293.15 K — 2273.15 K)
Thermal conductivity [W m^{-1} K^{-1}]		0.8 — 1.8 (293.15 K — 2273.15 K)
Coeff. of thermal expansion [K^{-1}]		$6.2\ 10^{-6}$ — $9.6\ 10^{-6}$ (293.15 K — 2273.15 K)
Maximal service temp. [K]		2873
Modulus of rupture[1] dense zirconia [MPa]		200 — 1000
Specific resistance [Ω cm^{-1}]		12.8 — 1.0 (1523 K — 2273 K)
Hooke's modulus [GPa]		200
Poisson's ratio ν		0.23
Average pore size[2]	10	1397
[μm]	20	838
Unit bulk density	10	0.93
[10^3 kg m^{-3}]	20	1.18
Unit porosity	10	81
[%]	20	77
Modulus of rupture	10	2.23
3 point bend test [MPa]	20	3.37

Table 3.2 Properties of ZAM Zirconia and its properties as ccm [Morganite, 1992].
1: de With [1991]
2: Pore size in ppi, being the number of pores per linear inch.

A complicating factor in case of a foam are the pores. These pores enhance the emissivity. When a pore is considered to be a cylindrical channel at constant temperature, the apparent emissivity can be estimated as function of the surface emissivity and the ratio of length and diameter of the cylinder (figure 3.5). When the poredepth is equal to the diameter, the ratio L/R is 2. With a surface emissivity of 0.3, the apparent emissivity of the pore becomes 0.65.

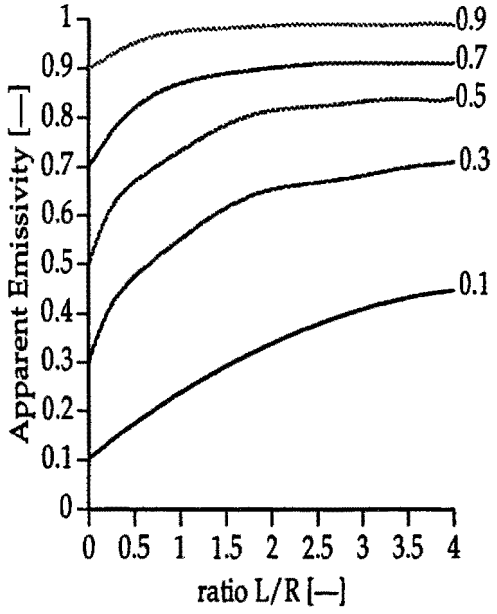

Figure 3.5 The apparent total emissivity of a cylinder with length L and radius R. The parameter is the total emissivity of the material. [Siegel&Howell, 1982].

Although zirconia can withstand high temperatures, it still can fail. The first failmode is oxidation. It is reported by Marmer [1971] that zirconia has a vaporization rate of 0.132 $\mu g/cm^2$ at 2200 K and 0.275 $\mu g/cm^2$ at 2300 K in vacuum. On the other hand Marmer states that zirconia can be used up to 2773 K in an oxidizing atmosphere. De With [1993] warns for evaporation of the stabilizing magnesia at high temperatures in an oxidizing atmosphere. This results in weakening of the strength of zirconia.

The second failmode is thermal shock, when the burner is turned off. When the burner is turned off, thermal stresses will occur due to temperature differences in the material. In appendix G the theory is explained and the critical temperature difference is calculated. The critical temperature difference is 592 K, if the influence of the shape is neglected. Thus cracks are expected due to thermal shock when the burner is turned off.

When cracks form and break a strut, pieces of material can come apart from the foam. Figure 3.6 shows a cross-section of a strut. It contains large pores, weakening the strut. Thus the design has to support the foam in order to keep it together, when struts break.

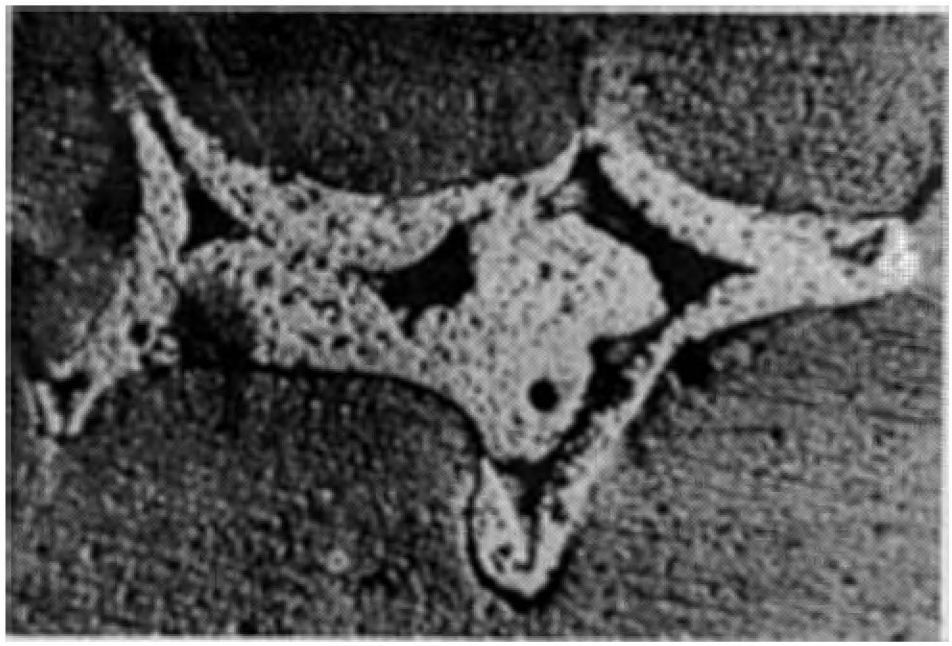

Figure 3.6 Cross-section of a strut.

Supporting the foam is done in two ways. The first is laying the foam on top of a ceramic board. Pieces of the foam can not fall down into the rest of the construction. In the ceramic board holes are drilled to let the gas/air mixture through. The second support is on the side of the foam. Around the foam ceramic alumina paper is winded. This alumina paper stays flexible up to 1873 K. Above 1873 K it will sinter and becomes solid. Thus the foam is gently clamped in a solid ring, when it is heated up. Material properties of the paper and board can be found in appendix D.

3.2.2 *Stabilization of the Flame zone*

The flame zone has to be kept on its place in the burner. E.g. the flame has to be stabilized somewhere inside the foam in order to achieve the best heat transfer from the flame to the foam. Stabilization can be realised by the gas-velocity and by cooling.

After some trial and error [Moonen, 1993] we found that the flame could be stabilized using a sieveplate. The sieveplate is made of ceraboard 1200 wherein holes are drilled (figure 3.8). In total 19 holes of 2.6 mm are drilled in the plate. In the holes the gas-velocity is 15 m/s at a power of 5 kW (calculation see appendix E.1).

The stabilization is realised by velocity because the velocity in the holes is higher than the flame speed. The flamespeed in a ccm can reach 7 times the adiabatic flamespeed [Sathe et.al., 1990a]. The adiabatic flamespeed is 0.4 m/s for a natural gas/air mixture and 6.5 m/s for a natural gas/oxygen mixture [Gaydon & Wolfhard, 1979]. So the flamezone is blown away from the holes. When the velocity is dispersed in the foam the flamezone stabilizes. The superficial velocity at 293 K is 0.4 m/s.

This mechanism prevents starting at full power. The burner has to be started on low power to prevent blow-off and to heat the foam. When the flamezone lies within the foam, the foam transports heat up- and

downstream. So the rest of the foam and the sieveplate are heated. When the part of the foam upstream of the flamezone is hot enough, it is able to heat the gasses above the auto-ignition temperature. For this reason the flame will move upstream. So it is necessary to cool the sieveplate otherwise the gasses will ignite before the plate, thus inducing flash-back.

When the furnace was not placed over the burner-head the plate was sufficiently cooled by the cold gasses [Moonen, 1993]. With the furnace over the burner-head it became hotter. The cooling of the gasses was not enough and flash-back occurred. Therefore an additional watercooling was placed under the sieveplate (figure 3.7).

The watercooling has to cool the sieveplate. The pattern of the sieveplate is drilled into a brass plate. With clamps the sieveplate is mounted to this brass plate. The slit between the sieveplate and the brass plate is cemented with gun-gum. The brass plate is cooled by water. There were several possibilities to build a heat exchanger. But due to a serious lack in time, a simple cross-stream heat exchanger with rectangular tubes was designed. The tubes were split into two circuits: the two outer, and the four inner tubes. The two circuits provide more freedom, the flows can be adjusted separately. The flows in the inner and outer circuit go in opposite directions to smooth out temperature differences. At the side of the sieveplate the tubes were soldered to the brass plate. The bottom of the tubes is glued on to a similar brass plate by silicone sealant.

A flow of 20 l/min could be established through the heat exchanger using the normal water-supply. This gives a maximum cooling capacity in Watts per Kelvin temperature difference over the heat exchanger at the waterside of:

$$\frac{Q}{\Delta T} = \rho_{water}\, \phi_v\, c_{p,\,water} = 1000 \cdot 3.3\ 10^{-4} \cdot 4200 = 1400\ \frac{W}{K} \qquad (3.1)$$

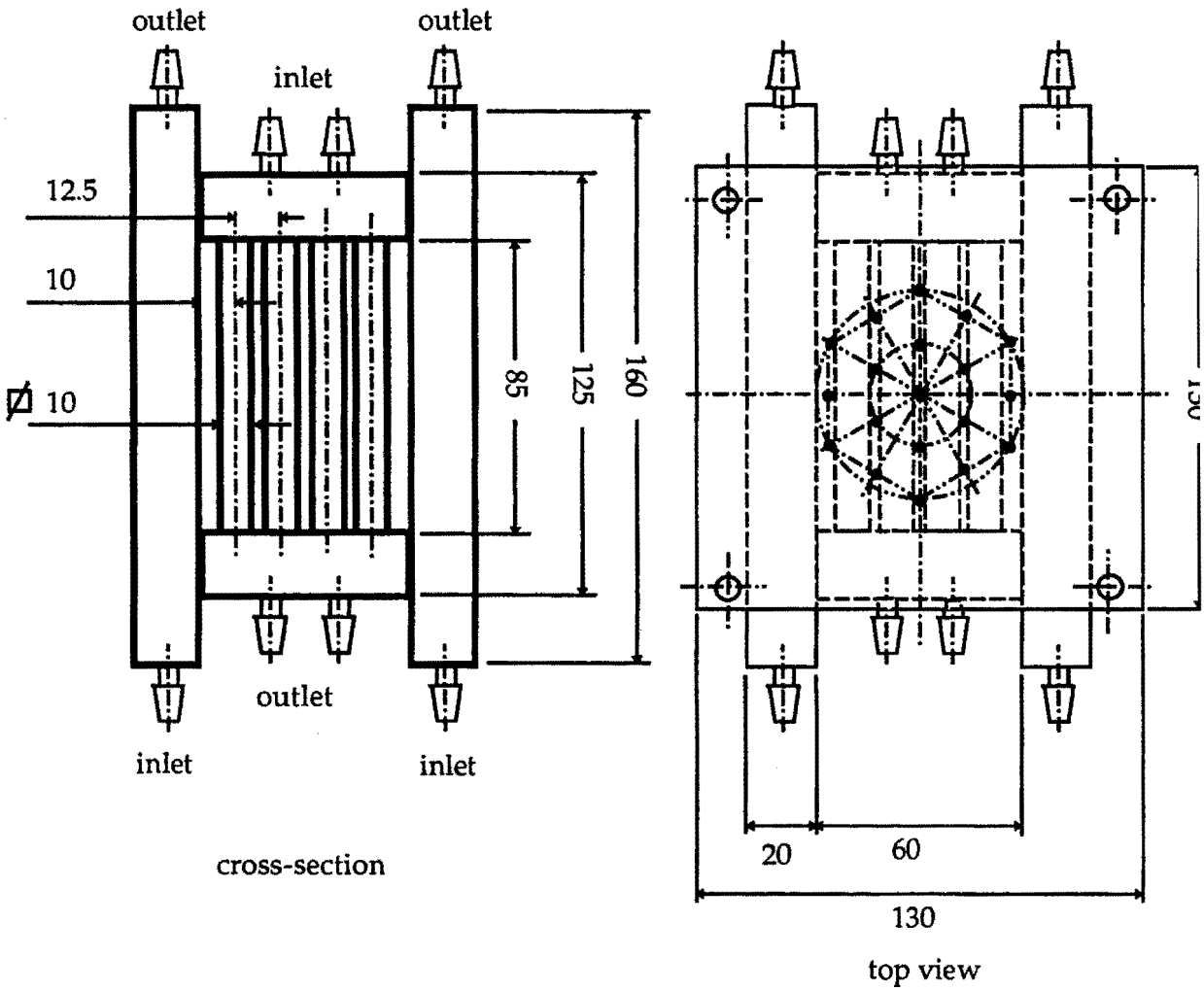

Figure 3.7 The watercooling.

3.2.3 *The Total Burner-Head*

Figure 3.8 shows an overview of the total burner-head including sieveplate and insulation. The foam lies on top of the sieveplate and ceramic paper is wound around the foam. Around the sieveplate a stainless steel ring is placed. The ring and sieveplate is mounted on the watercooling with two clamps and gun-gum. Durablanket is wound around the whole constitution, which is kept in place by stainless steel rings.

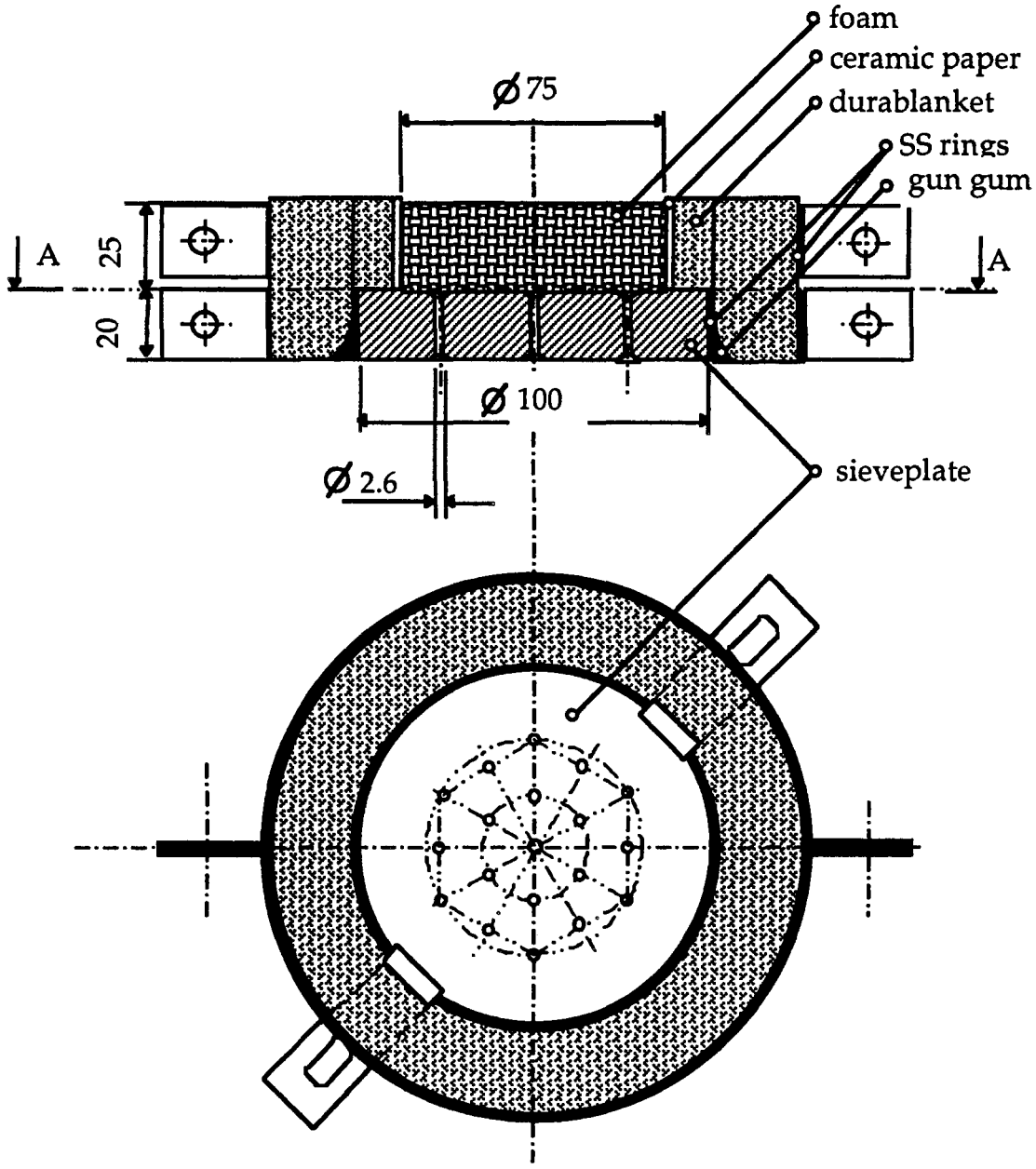

Figure 3.8 The total burner-head.

3.3 The Gas Supply

Three gas flows can be supplied to the burner: natural gas, air, and oxygen. The gasses are supplied to the burner-head premixed to achieve the highest temperature in the flamezone.

Each of the three gas-routes consists of a reservoir, a pressure control, a rotameter, a control valve, and a flame-extinguisher. In the mixing chamber the three flows are mixed and led into the support-tube of the burner-head. The flow-scheme of the installation is presented in figure 3.3.

As said, the different flows are measured by rotameters and controlled by valves. This set-up works due to the large pressure drop over the flame-extinguishers in comparison with pressure variations in the burner. So the variations in the burner do not influence the flows very much. Detailed information on the rotameters can be found in appendix F.

The three flows are mixed in the mounting of the burner-head. The mounting consists of two parts, a mixing chamber and a support for the head. Between the mixing chamber and the support, a restriction is placed to prevent flash-back.

As already is mentioned, attention has been paid to the safety of the design. The major risk is flash-back. It causes severe pressure-shocks or the flame front enters the supply piping. To prevent flash-back, the following actions are taken. A restriction is placed between the support-tube and the mixing chamber. At a design-point of 5 kW, the velocity in this restriction is 10 m/s, causing the flame to blow off. In each supply-channel a flame-extinguisher is mounted. The "piping" is made of polymer hoses, so a major flash-back causes the hoses to break or melt. Further the burner-head is detachable from the support. When the pressure increases in the support tube, the burner-head blows off.

3.4 A Simple Furnace

A furnace can be placed over the burner in order to diminish heat losses. The demands on the furnace are:

1. The furnace has to be movable,
2. It must be possible to measure the top-temperature of the foam,
3. The furnace has to withstand an oxidizing atmosphere of 2173 K,
4. The flue gasses have to be colder than 373 K, when they go into the ventilation system,
5. The furnace can be used to test the TEC.

Figure 3.9 shows the design of the furnace. The furnace is based on a cylinder of ZAL board (see appendix D.2 for material properties). Its (safe) maximum usage temperature is 1923 K. This is not according the demands, but high temperature boards are expensive ($500 for a cylinder of these dimensions). This cylinder was given for free by the MHD-group at the EUT. So it was decided to try this cylinder.

The cylinder is placed between two support plates. The support plate at the top is pressed against the cylinder by three springs. The springs allow the cylinder to expand or shrink. In the wall of the cylinder a quartz window is mounted. Through the window, the top temperature of the foam will be measured by a ratiopyrometer. Further the whole cylinder is insulated by a layer of durablanket.

The quartz window is first placed between ceramic paper to seal the slit. Then it is clamped between two ceraboard rings. In the ceraboard rings a slot is made to achieve a larger view-angle for the ratiopyrometer. The window can be cooled by pressurized air. The ceraboard rings are placed into a hole in the wall of the cylinder. This hole was made by the MHD-group.

A chimney is welded on the upper support plate. In the chimney, a 10 ppi foam is mounted. This foam diminishes the heat-loss through the chimney. After the foam the flue gasses will be cooler. In the experiments flue gas temperatures of 773-973 K were measured in the chimney. Between the chimney and the ventilation system a large slit of 100 mm was left open. Through this slit, enough cold air was sucked in together with the flue gasses to cool them to 343-353 K. In the chimney a tube is welded to insert a thermocouple and to suck combustion gasses to analyzers. The chimney and the two support plates are made from stainless steel AINSI 316.

The whole furnace is mounted to a cylinder, which can rotate and translate over a rod. The rod is mounted on the table. In this way the furnace can be easily placed over the burner and removed.

To test the TEC, the window is to be removed and this hole must be used as chimney. In the hole a foam must be placed to diminish heat-losses. The TEC can be mounted in place of the chimney. To measure the burner temperature, a new hole has to be made, or in the new chimney a hole is left open.

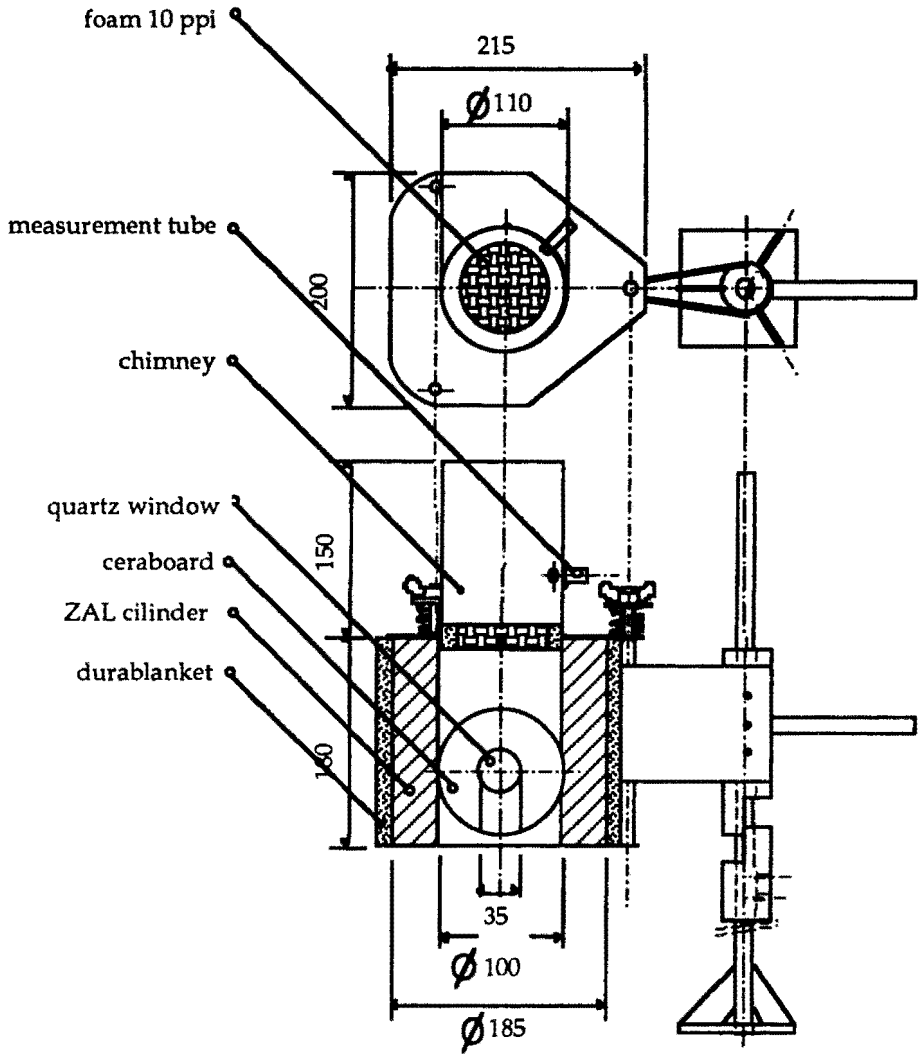

Figure 3.9 The furnace.

The burner and furnace are considered as one system to estimate the radiant power to be supplied by the burner. The power supplied must compensate the heat-sinks. The heat-sinks of the furnace are: loss through the cylinder, loss through the foam in the chimney, loss through the sieveplate, and loss through the burner insulation. The influence of the hot flue gasses is not taken into account, they disappear to the surroundings. Because the velocity of the gasses is low in the furnace, their convective heat transfer will be low compared to radiation. Only for the foam in the chimney, the gasses are taken into account. Other assumptions are that the heat-conduction is mainly one-dimensional and that the effects of the window and the thermocouples can be neglected. The calculations can be found in appendix E.2.

The loss through the cylinder is estimated 700 W, through the burner insulation 62 W, through the sieveplate 44 W, and through the foam 414 W. Added up, the total is 1220 W. These losses are delivered by radiation from the burner. To do so, the top burner must have a temperature of 2273 K (see section 2.3). The burner is heated by the flue gasses. An estimation of the amount of natural gas needed can be calculated, when the temperature difference of the flue gasses over the burner-head is known. It is assumed that the flue gasses leaving the burner-head have the same temperature as the top of the foam: 2273 K. The temperature in the flame zone is chosen to be 2773 K. This is the maximum temperature zirconia can stand, because the melting temperature of zirconia lies in the range from 2773 K to 2873 K [Richerson, 1992]. This flame temperature has to be realized by preheating or oxygen enrichment.

Thus based on the temperature difference of 500 K, 1.8 10^{-4} m^3/s gas must be supplied to compensate the losses being 1220 W. This flow presents a combustion heat of 5.6 kW (further called the burner power). This exercise can be repeated, when the TEC is added to the system. The radiant power needed with TEC becomes 1220 + 1500 = 1720 W, the flow of natural gas 3.9 10^{-4} m^3/s, and the burner power 12.4 kW.

4 Experimental Results

4.1 Measurement Strategy

In the design stage a number of questions are not answered. Amongst these questions are:

What are the optimum dimensions for the foam: length and porosity ?

Can the flame be stabilized using a sieveplate ?

How many holes are needed for the sieveplate to achieve a constant combustion in the foam without hot or cold spots ?

Which mixture of gas and air is optimal ?

Are the right materials chosen ?

How does the burner interact with a heat-load ?

Optimal means in our case maximum burner-output or maximum top temperature. These questions are to be answered by the measurement program.

Due to restrictions in time, no experiments are carried out with oxygen-enriched air. All experiments are carried out with a natural gas-air mixture. The status of this mixture is determined by the airfactor:

$$a = \frac{\phi_{v,\,air\ supplied}}{\phi_{v,\,air\ stochiometric}} = \frac{\phi_{v,\,air\ supplied}\ [m^3\ s^{-1}]}{\phi_{v,\,gas}{}^*\ 8.4303\ [m^3\ s^{-1}]} \qquad (4.1)$$

and the burner power:

$$P_{burner} = \phi_{v,\,gas}\ H_i = \phi_{v,\,gas}{}^*\ 31.669\ 10^6\ [W] \qquad (4.2)$$

Two additional parameters are defined. The first is the radiant power of the burner. The radiant power is defined as the net heat flux from the burner to its surroundings by radiation. The net heat flux is [Feijen, 1987]:

$$P_{rad} = \frac{A_{foam}\,\sigma\,(T_{foam}^4 - T_{surr}^4)}{\frac{1}{\varepsilon_{foam}} - 1 + \frac{1}{F_{foam\text{-}surr}} + \frac{A_{foam}}{A_{surr}}\left(\frac{1}{\varepsilon_{surr}} - 1\right)} \qquad (4.3)$$

This definition is based on the radiant heat exchange of two arbitrary grey surfaces. When the burner radiates to the laboratory without furnace, expression (4.3) simplifies to:

$$P_{rad} = \varepsilon_{foam} A_{foam} \sigma (T^4_{foam} - T^4_{surr}) \quad (4.4)$$

Second is the radiant efficiency of the burner:

$$\eta_{rad} = \frac{P_{rad}}{P_{burner}} \quad (4.5)$$

In appendix F.6 the random errors of these parameters are estimated. The relative random error of the airfactor a is 4%, of the burner power 0.6%, of the radiant power 0.8% (expression 4.4) and of the radiant efficiency 0.7%.
The following experiments are carried out:

— without furnace:
variation of the airfactor a at constant power P of 5 and 9.5 kW for a 10 ppi foam and a 20 ppi foam with a height of 25 mm.

— with furnace:
variation of the airfactor a at constant power P of 5 and 9.5 kW for 20 ppi foams with heights 10 & 25 mm and with a stack of a 10 ppi and a 20 ppi foam, both with a height of 25 mm.

4.2 The Instrumentation.

The instrumentation is described shortly in this paragraph. The reader is referred to appendix F for the used equations, working principles, and the background of systematic and random errors.

4.2.1 Flowmeters

In total three rotameters are used to measure the two gas flows; two parallel for natural gas, and one for air. The readings of the rotameters are calibrated and corrected for density, temperature and pressure. The relative error of the natural gas flow is 0.7% and of the airflow 4%.

4.2.2 The Pyrolaser

The Pyrolaser is a pyrometer operating at 865 nm. At 865 nm the pyrolaser measures the radiative flux. Using Planck's law, it calculates the temperature from the radiative flux. Further it shoots a laser at the surface. From the measured reflection of the laser beam, the reflectivity is derived. Using Kirchhoff's law the emissivity is found.

The pyrolaser is used to measure the top temperature of the foam. Unfortunately a filter was broken during this investigation. So the pyrolaser is only used for measurements without furnace by Moonen [1993].

Using the pyrolaser, two sources for systematic errors are identified. These sources are that the laser beam is not reflected diffusively and that the transmittance is not zero, due to the pores of the foam. Gelten [1993] showed that the influence of the first error source is small: the emissivity varies 3-

6% as function of the angle. For the moment this error will be neglected. But the influence of the reflection variation has to be studied.

The second error source makes that the pyrolaser will measure an effective top temperature: the mean of a certain volume of the foam. So not the true top temperature is measured. On the other hand the measured temperature is the temperature the surroundings experiences in radiant heat exchange with the burner.

The random error is mainly caused by the variation of the emissivity. The random error of the absolute temperature in Kelvin is 2%.

4.2.3 *The Ratiopyrometer*

The ratiopyrometer is used for the measurements with furnace. It measures the radiative flux at two wavelengths. Then the ratio of the two fluxes is calculated. This ratio is the same as for a black radiator, assuming that the emissivity is equal at both wavelengths.

Just like the pyrolaser, the ratiopyrometer measures the temperature at the top of the foam. This is done through a quartz window. During the experiment the window became smudgy leading to a systematic measurement error. This error is corrected by taking into account the transmittance of the window (see appendix F). Another systematic error is the transmittance of the foam. Here the same arguments apply as those for the pyrolaser.

Used without window, the random error of the pyrometer is ±12 K at 1473 K (1.6%) and ±17 K at 2873 K (1.2%). Using a correction for the window, the error becomes larger e.g. 2.5% (±21 K at 1823 K).

4.2.4 *Thermocouples*

The thermocouples measure the temperatures of flue gasses, the furnace walls, the temperatures in the burner-head, and the place of the flame zone. During the measurements without furnace, a couple is placed above the burner in the flue gas stream.

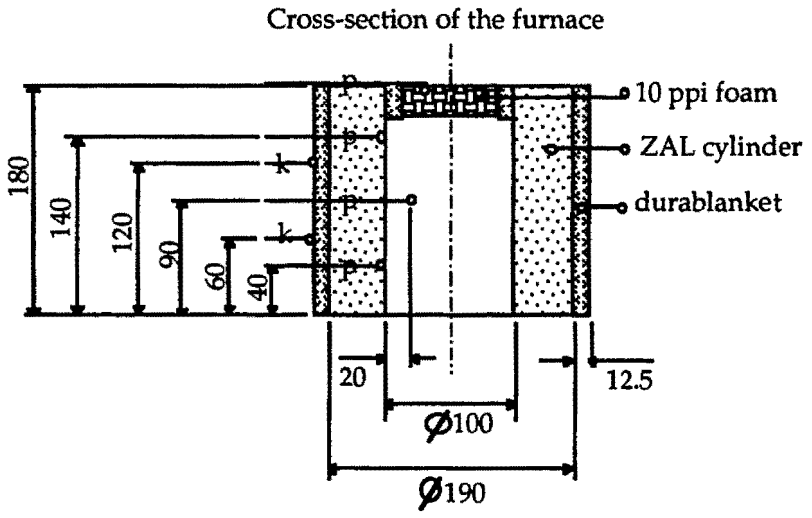

Figure 4.1 Mounting of the thermocouples in the furnace, k: chromel-alumel, p: Pt-PtRh13%.

Figure 4.1 shows where in the furnace Pt-PtRh13% and K-type thermocouples are mounted. Because a thermocouple is in thermal balance with its surroundings, systematic errors easily occur. The K-type thermocouples are not expected to have a systematic error because they are mounted along the durablanket for 100 mm.

The two Pt-PtRh couples, measuring the temperature of the inner furnace-wall, have a large systematic error in the order of 300 K [Smeets, 1980]. The Pt-PtRh couple in the foam at the outlet is placed in a pore. So it is a measure for the temperature of the foam.

The thermocouple in the gas flow has also a large systematic error. Its function is to measure the gas temperature. In practice the temperature of the couple differs from the gas temperature, because the couple radiates to the surroundings. Further the couple is heated by the foam. To find the flue gas temperature the heat balance of the thermocouple has to be solved. This is tried in appendix F.3, but it proved to be difficult. The relation between the couple temperature and the gas temperature is solved, but is very sensitive to emissivities of the materials used. And the emissivities are not well known.

Thus the systematic error for the couple in the flue gasses is recognized. It is in the order of 275 K, but a variation in emissivity of 0.1 results in a gas temperature variation of 180 K. For future experiments it is better to shield the couple by ceramic tubes. These ceramic tubes act as radiation shields. This minimizes radiation loss from the couple to the surroundings, and heating of the couple by the burner.

In the burner-head, three WRe5%-WRe26% are mounted pressing against the foam. Comparison of the temperature recordings with these couples gives an impression, where the flame zone is located. The couples lasted in the experiment for one hour.

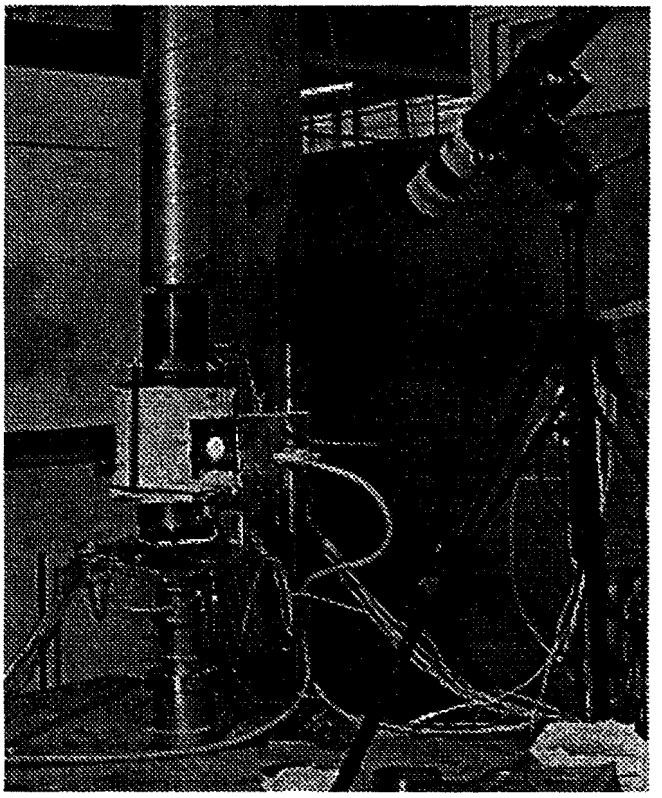

Figure 4.2 The test-rig with the ratiopyrometer.

4.3 General Remarks on the Performance

4.3.1 Behaviour of the Burner

Start-up has to be done carefully due to the high gas velocity in the sieveplate. In practice it is best to start the burner at low power (2.5 kW, being full gas flow without booster). Then the airflow is to be regulated such that the top of the foam starts to radiate. When the foam is hot (after 5 minutes), the booster can be turned on. The burner stabilizes at all powers without problem.

The flame-zone was during all experiments in the lower part of the foam and it is suspected that it starts in the sieveplate. This can be seen from the readings of thermocouples in the burner-head (figure 4.3) and from the temperature distribution of the insulation around the head (see also Moonen p. 57 [1993]).

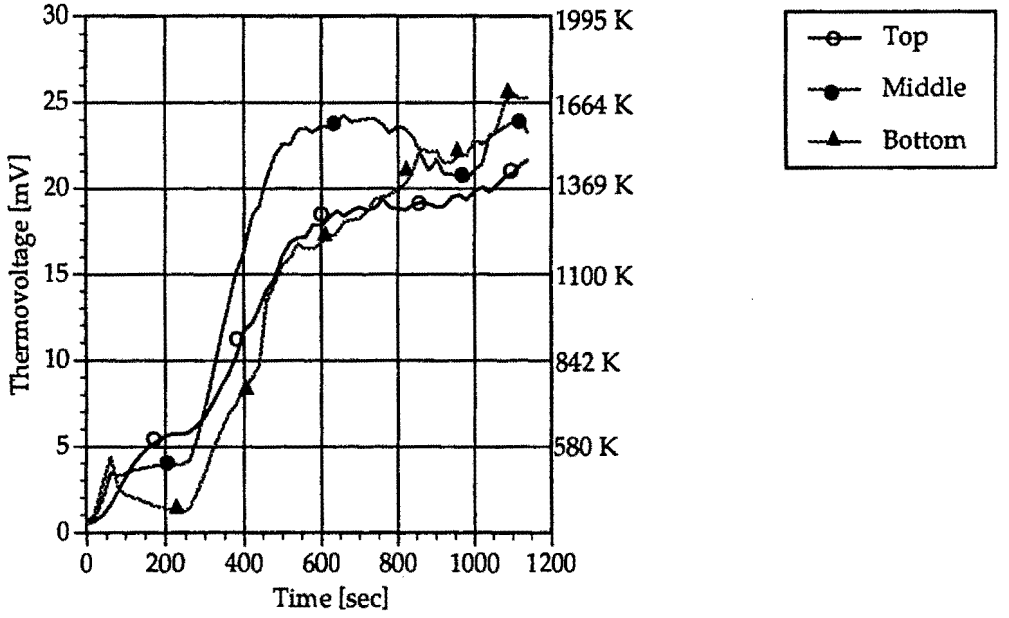

Figure 4.3 The readings of the couples in the burner-head during one of the experiments. The length of the foam is 25 mm.

Without furnace the reaction of the top temperature to a change in workpoint is fast, in the order of 30 seconds [Moonen, 1993]. With furnace it takes longer. Depending on the change, it varies from 1 minute to 15 minutes. Especially when the furnace is heated at start-up and when the workpoint is changed from high burner temperature to low burner temperature, the whole system is slow.

The sieveplate works reasonably well. When the height of the foam is 25 mm or more the radiation pattern is homogeneous. The foam of 10 mm gave some problems. After installation of the burner-head the velocity in the foam was too high. The combustion could only be stabilized for low power (4 kW) and the holes of the sieveplate were clearly visible in the radiation pattern of the foam. Increasing the power of the burner caused blow-off.

After 15 minutes the holes in the sieveplate became larger due to shrinking. This led to a faster stratification of the flow in the foam. Now the combustion was stable for higher power (9.5 kW).

Without furnace the burner worked without flash-back during several hours. The cooling by the cold mixture was enough. When the furnace is placed over the burner-head, flash-back occured after 20 minutes. Therefore the watercooling is designed and build. With watercooling flash-back did not occur anymore.

4.3.2 *Performance of the Materials*

As expected the foams broke during cooling down. But there was a large difference between cooling down with the furnace on top and without furnace. After several times starting and stopping the burner without furnace, the foams broke down completely when the burner-head was

dismantled. With furnace some cracks formed but the foam stayed intact. From the foam mounted in the chimney, little pieces fell down.

During the experiments no problems with the broken foams are experienced. Some foams burned up to 24 hrs. as long as they were not dismantled. The ceramic paper holds the foam together perfectly. The outer insulation of durablanket performed satisfactory.

Three materials are tested for the sieveplate: boronnitride, zircar board and ceraboard. The boronnitride is a dense ceramic tile. It stood up to a burner temperature of 1773 K. Above this temperature, the tile oxidized and vanished. Only some walls were left standing. The zircar board could stand the temperature demand. But due to shrinkage and thermal cycling it broke up in the end. The ceraboard performed well up to burner temperatures of 1773 K. When the temperature became higher, the board probably melted around the holes. The result was a dense solid ceramic tile with large holes.

The other materials of the furnace performed well. Only the lower stainless steel support plate became too hot. This can be solved by enlarging the hole to a diameter of 120 mm and folding durablanket around the plate. Another problem was the quartz window. It was cooled by an air stream, but when the burner temperature exceeded 1873 K the quartz became filthy. At the last experiments the window was left out. No difference in temperature was measured leaving the window out. So the measurement hole can be used without window. But it is advisable to make it as small as possible.

4.4 Results Without Furnace

Figure 4.4 shows a comparison between the top-temperature of a 10 ppi and a 20 ppi foam. No real difference can be discerned. On the whole the 20 ppi has a higher temperature but it falls within the error bands.

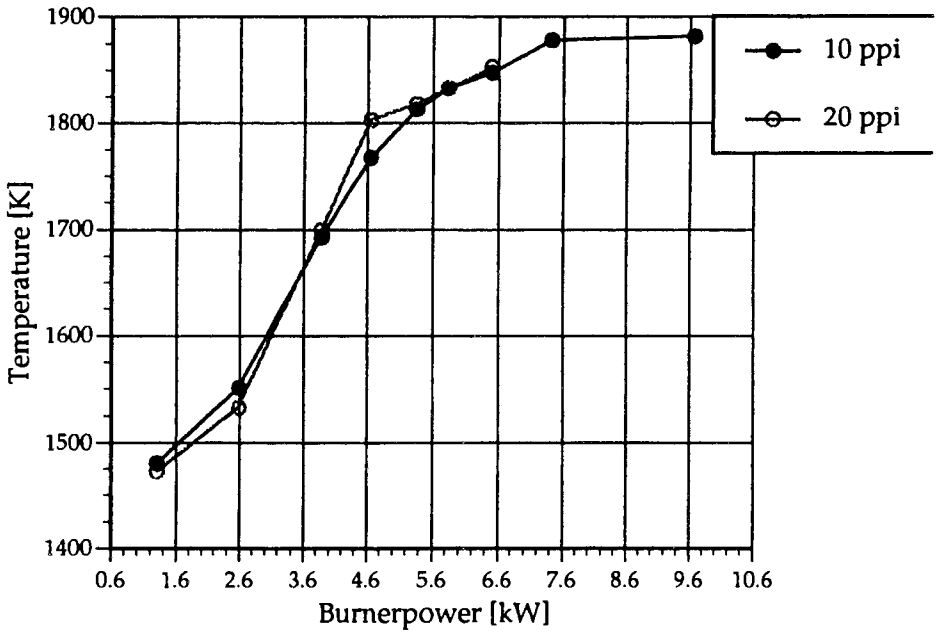

Figure 4.4 Top temperature of the foam as function of the burner power for the two porosities, at stochiometric conditions.

Figure 4.5 shows the top temperature as function of the airfactor. The parameter is the burner power. The foam used has a porosity of 10 ppi. The maximum temperature is achieved for a slight over-stochiometric mixture.

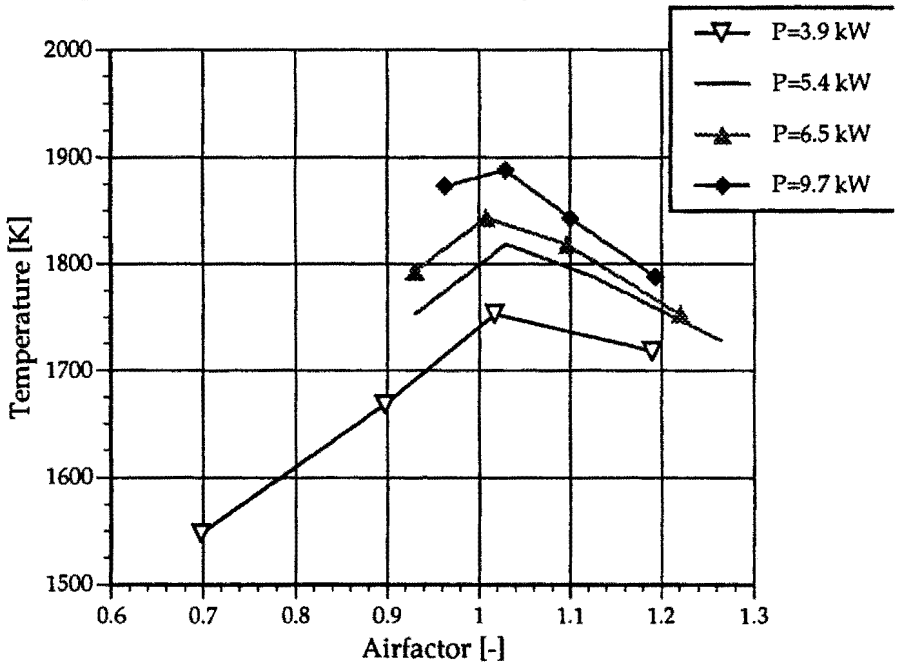

Figure 4.5 Top temperature of a 10 ppi foam as function of the airfactor for different powers. The measurements are without furnace.

From figure 4.5 the radiant power can be calculated. Ofcourse, the radiant power is directly coupled to the temperature. The radiant output power is calculated from the black body temperature, leading to a lower error. This temperature is the temperature, a body would have if it was black. The black body temperature is directly measured by the pyrolaser. To do so expression (4.4) is modified:

$$P_{rad} = A_{foam}\,\sigma\left(T^4_{b,\,foam} - \varepsilon_{foam}\,T^4_{surr}\right) \tag{4.6}$$

The emissivity of the foam is still unknown. But it can be derived from the ratio of the black body temperature and the emissivity corrected temperature. These two temperatures are reported by the pyrolaser. Thus,

$$\varepsilon_{foam,\,total} = \frac{T^4_{b,\,foam}}{T^4_{\varepsilon,\,foam}} \tag{4.7}$$

The result is shown in figure 4.6 for a 10 ppi foam.

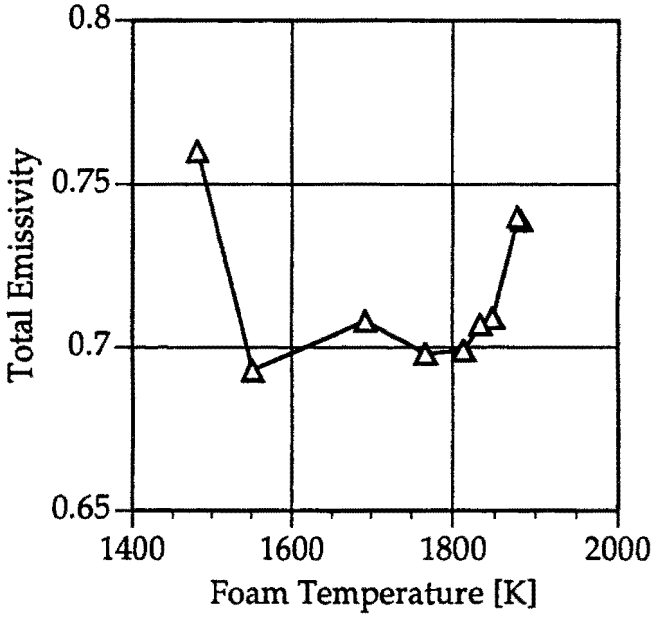

Figure 4.6 The total emissivity of a 10 ppi foam as function of its temperature.

The measurements presented in figure 4.6 differ from the previous used data of Bramson [1968] (figure C.2). The emissivity is 200-300 % higher than measured by Bramson. The reason for the large difference is the influence of the pores. The pores augment the emissivity as described in section 3.2.1. Because this effect is very significant, emissivity measurements have to be carried out on the ccm's in the near future.

Figure 4.7 shows the radiant power. The emissivity of the foam is 0.7, based on figure 4.6. The temperature of the surroundings is 293 K.

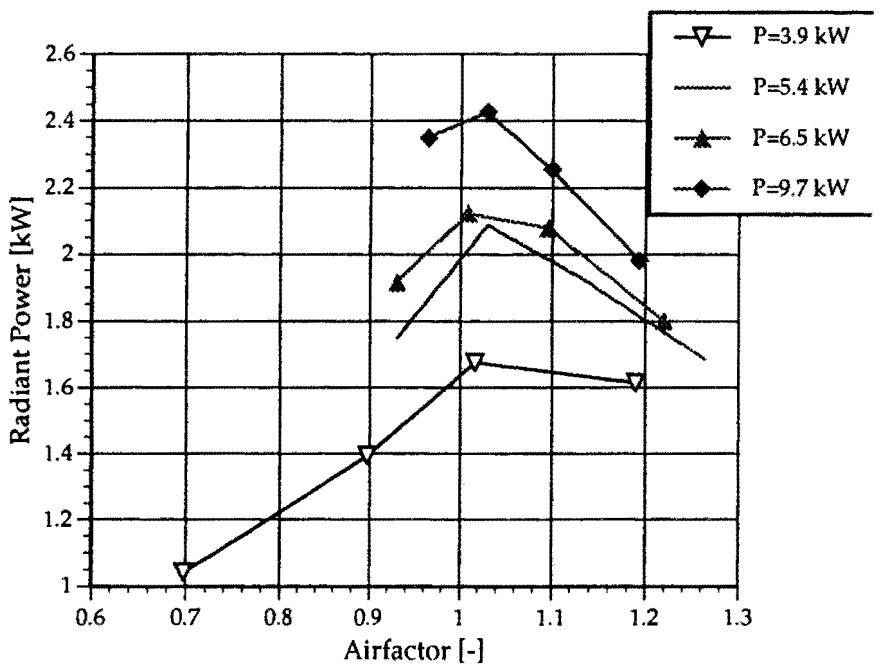

Figure 4.7 Radiant power of a 10 ppi foam as function of the airfactor for different burner powers.

Figure 4.8 combines figure 4.7 with the burner power in the radiant efficiency. Interesting to see is that the efficiency decreases when the burner power increases. This means that the convective heat transfer in the foam and the radiant output are not coupled linearly.

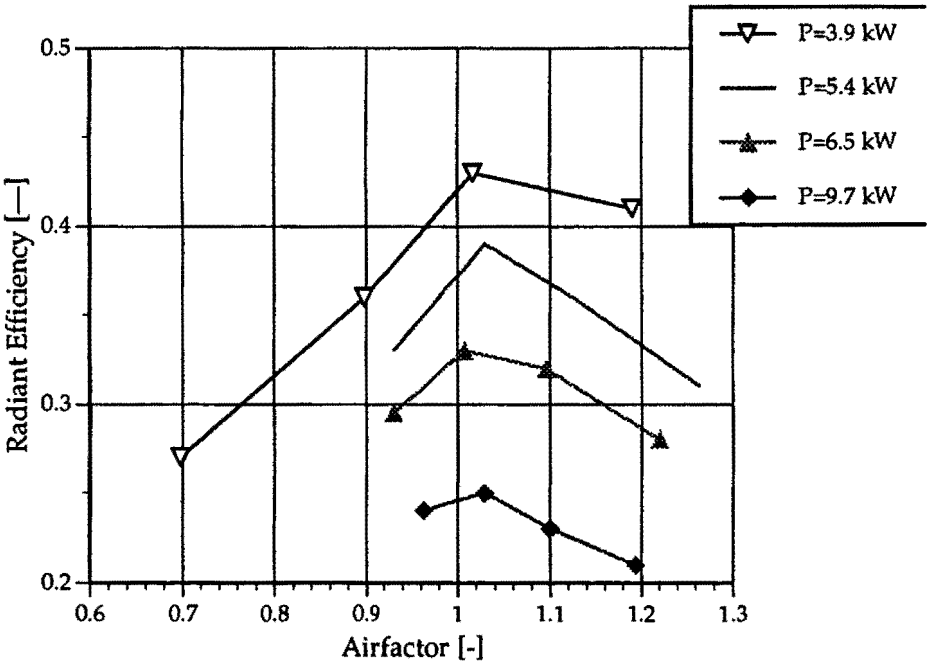

Figure 4.8 Radiant efficiency of a 10 ppi foam as function of the airfactor for different burner powers

4.5 Results With Furnace

Figure 4.9 shows the top temperatures of the foam for three different lengths for the foams. The foams used have a porosity of 20 ppi. The shortest foam (10 mm) achieves the highest temperature. In figure 4.9 the adiabatic flame temperature is also drawn [de Goey, 1990]. The temperature of the foam stays at its maximum 280 K underneath the adiabatic flame temperature. Further it is clearly seen that in accordance with theory the highest temperatures are reached for a slight over-stochiometric mixture.

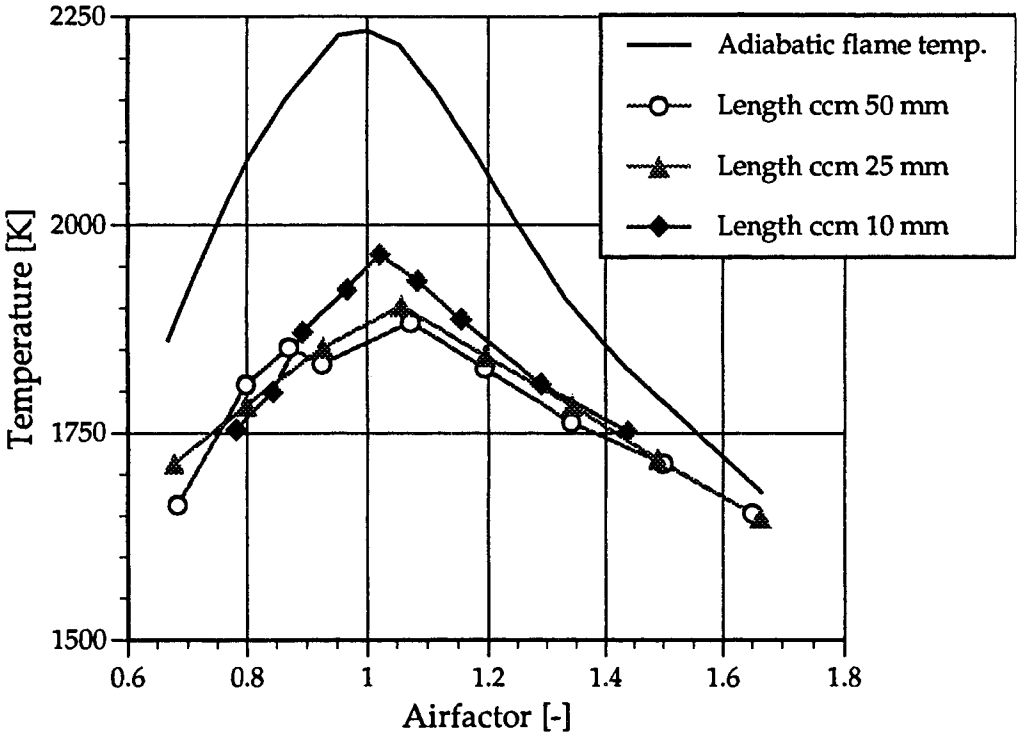

Figure 4.9 Top temperatures of the foam at 9.5 kW for the three configurations compared to the adiabatic flame temperature.

Figure 4.10 shows the temperature measured by the thermocouple in the flue gasses 90 mm above the burner. The shortest foam has the highest flue gas temperature for stochiometric conditions. Between the other two configurations (25 & 50 mm) there is no significant difference.

In figure 4.11 the temperatures of the inner furnace wall are shown, with the temperature of the thermocouple in the foam at the outlet. The temperatures are higher for the configuration with one foam than for two foams for stochiometric conditions. This is consistent with the burner temperature itself. From figure 4.11a it is also seen that the furnace wall is colder for low airfactors. These measurements were taken too soon after start-up when the furnace was not yet stationary.

The readings of the thermocouples are not corrected for their systematic errors.

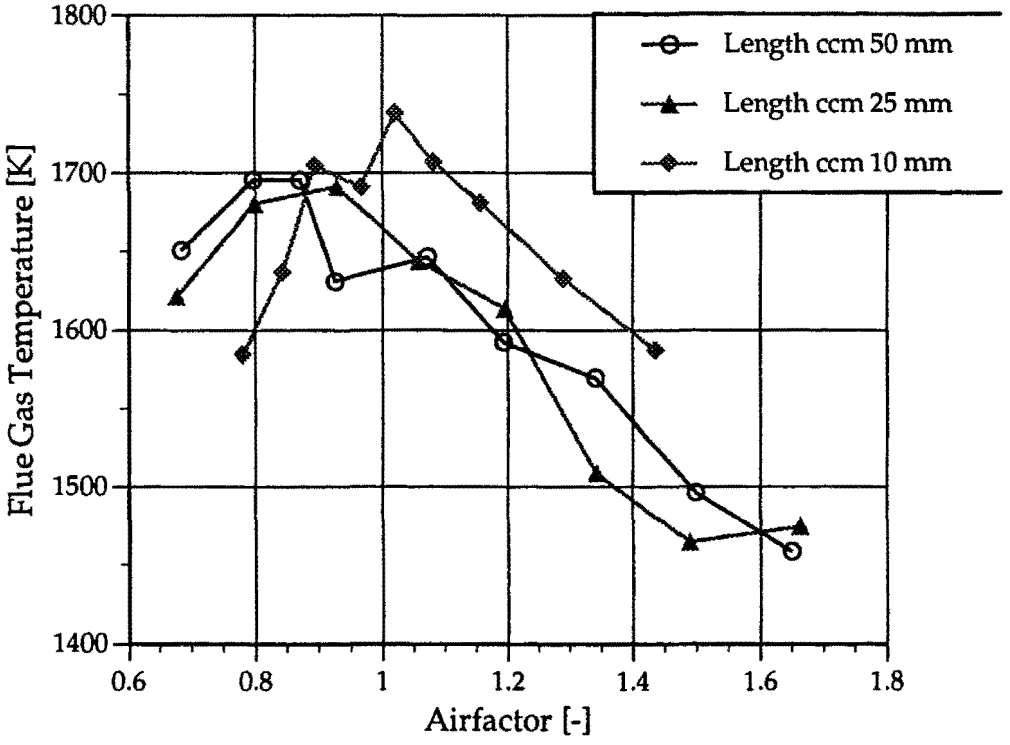

Figure 4.10 The temperature of the thermocouple in the flue gasses as function of the airfactor. Parameter is the thickness of the foam.

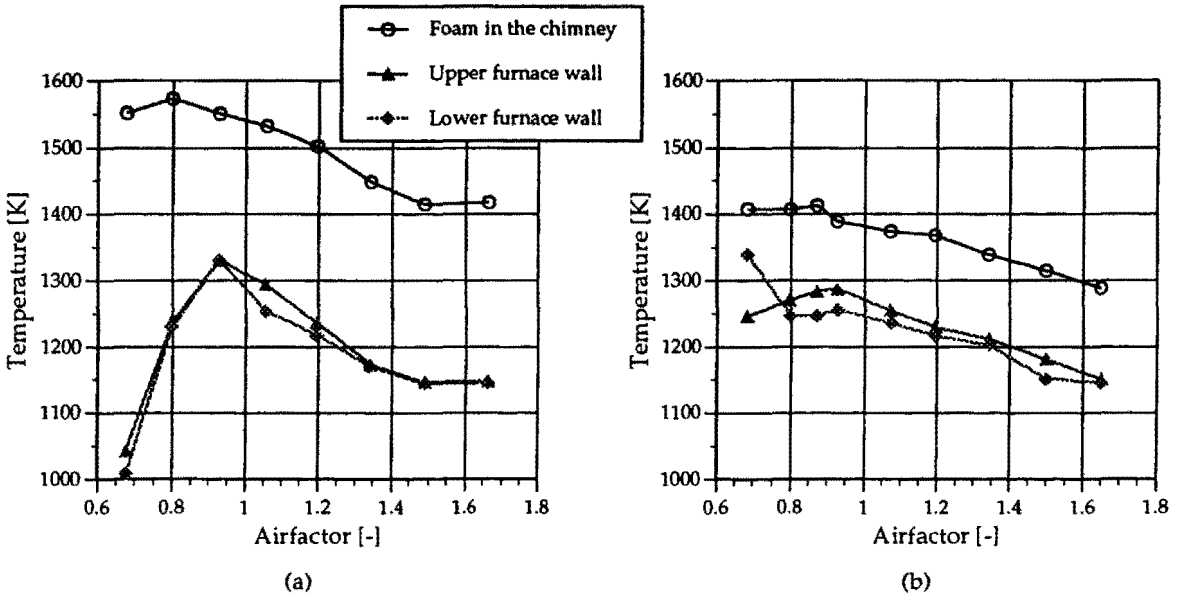

Figure 4.11 The temperatures of the thermocouples in the furnace wall and in the foam at the outlet. (a) length of the foam is 25 mm (b) length of the foam is 50 mm. The burner power is 9.5 kW.

Figure 4.12 shows the temperatures measured in the furnace for the three burner configurations. Figure 4.12a shows a difference in procedure with the other two. The thermocouple in the flue gasses was broken, so the thermocouple in the foam at the outlet was placed underneath the foam

measuring the gas temperature. The temperatures of the thermocouples are not corrected for their systematic errors.

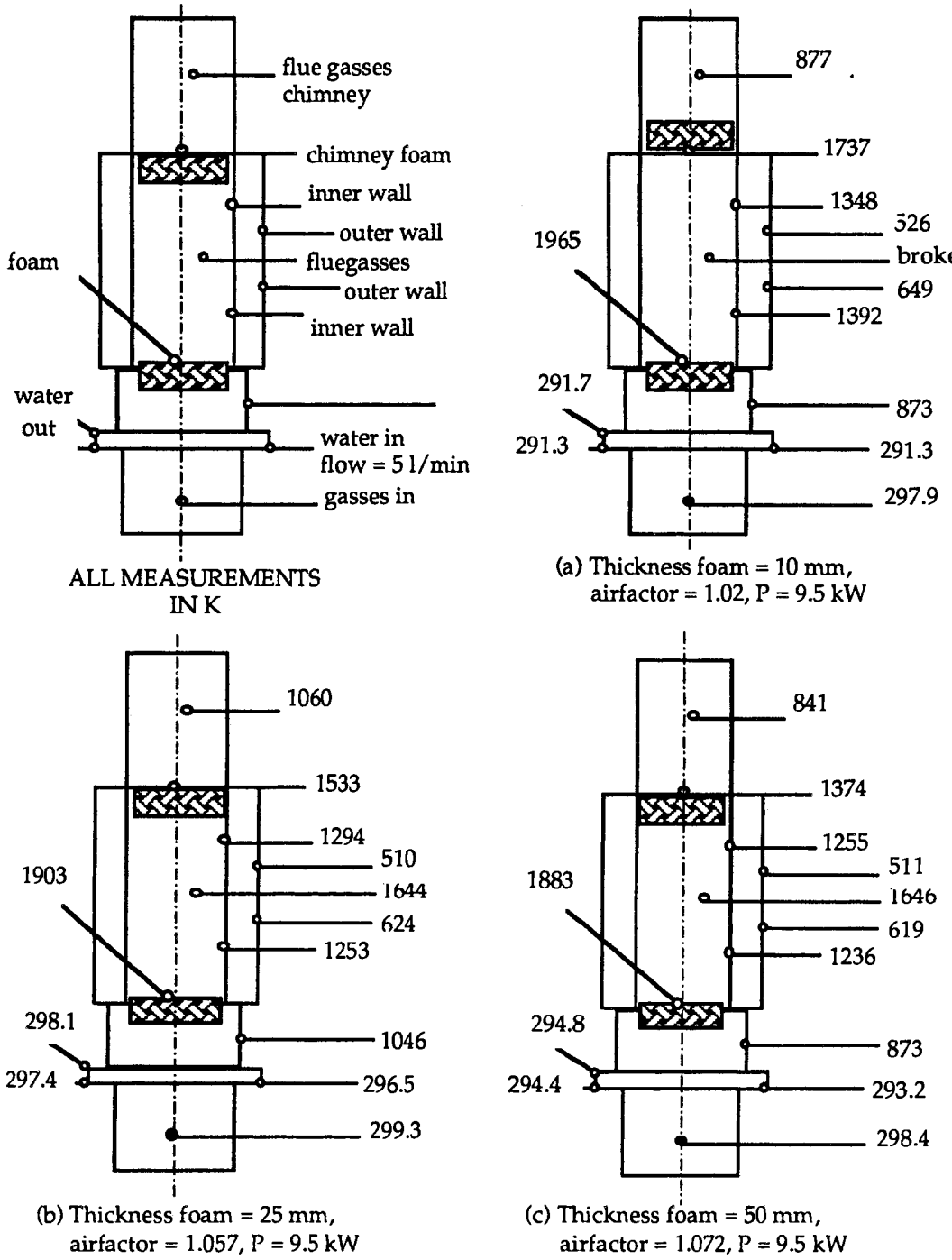

Figure 4.12 Temperatures measured in the furnace with the three burner configurations at stochiometric conditions.
(a) foam length 10 mm, (b) 25 mm, (c) 50 mm.

With these data an energy balance of the burner-head can be made. The burner-head loses its burner power in four ways: first it radiates to the furnace,

$$Q_{rad} = \frac{A_{foam}\,\sigma\,(T_{foam}^4 - T_{furnace}^4)}{\frac{1}{\varepsilon_{foam}} - 1 + \frac{1}{1} + \frac{A_{foam}}{A_{furnace}}\left(\frac{1}{\varepsilon_{furnace}} - 1\right)} \qquad (4.8)$$

Second heat is transported by the flue gasses,

$$Q_{flue} = \phi_m\,\overline{c_p}\,(T_{flue\ gasses} - 293.15) \qquad (4.9)$$

The isobaric heat capacity is averaged over ($T_{flue\ gasses}$ - 293.15 K). Values can be found in Gasunie [1988]. Third the foam loses heat through its insulation to the surroundings,

$$Q_{ins} = \frac{2\,\pi\,L_{foam}\,(T_{foam} - T_{ins,\,out})}{\frac{1}{k_{durabl.}}\ln\left(\frac{r_{ins}}{r_{foam}}\right)} \qquad (4.10)$$

It is assumed that the foam temperature is constant, equal to the top value. Fourth and last is heat loss through the sieveplate. This flow is estimated by evaluating the heat absorbed by the watercooling,

$$Q_{water} = \phi_m\,c_p\,(T_{out} - T_{in}) \qquad (4.11)$$

The temperatures follow from the experiments. The calculations are performed at the airfactor yielding maximum foam temperature. In table 4.1 also the radiant efficiency is calculated.

The following values for material properties are used to perform the calculations. The emissivity for the foam is again based on figure 4.6. The emissivity for the furnace is estimated on data from Mikron. The heat content of the flue gasses can be found in Gasunie [1988] and of water in VDI [1988].

$$\begin{aligned} \varepsilon_{foam} &= 0.7;\ \varepsilon_{furn} = 0.3 \\ \overline{c_{p,\,flue}} &= 1430\ J\,kg^{-1}\,K^{-1} \\ c_{p,\,water} &= 4128\ J\,kg^{-1}\,K^{-1} \end{aligned} \qquad (4.12)$$

Foam length	P_{burner} [kW]	Q_{rad} [kW]	Q_{flue} [kW]	Q_{ins} [kW]	Q_{water} [kW]	P_b-Q_{tot} [kW]	η_{rad} [%]
10 mm	9.6	1.1	6.9	0.037	0.052	1.5	11
25 mm	9.6	0.96	6.4	0.029	0.44	1.8	10
50 mm	9.6	0.92	6.4	0.027	0.49	1.8	10

Table 4.1 Heat balances of the furnace for the three configurations.

In this way the heat balance of the burner-head is not closed; a discrepancy of 15-18 % remains. The difference is probably caused by the systematic measurement errors of the thermocouples.

4.6 Estimation of the Performance with TEC

Based on the experimental results, the performance of the test-rig can be calculated, when the TEC is mounted. Point of interest is the heat flux on the TEC. The temperature of the TEC is assumed to be 1723 K and the burner temperature 1965 K (figure 4.12a). Now the other temperatures and heat fluxes are calculated with Gebhart's zone method (see section 2.3 and appendix C).

The material properties needed are the heat conductivities and the emissivities. The heat conductivities of zircar and durablanket are given in appendix D. The emissivity of the TEC is 0.9. The emissivity of the burner is 0.7 based on figure 4.6. The emissivity of the insulation is 0.3 [Mikron].

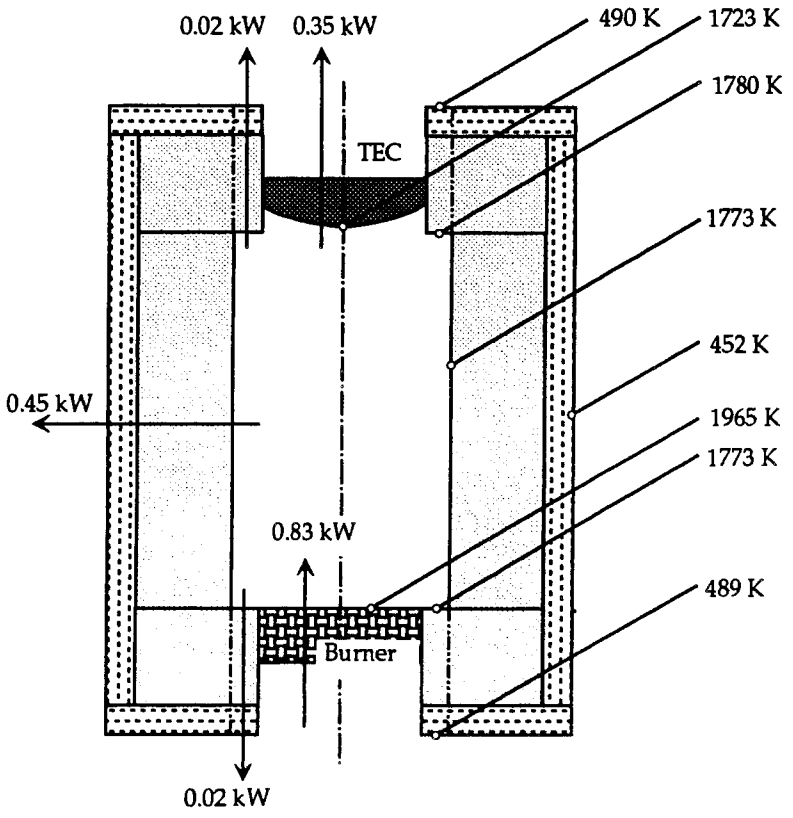

Figure 4.13 The calculated temperatures of the five zones and the heat fluxes through the zones.

Figure 4.13 shows the temperatures of the five zones with the heat fluxes through the zones. Thus, when in the experiment of figure 4.12a the TEC is mounted, it receives 0.35 kW. The goal is 1.5 kW. Figure 4.14 shows the heat fluxes of the burner and TEC as function of the burner temperature. When the burner reaches the temperature of 2273 K, the TEC receives 1.5 kW.

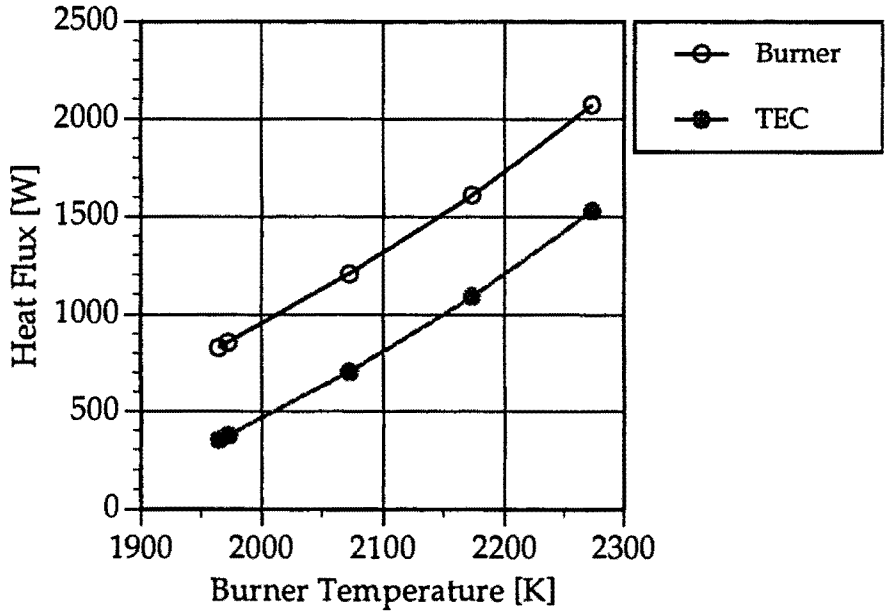

Figure 4.14 The calculated heat flux of the burner and TEC as function of the burner temperature.

In the course of this report, it is emphasized that the emissivity of the burner is not known exactly. Therefore figure 4.15 is constructed. It shows the variation of the heat fluxes of the burner and the TEC versus the emissivity of the burner. The burner temperature is 1965 K, the TEC temperature 1723 K.

The heat flux depends strongly on the emissivity. The heat flux received by the TEC varies 150 Watts for the change in emissivity from 0.6 to 0.8. This is another argument to measure the total emissivity of the foam in the future.

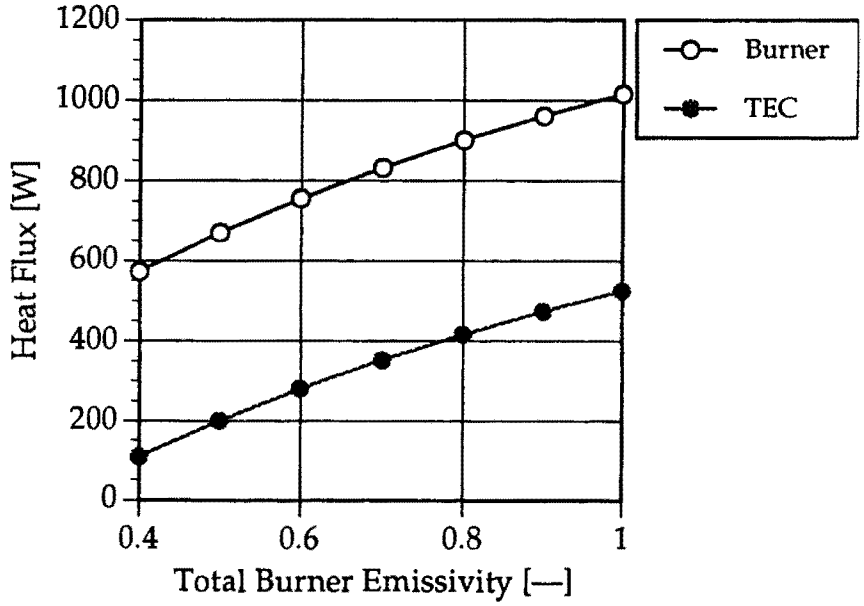

Figure 4.15 The calculated heat flux of the burner and TEC as function of the burner emissivity.

Figure 4.16 shows the two heat fluxes as function of the emissivity of the insulation. It is clear that the emissivity of the insulation material has a small influence on the heat balance of the furnace. Thus the heat balance of the insulation is ruled by the conductive loss.

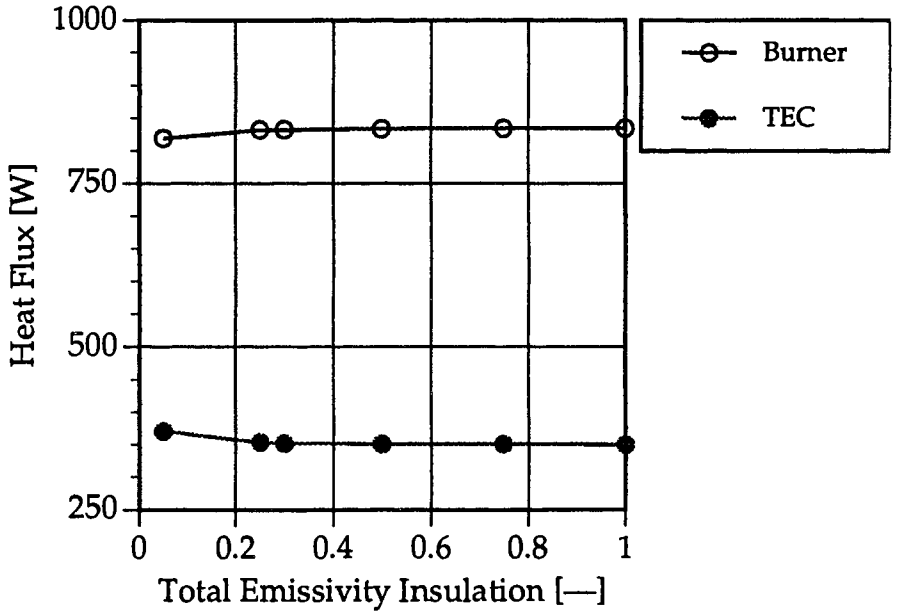

Figure 4.16 The calculated heat flux of the burner and TEC as function of the insulation emissivity.

5 Concluding Discussion

The thermionic energy converter imposes large demands on its heat-source: the heat-source has to deliver a heat flux of 1500 W at an emitter temperature of 1723 K. The heat-source has to be a burner fuelled by natural gas. The TEC and burner will form a complete unit, which can be used for heating of (green)houses and other purposes.

In the design process the concept of a porous radiant burner is chosen. By evaluation of a furnace, it is found that the radiative body of the burner has to reach a temperature of 2273 K to heat the TEC in combination with a well insulated furnace. This implies that the combustion temperature has to be higher, which is not possible using natural gas with air (293 K): the adiabatic flame temperature is 2293 K [Gasunie, 1988]. To increase the combustion temperature two solutions are discussed. The first is preheating, which can lead to temperatures up to 2873 K. The second is enriching the combustion air with oxygen with a maximum temperature of 3053 K for pure oxygen [Gaydon&Wolfhard, 1979]. In the final commercial design, preheating must be used because the use of oxygen is too expensive in a home situation.

Based on these findings, a pilot burner was designed and built. The burner is fuelled by natural gas and the possibility to enrich the combustion air with oxygen is provided. Enrichment is chosen, because preheating is too complex for a laboratory burner testing the TEC. Preheating the combustion air introduces additional problems like an efficient heat exchanger and separate supply of hot combustion air and gas. So to start this study enrichment is chosen because it is easier to implement and control. Unfortunately no serious experiments are carried out with oxygen enrichment due to insufficient time.

The burner itself is built modularly. The most important module is the burner-head. The head consists of a sieveplate and a cellular ceramic foam. The whole construction is insulated by a ceramic blanket. Over the burner-head a simple furnace can be placed to diminish losses to the surroundings. The function of the sieveplate is to stabilize the combustion by a velocity step and by insulating the gas mixture upstream from the combustion. When the burner radiates freely to the surroundings, this is sufficient. When the furnace is placed over the burner, this proves to be insufficient. More heat is transported upstream, because the burner can not lose its heat downstream as easily, when there is no furnace placed over the burner. The sieveplate becomes too hot, and flash-back occurs. A watercooling is placed underneath the sieveplate, preventing flash-back.

The performance of the burner is monitored experimentally to evaluate the design and materials. The other function of the experiments was to find trends towards an optimum design. The optimum is stated as the highest temperature on the top of the foam (so-called burner temperature) with

equal heat-load and power. Using the same material, the temperature must be as low as possible, while heating the TEC. The demands on the material are very severe. Thus the material is the bottle-neck, when the burner is commercialized. A more efficient heat-transfer set-up lowers the demand on the material. Tuning parameters for the foam are its porosity, thickness, emissivity and number of pores. Tuning parameters for the sieveplate are the number of channels, speed in the channels, heat-conductivity, and the thickness.

The sieveplate works satisfactory for foams thicker than 25 mm. But for the thin foams (10 mm) the velocity step is too large. The flow does not break up in the foam. The holes of the sieveplate are visible and at full burner power the flame blows off. To straighten out the radiation pattern more holes can be used.

Several materials were used for the sieveplate. The best appears to be zirconia board. But the board broke due to densification and shrinking. After dismantling the burner-head, it could not be reused. Also a dense ceramic was used: boronnitride. It performed very well for burner temperatures below 1773 K, and did not break even after several cycles. But it corroded heavily when the burner temperature was increased to 1873 — 1923 K. Eighty percent of the boronnitride was burned away.

Thus for the sieveplate better materials must be found, possible alternatives are zirconia and alumina. These materials can withstand the conditions in the flame-zone, which stabilizes on top of the sieveplate. The advantage of zirconia is its ability to withstand thermal shock. Alumina is less thermal shock resistant. Both materials must be tested in dense and in board form. The main advantage of board is that it is easily machinable. To make holes in dense zirconia and alumina is not easy. Further cracks are induced due to machining, making dense material less resistant to thermal cycling.

The other important module of the burner is the foam. It is heated by the flue gasses and loses heat through radiation to the load, in this case the surroundings or the furnace. In a later stage the load will be the TEC. The foam is characterized by the material, its porosity and its dimensions. The material used is partially stabilized zirconia by magnesia. Chemically and physically it is able to withstand temperatures up to 2873 K. Mechanically it is expected to fail due to thermal shock. During the experiments cracks were formed in the struts of the foam, but the design did allow this. The ceramic paper wound around the foam kept the foam together and the global structure remained intact. Chemical corrosion was not observed.

The diameter of the foam equals the TEC diameter (75 mm). The height of a standard foam is 25 mm. The foams are tested in two porosities of 10 and 20 pores per linear inch (ppi). The first experiments showed that the 20 ppi foam reaches the highest temperature. The reason is probably the higher heat exchanging area and the denser radiation surface. In further experiments the height of the foam was varied: 10, 25 and 50 mm. The thinnest foam reached the highest temperature (1965 K at an input power of 9.5 kW). It is also shown that the burner temperature follows the adiabatic flame temperature very well when the airfactor is varied.

Thus the following trends for the foam are shown: a 20 ppi foam seems to become hotter than a 10 ppi foam and the thinner the foam, the hotter it gets. It is expected that somewhere a maximum will be found for both trends. Also other parameters become important in the optimalisation of the total design, like for instance the pressure drop over the foam.

Based on the experiments, an estimation is made of the performance of the burner in combination with the TEC. When the TEC will be mounted in the test-rig, it will receive 0.35 kW with a burner temperature of 1965 K. The design-point of 1.5 kW for the TEC will be reached, when the burner achieves the temperature of 2273 K. This burner temperature must be achieved by enrichment of the combustion air with oxygen.

6 Recommendations

This study reports the experimental route followed to gain some insight in the optimum design of a radiant burner. This route must be followed further. New choices for materials must be tried. For the sieveplate all materials failed one way or another, when the sieveplate was used for several hours.

The same applies to the foam material; it is necessary to follow the market to see if new alternatives are being developed. Another point is the form of the cellular ceramic. The foam used here was just a starting point. As discussed, a tunnel is expected to provide better heat transfer to the TEC.

A very important property of the foam is its total emissivity. The total emissivity has a large influence on the heat transfer characteristics of the foam. During this investigation, it is argued that the emissivity of a foam is not well known. For the calculations, some guessed estimate was used. Therefore, it is important that the total emissivity of a foam is measured. The emissivity has to be measured as function of the foam temperature and as function of the number of pores per linear inch (ppi).

The proposed experiments with oxygen enrichment have to be carried out, to verify wether a higher combustion temperature will lead to higher burner temperatures. A gas-oxygen flame radiates less than a gas-air flame, so the results of these experiments depend on the importance of radiation in the heat transfer from gas to solid. To perform these experiments, the sieveplate has to be redesigned. In tentative experiments with oxygen, flash-back occurred regularly. Thus the velocity in the channels of the sieveplate must be higher. This is easily done by adjusting the diameter of the channels in the sieveplate. Also the diameter of the holes in the top and bottom plate of the watercooling must be adjusted. When the same number of channels is used, a plate with smaller holes in the same arrangement can be bolted on top of the watercooling.

Uptil now the burner is only loaded by its surroundings. A next step is to test the burner, while it is loaded with a real heat-sink, preferably the TEC. Otherwise a controlled heat-sink has to be developed. Such heat-sink could consist of a ceramic cylinder or a metal cylinder with on top a thermal barrier coating. At the bottom the cylinder would be cooled by water, designed to cool 1500 Watt while the top gets a temperature of 1723 K. By measuring the temperature difference over the length of the cylinder the heat flow can be estimated. Figure 6.1 gives an impression of this concept.

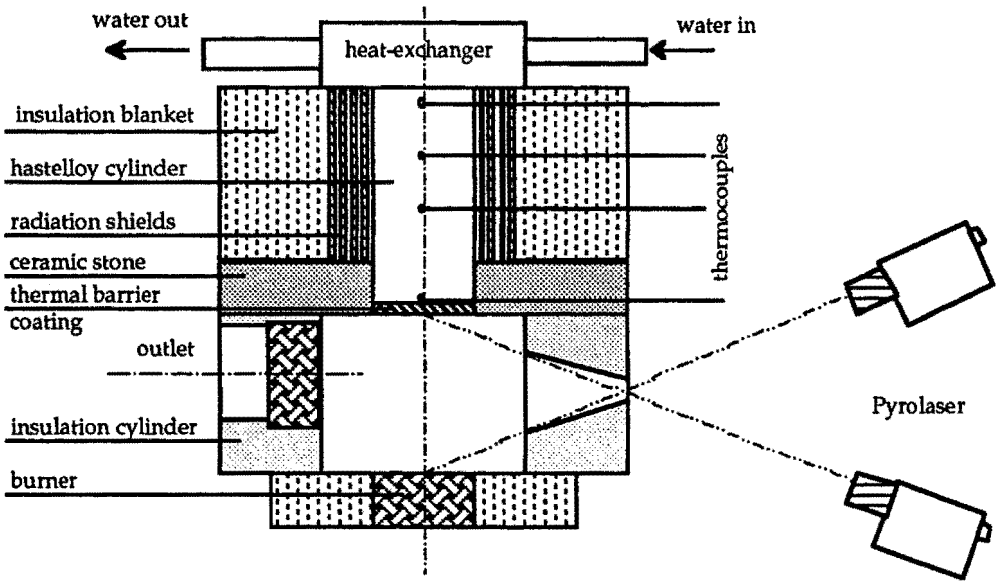

Figure 6.1 Concept of an adjustable heat-sink.

Contrary to the laboratory test-rig enrichment of the combustion air with oxygen is not feasible for a commercial burner-TEC combination. Therefore the air has to be preheated to increase the combustion temperature. In the current test-rig a stainless steel heat exchanger can be placed in the chimney. There the flue gasses heat the combustion air. A problem is that the preheated air can not be mixed with the natural gas before the burner-head. Otherwise it will ignite spontaneously, when the mixture temperature is higher than 903 K. Some system has to be designed to inject the gas in the air, for example a double sieveplate. The first delivers the air. Its holes are smaller than the second sieveplate. In the sieveplate stainless steel injection tubes are mounted for the gas. The foam is placed on top of the second plate (see figure 6.2).

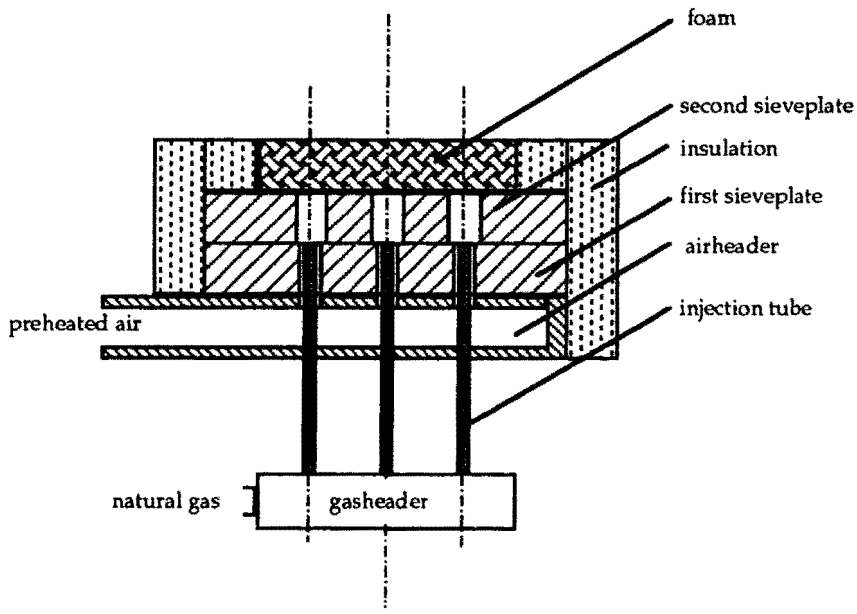

Figure 6.2 Cross-section for a burner-concept using preheated air and gas injection.

As discussed earlier, the design of the foam and of the sieveplate must be optimized. While this report mainly discusses experimental/empirical methods, numerical modelling will also provide useful information. A one-dimensional heterogeneous model can be formulated, for example along the lines of those by Sathe et.al. [1990, 1991]. Using such model the porosities of the sieveplate and the foam can be optimized, thus balancing the velocities. Further the influence of thickness, being a measure for the heat-exchanging area, can be evaluated.

The heat transfer properties of cellular ceramics are a tricky problem in modelling a cellular ceramic material (ccm). Two recent studies on the convective heat transfer within a ccm [Youis & Viskanta, 1993] and another on the thermal conductivity and optical properties [Hsu & Howell, 1992] provide data that can model and predict the performance of the burner. For the boundary conditions, the burner model can be coupled to the Gebhart zone model. To evaluate the whole system, the model of the TEC by Veltkamp & van Kemenade [1993] can be coupled to the zone model.

During this study no attention has yet been paid to environmental effects. First the emissions of NO_x and CO simply have to be measured. If these are too high, methods must be found to lower the emissions. A possible solution could be two-stage combustion.

Literature

Baustian U., Matthews E.K., Improved Infrared Temperature Measurement by Utilization of Laser Technology, Proc. 8th International Congress on Optoeletronics in Engineering, 1987.

Boch P., Thermal Shock Properties of Ceramics, In: Fracture of Non-Mettallic Materials, pp. 117-135, editors: Herrmann K.P., Larsson L.H., ISPRA Courses on Materials, Engineering and Mechanical Science, D. Reidel Publishing Company, Brussels, 1987.

Bramson M.A., Optical Physics and Engineering Infrared Radiation, a Handbook for Applications, Plenum Press, 1968.

Brooks D.L., Winter E.M., Material Selection of Cellular Ceramics for a High Temperature Furnace, Fossil Fuel Combustion Symposium 1990, 13th Annual Energy-Sources Technology Conference , ASME PD vol. 30, pp. 117-125, 1990.

Chen D.C.C., McGrath I.A., Convective Heat Transfer in Chemically Reacting Systems, J. of the Inst. of Fuel, pp. 12-18, January 1969.

Coles K.F., Grimm W., Design and Operation of new Radiation and Tunnel Burners and their Application to Furnaces (in german), In: Gas-Wärme International, Vol. 24, pp. 512-526, 1975.

de Goey L.P.H., Combustion Science (in dutch), report WOC.WF 90.002, Eindhoven University of Technology, 1990.

de With G., Lecture Notes on Ceramics, Eindhoven University of Technology, 1991.

de With G., Personal Communication, Philips Research & Department of Chemical Engineering, Eindhoven University of Technology, February 12, 1993.

Echigo R., Effective Energy Conservation Method Between Gas and Thermal Radiation and Application to Industrial Furnace, In: Proc. of the 7th International Heat Transfer Conference, Munich, vol. VI, pp. 361-366, 1982.

Feijen J.J., Introduction to Heat Engineering (in dutch), 2nd. ed., B.V. Uitgeverij Nijgh & Van Ditmar, The Hague, 1987.

Gasunie N.V., Physical Properties of Natural Gasses (in dutch), Groningen, 1980.

Gasunie N.V., Physical Properties of Natural Gasses, Groningen, 1988.

Gaydon A.G., Wolfhard H.G., Flames their Structure, Radiation and Temperature, Chapman and Hall, London, 1979.

Gelten M.P.W., Temperature Measurements with the Pyrolaser - Analysis of the Problems- (in dutch), report WOC-WET 93.015, Eindhoven University of Technology, 1993.

God C., Ebner-Brunner F., Testing a Recuperator Burner for Use in Gas-Fired Reheating and Heat-Treating Furnaces (in german), In: Gas-Wärme International, Vol. 33, No. 2/3, pp. 66-76, 1984.

Golombok M., Shirvill L.C., Emissivity of Layered Fibrous Materials, In: Applied Optics, Vol. 27, No. 18, 1988.

Harbeck W., Holze D., Kühne W., Seddig M., Radiation Burner STB - on the Development of a Series with high Usage Specifications (in german), In: Energietechnik, Vol. 35, No. 5, May 1985.

Hinze J.O., Turbulence; an Introduction to its Mechanism and Theory, McGraw-Hill Book Company, New York, 1959.

Hsu P., Howell J.R., Measurements of Thermal Conductivity and Optical Properties of Porous Partially Stabilized Zirconia, In: Experimental Heat Transfer, vol. 5, pp. 293-313, 1992.

Kreith F., Bohn M.S., Principles of Heat Transfer, 4th. ed., Harper & Row Publishers, New York, 1986.

Levinson R.E., Oxy- Gas Combustion System Developed for High Temperature Applications, In: Industrial Heating, November 1986.

Leybold-Heraeus GmbH, Manual for Ratiopyrometer QP 31, Colour Pyrometer for Measurement of Temperatures between 1000 °C and 3000 °C, Hanau, Germany.

Marmer E.N., Gurvich O.S., Maltseva L.F., High Temperature Materials, Freund Publishing House, Holon, Israel, 1971.

McGee T.D., Principles and Methods of Temperature Measurement, John Wiley & Sons, New York, 1988.

Mikron Instrument Company Inc., Table of Emissivity of Various Surfaces for Infrared Thermometry, New Jersey.

Moonen E.J., Theoretical and Experimental Research on a Radiant Ceramic Burner for High Temperature Applications, report WOC-WET 93.003, Eindhoven University of Technology, 1993.

Morganite Thermal Ceramics Ltd., Refractory Mouldings and Castings, Data sheet ZAL/ZAM Zirconia, Derby, England, 1992.

Nicholson R., Recuperative and Regenerative Techniques at High Temperature, In: Heat Recovery Systems, Vol. 3, No. 5, pp. 385-404, 1983.

Pritchard R., Guy J.J., Connor N.E., Industrial Gas Utilization, Engineering Principles and Practice, Bowker Publishing Company Limited, Epping, Essex, pp. 282-284, 1977.

Richerson D.W., Modern Ceramic Engineering: Properties, Processing and Use in Design, 2nd revised and expanded ed., Marcel Dekker Inc., New York, 1992.

Rhine J.M., Tucker R.J., Modelling of Gas-Fired Furnaces and Boilers, and Other Industrial Heating Processes, McGraw-Hill Book Company, New York, 1991.

Sathe S.B., Peck R.E., Tong T.W., A Numerical Analysis of Heat Transfer and Combustion in Porous Radiant Burners, In: Int. J. Heat Mass Transfer, Vol. 33, No. 6, pp 1331-1338, 1990a.

Sathe S.B., Peck R.E., Tong T.W., Flame Stabilization and Multimode Heat Transfer in Inert Porous Media: A Numerical Study, In: Combust. Sci. and Tech., Vol. 70, pp 93-109, 1990b.

Sathe S.B., Tong T.W., Heat Transfer Characteristics of Porous Radiant Burners, In: Transactions of the ASME, J. of Heat Transfer, Vol. 113, pp 423-428, 1991.

Schmid K., Research on a System of a Chamber Furnace and Gas Burners with Integrated Burner Head Cooling and Air Preheating to Produce High Temperature Gas with a Large Temperature Range (in german), Dissertation Technischen Hochschule Aachen, 1980.

Siegel R., Howell J.R., Thermal Radiation Heat Transfer, 2nd ed., Hemisphere Publishing Corporation, New York, 1982.

Seuren J.A.T., Designstudy for a Gas-Fired High-Temperature Test Furnace (in dutch), report WOC-WET 91.004, Eindhoven University of Technology, 1991.

Smeets M.C.M., Heat Technical Study of a 5 MW Blow Down Installation (in dutch), report EG/80/282, Department of Electrotechnical Engineering, Eindhoven University of Technology, 1980.

Veltkamp W.B., van Kemenade H.P., Combustion Heated Thermionic Systems, Short Course Thermionic Energy Conversion II Conference, Göteborg, may 3-4, 1993.

Verein Deutscher Ingenieure, VDI Wärmeatlas, VDI Verlag, Düsseldorf, 1988.

Webb R.J., Developments in Recuperative and Regenerative Burners for Use in High Temperature Furnaces, Recovery and Utilization Symposium, Portsmouth, September. 25, 1985.

Youis L.B., Viskanta R., Experimental Determination of the Volumetric Heat Transfer Coefficient Between Stream of Air and Ceramic Foam, In; Int. J. Heat Mass Transfer, Vol. 36, No. 6, pp. 1425-1434, 1993.

A Calculation of the Adiabatic Flame Temperature

A simple way to calculate the adiabatic flame temperature is splitting the combustion in two stages. The first is the reaction. The reaction takes place at room-temperature and the heat liberated to form of water, carbondioxide and other products is determined. The second stage is to heat the flue gasses up to that temperature, whereas the enthalpy of the flue gasses equals the heat of reaction.

For hot flames this method is not accurate, it will predict far to high flame temperatures. These high temperatures are not actually attained, due to the dissociation of the flue gasses. This dissociation uses much energy and limits the flame temperature.

To account for dissociation, a scheme proposed by Gaydon & Wolfhard [1979] is used to calculate the flame temperature. Their model incorporates the following assumptions:

- — the flame is at constant pressure,
- — the calculated flame temperature is attained only if there is no heat loss,
- — in the flue gasses equilibrium is assumed,
- — at very high flame temperatures, the method will not be correct because additional dissociation of the flue gasses is not taken into account.

A simplification is the use of methane instead of natural gas to calculate the adiabatic flame temperatures. The composition of dutch natural gas is 81.21 %(mol) methane, 3.5 %(mol) other organic gasses, and 14.32 %(mol) N_2. The exact influence of this assumption can not be estimated because of two contrary effects: the extra combustion heat due to the higher organic fuels and on the other hand the additional nitrogen has to be heated.

The first step in the iterative scheme is to calculate the composition of the flame gasses for an estimated flame temperature. The dissociation equilibria considered are in case of a mixture containing carbon, oxygen, hydrogen and nitrogen:

$$CO_2 \Leftrightarrow CO + 0.5\,O_2$$

$$H_2O \Leftrightarrow H_2 + 0.5\,O_2$$

$$H_2O \Leftrightarrow 0.5\,H_2 + OH$$

$$0.5\,H_2 \Leftrightarrow H$$

$$0.5\,O_2 \Leftrightarrow O$$

$$0.5\,N_2 + 0.5\,O_2 \Leftrightarrow NO$$

The equilibrium constants at the estimated flame temperature can be found in tables of thermochemical data. Using the equilibrium constants, the composition of the flue gasses is calculated. Therefore the iterative method of Damköhler & Edse is used. This method is explained in detail by Gaydon & Wolfhard [1979].

Now the composition for a given flame temperature is known. The next step is to check the energy balance. Heat is used to form free atoms and radicals. Heat is liberated by formation of stable molecules and by the decomposition of the fuel. The heat produced by the reaction is the net.

In case of preheating, the initial temperature of the gas mixture is not necessarily standard room temperature. Then the heat of reaction has to be corrected using Kirchhoff's law [Gaydon & Wolfhard, 1979]:

$$H_{preheat}=H_{room\ temperature}+\int_{T_{room}}^{T_{preheat}}(c_{p,unburnt\ gases}-c_{p,flue\ gasses})dT \qquad (a.1)$$

where H is the reaction heat produced, evaluated at respectively preheat and room temperature, and c_p is the specific heat of the unburnt mixture respectively the flue gasses.

Finally the net produced heat is compared to the energy content of the flue gasses at the flame temperature. When for example the net produced heat is higher than the energy content of the flue gasses to the estimated temperature, the whole procedure has to be repeated with a higher estimation for the flame temperature. This iteration has to be carried on till the heat balance is satisfied.

B Heat Transfer by Normal Impinging Jets

A jet is often used to augment heat transfer from a fluid to a surface. A sketch is given in figure 2.3. The basic heat transfer mode is convection. For practical calculations correlations for the radial Nusselt number are presented in literature [Rhine & Tucker, 1991], like

$$\frac{Nu}{Pr^{0.42}} = \frac{D}{r}\frac{1 - 1.1\,D/r}{1 + 0.1\,(z/D - 6)\,D/r} f(Re)$$

$$\text{where } f(Re) = 2\,Re^{0.5}\sqrt{(1 + Re^{0.55}/200)}$$

$$\text{and } Nu = \frac{2}{r^2}\int_0^r Nu\,(\rho)\;d\rho \qquad \text{(b.1)}$$

This correlation is valid for $2000 \le Re \le 400000$, $2.5 \le r/D \le 7.5$ and $2 \le z/D \le 12$. D is the jet diameter and r the radial distance from the jet centre line. The Nusselt, Prandtl and Reynolds numbers are based on the conditions at the mouth of the jet. The characteristic dimension is the jet diameter D.

The heat transfer of a jet to the TEC can be estimated using the following expression:

$$Q = h\,A_{TEC}\,(T_{jet} - T_{TEC}) \qquad \text{(b.2)}$$

The following relation can be found using the definitions of the Nusselt, Prandtl and Reynolds numbers and by substituting relation (b.1) into (b.2):

$$0 = 2\frac{(T_{jet} - T_{TEC})\,A_{TEC}\,Pr^{0.42}\,k_{gas}\left(-1.1\frac{D}{r} + 1\right)\left(\frac{1}{200}\left[\frac{Du\,\rho}{\mu}\right]^{0.55} + 1\right)^{0.5}\left(\frac{Du\,\rho}{\mu}\right)^{0.5}}{-0.6D + r + 0.1z} - Q \qquad \text{(b.3)}$$

This relation can be solved for the jet velocity u and jet temperature T_{jet}. For the temperature-dependent properties of the gas the reader is referred to appendix D.

However for burners placed on a small distance of the surface dissociative effects (mass transfer) can augment the heat transfer. The different radicals in the combustion gasses (see appendix A) recombine on the surface thus liberating their formation enthalpy. According to Chen & McGrath [1969] this process can augment the heat transfer coefficient h by 100 % or even more.

C Radiant Heat Exchange in a Cylindrical Furnace

C.1 Viewfactors

In this section the viewfactors for a cylindrical furnace (figure C.1) are summarized. The viewfactors are derived from the standard cases of parallel, directly opposed plane ring areas [example 7-10, Siegel & Howell, 1982] and two parallel circular disks with centres along the same normal [Appendix C, case 21, Siegel & Howell, 1982].

From these basic cases the other viewfactors can be computed using the following three relations. The first relation is that of subdivision of a surface. A surface area i exchanges energy with a surface area j. The surface j is divided for example in two areas k and l. The viewfactor F_{i-j} can be divided as follows:

$$F_{i-j} = F_{i-(k+l)} = F_{i-k} + F_{i-l} \tag{c.1}$$

The second is the reciprocity relation:

$$F_{j-i} = \frac{A_i}{A_j} F_{i-j} \tag{c.2}$$

The third is valid for enclosures only. In a black enclosure, all the fractions of energy leaving one surface and reaching the surfaces of the enclosure must total to unity, thus for each plane k:

$$\sum_{j=1}^{N} F_{k-j} = 1 \tag{c.3}$$

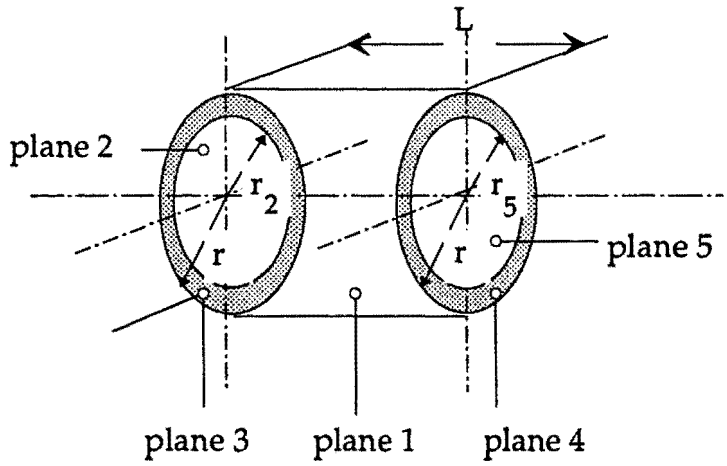

Figure C.1 The furnace divided in five zones: burner (2), TEC (5) and insulation (1,3,4).

The required viewfactors in this system are (the others can be derived through relation (c.2):

$$F_{1\text{-}1} = \frac{1}{2}\frac{L}{r} - \frac{1}{2}\sqrt{\frac{L^2}{r^2} + 4} + 1 \qquad \text{(c.4)}$$

$$F_{1\text{-}2} = \frac{1}{4}\frac{\sqrt{(L^2 + r^2)^2 + r_2^2(r_2^2 + 2L^2 - 2r^2)} - L^2 - r^2 + r_2^2}{Lr} \qquad \text{(c.5)}$$

$$F_{1\text{-}3} = \frac{1}{4}\frac{-\sqrt{(L^2 + r^2)^2 + r_2^2(r_2^2 + 2L^2 - 2r^2)} + L\sqrt{L^2 + 4r^2} + r^2 - r_2^2}{Lr} \qquad \text{(c.6)}$$

$$F_{1\text{-}4} = \frac{1}{4}\frac{-\sqrt{(L^2 + r^2)^2 + r_5^2(r_5^2 + 2L^2 - 2r^2)} + L\sqrt{L^2 + 4r^2} + r^2 - r_5^2}{Lr} \qquad \text{(c.7)}$$

$$F_{1\text{-}5} = \frac{1}{4}\frac{\sqrt{(L^2 + r^2)^2 + r_5^2(r_5^2 + 2L^2 - 2r^2)} - L^2 - r^2 + r_5^2}{Lr} \qquad \text{(c.8)}$$

$$F_{2\text{-}2} = 0 \qquad \text{(c.9)}$$

$$F_{2\text{-}3} = 0 \qquad \text{(c.10)}$$

$$F_{2\text{-}4} = \frac{1}{2r\frac{2}{2}}\left(-\sqrt{(L^2 + r^2)^2 + (2L^2 - 2r^2 + r_2^2)r_2^2}\right.$$
$$\left. + \sqrt{(L^2 + r_2^2)^2 + (2L^2 - 2r_2^2 + r_5^2)r_5^2} + r^2 - r_5^2\right) \qquad \text{(c.11)}$$

$$F_{2\text{-}5} = \frac{-\sqrt{\left(L^2 + r_2^2\right)^2 + r_5^2\left(r_5^2 + 2L^2 - 2r_2^2\right)} + L^2 + r_5^2}{2r_2^2} + \frac{1}{2} \tag{c.12}$$

$$F_{3\text{-}3} = 0 \tag{c.14}$$

$$F_{3\text{-}4} = \frac{1}{2(r^2 - r_2^2)}\left(\sqrt{\left(L^2 + r^2\right)^2 + r_2^2\left(r_2^2 + 2L^2 - 2r^2\right)} + \sqrt{\left(L^2 + r^2\right)^2 + r_5^2\left(r_5^2 + 2L^2 - 2r^2\right)} - \sqrt{\left(L^2 + r_2^2\right)^2 + r_5^2\left(r_5^2 + 2L^2 - 2r_2^2\right)} - L\sqrt{L^2 + 4r^2}\right) \tag{c.15}$$

$$F_{3\text{-}5} = \frac{1}{2} + \frac{1}{2(r^2 - r_2^2)}\left(-\sqrt{\left(L^2 + r^2\right)^2 + r_5^2\left(r_5^2 + 2L^2 - 2r^2\right)} + \sqrt{\left(L^2 + r_2^2\right)^2 + r_5^2\left(r_5^2 + 2L^2 - 2r_2^2\right)}\right) \tag{c.16}$$

$$F_{4\text{-}4} = 0 \tag{c.17}$$

$$F_{4\text{-}5} = 0 \tag{c.18}$$

$$F_{5\text{-}5} = 0 \tag{c.19}$$

I hope that above equations do not contain any type-errors. Hence I advise the reader to perform the check according to equation (c.3), as I did myself in the computations.

C.2 Gebhart's Zone Method

Gebhart's zone method [Siegel & Howell, 1982] provides a method to solve radiative heat exchange in an enclosure. The method calculates coefficients that provide the fraction of energy emitted by a surface that is absorbed at another surface after reaching the absorbing surface by all possible paths. In developing the scheme, an enclosure having N diffuse gray surfaces is considered. Over each of these areas the following restrictions are met:

- The temperature is uniform.
- The emissivity, absorptivity and reflectivity are independent of wavelength and direction.
- All energy is emitted and reflected diffusively.
- The incident and hence reflected energy flux is uniform over each individual area.

For a typical surface A_k the net energy loss is the emission from the surface minus the energy that is absorbed by the surface from all incident sources. We define G_{jk} as the fraction of the emission from surface A_j that reaches A_k and is absorbed. Then a heat balance on A_k gives:

$$\begin{aligned} Q_k &= A_k\varepsilon_k\sigma T_k^4 - (A_1\varepsilon_1\sigma T_1^4 G_{1k} + \ldots + A_j\varepsilon_j\sigma T_j^4 G_{jk} + \ldots + A_N\varepsilon_N\sigma T_N^4 G_{Nk}) \\ &= A_k\varepsilon_k\sigma T_k^4 - \sum_{j=1}^{N} A_j\varepsilon_j\sigma T_j^4 G_{jk} \end{aligned} \qquad \text{(c.20)}$$

This relation can be written for each surface. Q_k is the energy supplied to the surface by other mechanisms than radiation. For the quantity G_{jk} the following set of N relations for an area A_k is obtained:

$$\begin{aligned} G_{1k} &= F_{1\text{-}k}\varepsilon_k + F_{1\text{-}1}\rho_1 G_{1k} + \ldots + F_{1\text{-}k}\rho_k G_{kk} + \ldots + F_{1\text{-}N}\rho_N G_{Nk} \\ G_{2k} &= F_{2\text{-}k}\varepsilon_k + F_{2\text{-}1}\rho_1 G_{1k} + \ldots + F_{2\text{-}k}\rho_k G_{kk} + \ldots + F_{2\text{-}N}\rho_N G_{Nk} \\ &\ldots\ldots\ldots\ldots\ldots\ldots\ldots\ldots\ldots\ldots\ldots\ldots\ldots\ldots\ldots\ldots \\ G_{Nk} &= F_{N\text{-}k}\varepsilon_k + F_{N\text{-}1}\rho_1 G_{1k} + \ldots + F_{N\text{-}k}\rho_k G_{kk} + \ldots + F_{N\text{-}N}\rho_N G_{Nk} \end{aligned} \qquad \text{(c.21)}$$

To solve the set (c.21) the black-body viewfactors $F_{j\text{-}k}$ have to be known. By solving this set the G-factors for each area are calculated. They can be related to the area-temperatures by substitution of the G-factors in equation (c.20).

C.3 Algorithm to Solve the Radiant Heat Exchange in the Furnace

The program first solves the radiation within the enclosure. It calculates the temperatures of the insulating zones, the temperature of the burner and the power to be delivered by the burner. Using the inner temperatures the casing temperatures are calculated for the different zones. This gives the heat fluxes through the insulation zones.

When the insulation losses remain constant, a second iteration is entered. The emissivity of the burner is not constant but dependent on temperature. A new emissivity for the burner is calculated based on the burner temperature resulting from the previous iteration. Then the iteration over the heat losses is carried out again. This process continues until the emissivity of the burner remains constant and the actual solution is achieved.

In the resulting Pascal-program based on Gebhart's method, two additional iterations must be implemented. As said the temperatures of the five areas (figure 2.6) are solved using equations (c.20) and (c.21). Then the heat loss by conduction through the insulation is solved. To calculate the heat loss a heat balance is made over the insulation. Using the heat balance the casing temperature is calculated, which in return can be used to calculate the heat flux. For the two rings around the TEC and around the burner the heat-balance yields [VDI, 1988];

$$\frac{A\,(T_{in}-T_{casing})}{\sum_{i=1}^{n}\frac{\delta_i}{k_i}} = h\,A\,(T_{casing}-T_{surr}) + \sigma\,\varepsilon_{casing}\,A\,(T^4_{casing}-T^4_{surr}) \qquad (c.22)$$

A is the surface of the ring, δ the thickness of each insulation layer (see figure 2.5). The left-hand term represents conduction through a total of n insulation layers. The right-hand term presents the heat transfer from the casing to the surroundings.
For the cylindrical body the left-hand term is replaced by:

$$\frac{2\pi L\,(T_{in}-T_{casing})}{\sum_{i=1}^{n}\frac{1}{k_i}\ln\left(\frac{r_{i+1}}{r_i}\right)} \qquad (c.22a)$$

here is L the length of the furnace, A the outer area of the casing and r_i the radii of the insulation-layers. The inner temperature T_{in} is known from the Gebhart-routine. So by means of a simple rootfinder the casing temperature can be calculated. The flux is found by calculating only the right-hand or left-hand term of equation (c.22).

The emissivity of the casing is 0.95 for paint [VDI, 1988]. The heat transfer coefficient is found by means of a diagram correlating the conditions of the surroundings and the diameter of a pipe with the heat transfer coefficient [page Eb.3, Bild 4, VDI, 1988]. The value for h is 20 W m^{-2} K^{-1} for a slight wind and a diameter of 0.2 m.

The calculated fluxes are used to estimate the area-temperatures anew. This process is repeated till the temperature does not change anymore.

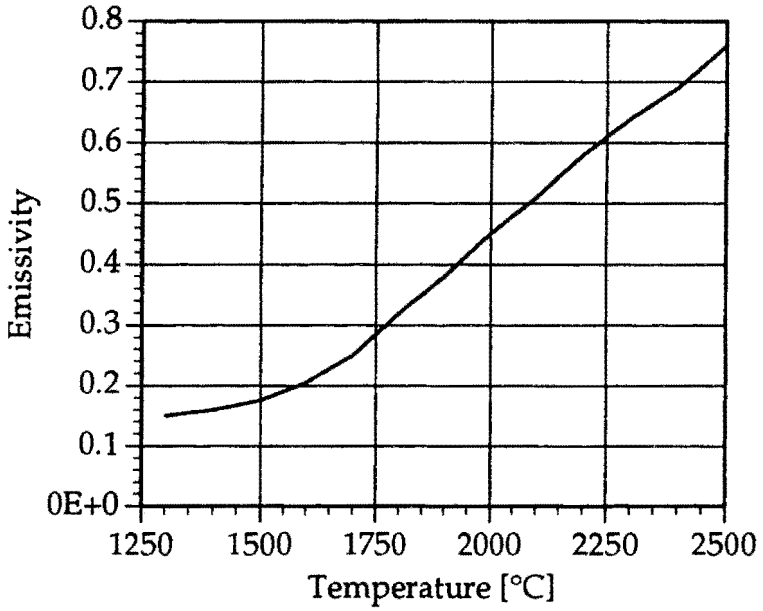

Figure C.2 Emissivity of dense zirconia [Bramson, 1968].

Now the second iterative process comes in action. As seen in figure C.2 the emissivity of the burner is dependent on temperature. This relation can be fitted by (valid between 1250 °C and 2700 °C (extrapolated)):

$$\varepsilon = -4.137529 \cdot 10^{-10} (T - 273.15)^3 + 2.565435 \cdot 10^{-6} (T - 273.15)^2 - 4.617840 \cdot 10^{-3} (T - 273.15) + 2.727008 \qquad \text{(c.23)}$$

T is the temperature in Kelvin. The estimated temperature of the burner is used to calculate a new emissivity. Using this new emissivity, the whole process of calculating the G-factors, temperatures and insulation losses is repeated. In the end this leads to a solution for which the temperatures will not change anymore. Figure (C.3) gives a flowchart of the described algorithm. The listing can be obtained from the author.

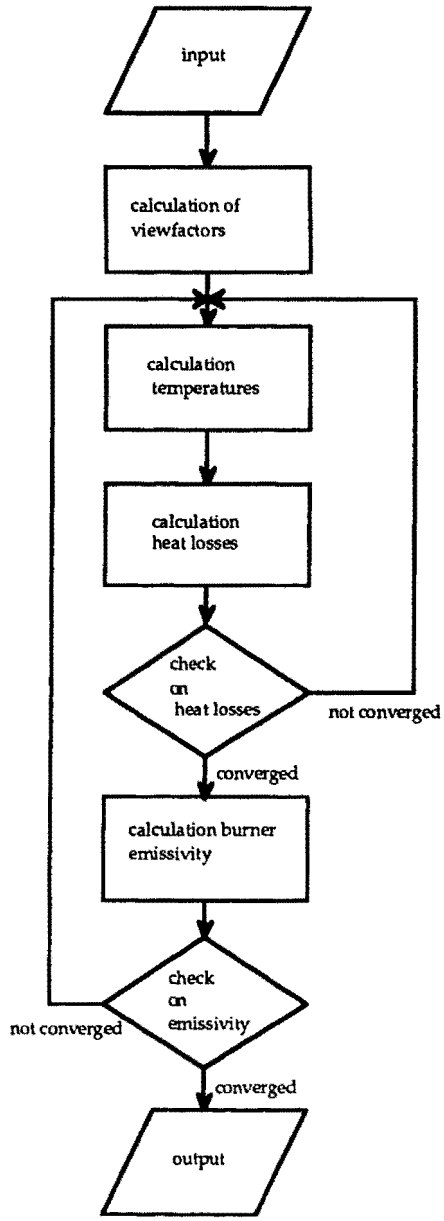

Figure C.3 Flow-chart of the algorithm to calculate the heat exchange in the furnace.

C.4 Heat Exchange between the TEC and Burner without a Furnace

The net radiative heat flux from the burner to the TEC is written as [Feijen, 1987]:

$$Q_{b\text{-}TEC} = \frac{A_b \sigma (T_b^4 - T_{TEC}^4)}{\left(\frac{1}{\varepsilon_b} - 1\right) + \frac{1}{F_{b\text{-}TEC}} + \frac{A_b}{A_{TEC}}\left(\frac{1}{\varepsilon_{TEC}} - 1\right)} \qquad \text{(c.24)}$$

The viewfactor $F_{b\text{-}TEC}$ is derived for two parallel circular disks with centres along the same normal [Siegel & Howell, 1982]:

$$F_{b\text{-}TEC} = \frac{1}{2}\left(-\sqrt{\left[\frac{\left(\frac{r_{TEC}}{L}\right)^2 + 1}{\left(\frac{r_b}{L}\right)^2} + 1\right]^2 - 4\left[\frac{r_{TEC}}{r_b}\right]^2} + \frac{\left[\frac{r_{TEC}}{L}\right]^2 + 1}{\left[\frac{r_b}{L}\right]^2} + 1\right) \qquad \text{(c.25)}$$

Where L denotes the distance between the burner and the TEC. When expression (c.25) and (c.23) are substituted in (c.24), a relation between the distance L and the required burner temperature T_b is found. This expression is not written down, because it becomes very bulky.

The unknown parameters left are the burner radius r_b, the TEC radius r_{TEC}, the TEC emissivity ε_{TEC}, the net power $Q_{b\text{-}TEC}$, and the TEC temperature T_{TEC}. When these parameters are defined, the relation between the required burner temperature and the distance can be solved. The result is shown in figure 2.8.

D Material Properties

D.1 Properties of Gasses

For the properties of gasses, two sources are used: Gasunie [1988] and Rhine & Tucker [1991]. The last two authors propose the following fits:

$$\Phi = a + b\,z + c\,z^2 + d\,z^3 + e\,z^4 + f\,z^5$$
where $z=(T-1400)/200$ T in K (d.1)

The coefficients are listed in the table below.

Coefficients	a	b	c	d	e	f
Air						
c_p [J kg^{-1} K^{-1}]	1206.0343	22.779916	-3.455606	0.426062	0.042889	-0.011736
μ [10^{-6} Pa s]	51.537354	4.858258	-0.106514	-.002914	-0.001630	0.000448
k [W m^{-1} K^{-1}]	0.089086	0.009956	-0.000250	-0.000003	0.000001	0.0
Pr	0.697492	0.001118	-0.000204	0.000023	0.000002	-0.000001
Stochiometric combustion products						
c_p [J kg^{-1} K^{-1}]	1401.6596	36.60067	-4.43026	0.316066	0.046715	-0.0099
μ [10^{-6} Pa s]	50.249626	4.731996	-0.12346	0.008790	-0.001328	0.000167
k [W m^{-1} K^{-1}]	0.099972	0.012950	-0.000153	-0.000016	0.0	0.0
Pr	0.704524	-0.006326	-0.000334	0.000137	0.000014	-0.000003

Table D.1 Polynomial coefficients for the properties of air and stochiometric natural gas combustion products over the temperature range 200-2400 K.

Table D.2 summarizes the composition of natural gas and presents some material properties.

Components	Vol%	Density (kg/m^{-3})
CH_4	81.3	0.717
C_2H_6	2.85	1.355
C_3H_8	0.37	2.011
C_4H_{10}	0.14	2.701
C_5H_{12}	0.04	3.454
C_6H_{14}	0.05	4.204
N_2	14.35	1.250
O_2	0.01	1.429
CO_2	0.89	1.977
Natural Gas	100	0.833

Table D.2 Composition of natural gas [Gasunie, 1988].

Other properties of natural gas:

H_s=35.096 MJ/m^3

H_i=31.669 MJ/m^3

Air requirement dry air 8.4303 m^3/m^3

Air requirement wet air 8.5280 m^3/m^3

D.2 Ceramics

The ceramics used are listed here with their properties and the resellers.

Ceramic Cellular Material ZAM Zirconia

Components	SiO_2 (0.4%), TiO_2 (0.2%), Fe_2O_3 (0.1%), Al_2O_3 (0.1%), CaO (0.1%), MgO (3.0%), ZrO_2 + HfO_2 (96.2%)
Max. service temp.	2873 K
Specific heat	550 — 810 J kg^{-1} K^{-1} (293 — 2273 K)
Density	4580 kg/m^3
Conductivity	0.8 — 1.8 W m^{-1} K^{-1} (293 — 2273 K)
Producer	Morganite Thermal Ceramics Ltd., Market Place, Kegworth, Derby DE7 2EF, England.
Reseller	Profiltra B.V., Meerpaalweg, 1332 BB Almere

Ceramic fibre paper ASH 1600 °C

Components	Al_2O_3 (92%), SiO_2 (7%)
Organic components	Binders 5 %
Shrink after 24 hr.	4 %
Melting temperature	2273 K
Density	200 kg/m^3
Thickness	1 mm
Conductivity	0.2 — 0.5 W m^{-1} K^{-1} (1073 — 1873 K)
Producer	Ash Fibre processors Ltd.
Reseller	Profiltra B.V., Meerpaalweg, 1332 BB Almere

Ceraboard 100

Components	SiO_2 (47%), Al_2O_3 (44%), Fe_2O_3 (1%), others
Shrink after 24 hr.	3 %
Massloss after 5 hrs.	5 %
Max. temperature	1533 K
Density	260 kg/m^3
Thickness	20 mm
Conductivity	0.05 — 0.2 W m^{-1} K^{-1} (473 — 1273 K)
Producer	Manvilee de France S.A., B.P. 240, 92504 Rueil-Malmaison Cedex, France
Reseller	Profiltra B.V., Meerpaalweg, 1332 BB Almere

Alumina board ZAL 45

Components	Al_2O_3 (85%), SiO_2 (15%)
Shrink after 1 hr.	3 %
Max. temperature	1923 K
Density	720 kg/m^3
Conductivity	0.15 — 0.45 W m^{-1} K^{-1} (523 K — 1923 K)
Producer	Zircar Products Inc., 110 North Main Street, Florida, New York 10921, USA.
Reseller	Gimex, Postbus 220, 4190 CE Geldermalsen.

Zirconia board ZYFB-3

Components	ZrO_2 (92%), Y_2O_3 (8%), SiO_2 (<0.3%)
Shrink after 1 hr.	1 %
Porosity	92 %
Max. temperature	2473 K
Density	480 kg/m^3
Conductivity	0.08 — 0.24 W m^{-1} K^{-1} (673 K — 1923 K)
Producer	Zircar Products Inc., 110 North Main Street, Florida, New York 10921, USA.
Reseller	Gimex, Postbus 220, 4190 CE Geldermalsen.

Fiberfrax Durablanket 1400

Components	Al_2O_3, SiO_2, ZrO_2: 99.75 % minimum, Na_2O, Fe_2O_3 (rest)
Shrink after 1 hr.	3 %
Classification temp.	1703 K
Melting point	2013 K
Density	128 kg/m^3
Conductivity	0.03 — 0.26 W m^{-1} K^{-1} (373 — 1273 K)
Specific heat	1130 J kg^{-1} K^{-1} at 1363 K
Thickness	12.7 mm
Producer	Carborundum Resistant Materials Ltd., Mill Lane, Rainford, St. Helens, Merseyside. WA11 8LP, England.
Reseller	Insulcon B.V., Postbus 134, 4650 AC Steenbergen.

Gun-Gum

Classification temp.	923 K
Drying time	12 hrs.
Producer	Holts Products Ltd., England.
Reseller	Car parts shops.

E Design Calculations for the Burner

E.1 The Sieveplate

The main function of the sieveplate is to stabilize the flame zone. In the sieveplate a number of holes are drilled. In these holes the velocity has to be much higher as the flame speed. The flame speed for a stochiometric natural gas with air mixture is 40 cm/s. The flame speed for a stochiometric natural gas with oxygen mixture is 6.5 m/s.
Two degrees of freedom are left for the designer: the number of holes and the diameter. At 5 kW the total flow through the burner is:

$$\phi_v = \frac{P}{H_i}(1 + \text{Air Requirement}) =$$
$$= \frac{5\ 10^3}{31.669\ 10^6}(1 + 8.4303) = 1.489\ 10^{-3}\ m^3/s \qquad \text{(e.1)}$$

The superficial velocity of the mixture in the burner-head is:

$$u_{superficial} = \frac{\phi_v}{\pi/4\ D_{foam}^2} = \frac{1.489\ 10^{-3}}{\pi/4\ 0.075^2} = 0.337\ m/s \qquad \text{(e.2)}$$

This gives a real velocity in the burner-head of:

$$u = \frac{u_{superficial}}{porosity} = \frac{0.337}{0.8} = 0.42\ m/s \qquad \text{(e.3)}$$

For the channels a speed of 15 m/s is chosen. This velocity is based on the numerical results of Sathe et.al. [1990a], who states that the flame speed can be 7 times the adiabatic flame speed. Thus;

$$n_{channel}\ \pi/4\ D_{channel}^2 = \frac{\phi_v}{u} = \frac{1.489\ 10^{-3}}{15} = 9.93\ 10^{-5}\ m^2 \qquad \text{(e.4)}$$

After some trials to make a lay-out for the channels 19 channels are chosen according to figure E.1. This leads to a channel diameter of 2.6 mm according to expression (e.3). The pattern is based on equal sided triangles. So all channels have the same distance to eachother.

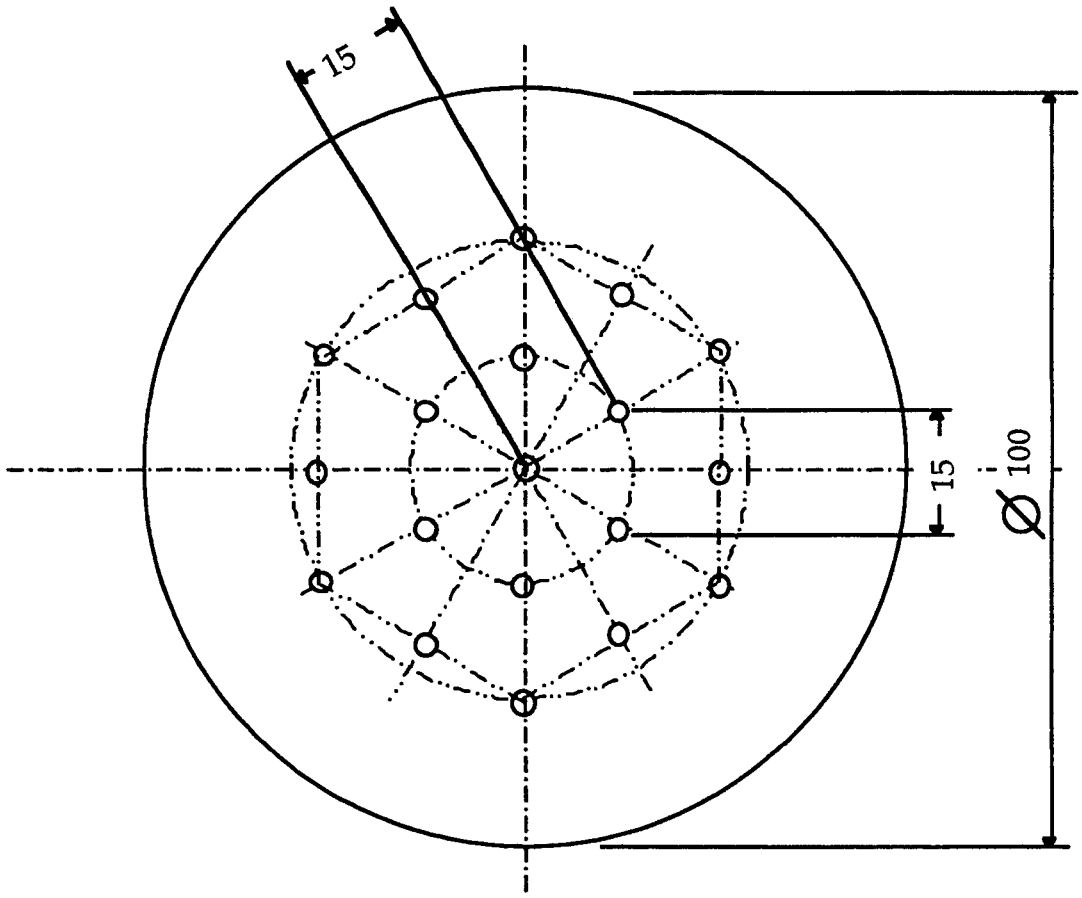

Figure E.1 The pattern of the channels in the sieveplate.

E.2 The Power of the Burner

The burner and furnace are considered as one system to estimate the radiant power to be supplied by the burner, The power supplied must compensate the heat-sinks. The heat-sinks of the furnace are: loss through the cylinder, loss through the foam in the chimney, loss through the sieveplate, and loss through the burner insulation. The influence of the hot flue gasses is not taken into account, they disappear to the surroundings. Because the velocity of the gasses is low in the furnace, their convective heat transfer will be low compared to radiation. Only for the foam in the chimney the gasses are taken into account. Other assumptions are that the heat conduction is mainly one-dimensional and that the effects of the window and thermocouples can be neglected. The dimensions of the furnace can be found in figure 3.9.

The first is insulation loss through the furnace. The inner temperature of the furnace is taken 2173 K, based on the calculations in chapter 2. The loss is estimated as [VDI, 1988]:

$$Q = \frac{2\pi L (T_{in} - T_{out})}{\frac{1}{k_{ZAL}} \ln\left(\frac{r_2}{r_1}\right) + \frac{1}{k_{durabl.}} \ln\left(\frac{r_3}{r_2}\right)} = \frac{2\pi 0.18 (2173 - 423)}{\frac{1}{0.35} \ln\left(\frac{0.095}{0.05}\right) + \frac{1}{0.15} \ln\left(\frac{0.1102}{0.095}\right)} = 700 \text{ [W]} \quad \text{(e.5)}$$

where r_1 is the inner and r_2 the outer radius of the ZAL cylinder, r_3 is the radius of the outside of the durablanket layer. T_{in} is the temperature of the inner furnace wall, T_{out} of the outer furnace wall.
The same expression applies to the loss through the radial insulation around the foam. The foam temperature is taken constant, equal to the demanded 2273 K:

$$Q = \frac{2\pi L (T_{foam} - T_{out})}{\frac{1}{k_{durabl.}} \ln\left(\frac{r_2}{r_1}\right)} = \frac{2\pi 0.025 (2273 - 423)}{\frac{1}{0.15} \ln\left(\frac{0.0756}{0.0375}\right)} = 62 \text{ [W]} \quad \text{(e.6)}$$

The third heat loss is through the sieveplate:

$$Q = \frac{\pi r^2 k_{ceraboard} (T_{foam} - T_{gas})}{\delta_{sieveplate}} = \frac{\pi 0.0375^2 0.1 (2273 - 293)}{0.02} = 44 \text{ [W]} \quad \text{(e.7)}$$

The last heat loss is through the foam in the chimney. The thermal conductivity including radiation effects is estimated to be 2.5 W m^{-1} K^{-1} [Hsu & Howell, 1993]. The temperature difference is estimated to be of the order of 900 K. Because the foam is not only heated by the burner, but also by the flue gasses.

$$Q = \frac{\pi r^2 k_{foam} (T_{foam,\,bottom} - T_{foam,\,top})}{\delta_{foam}} = \frac{\pi 0.0375^2 2.5 (2173 - 1273)}{0.024} = 414 \text{ [W]} \quad \text{(e.8)}$$

Added up, the needed radiant power is 700 + 62 + 44 + 414 = 1220 Watt. This energy is supplied to the burner by cooling the flue gasses. To estimate the amount of flue gasses, it is assumed that the gasses are cooled from 2773 K to 2273 K. During this cooling heat is transferred to the foam. Thus,

$$\phi_m = \frac{Q}{c_p (T_{flame} - T_{out})} = \frac{1220}{1277 (500)} = 1.91\ 10^{-3} \text{ [kg } s^{-1}\text{]} \quad \text{(e.9)}$$

$$\phi_{v,\,natural\ gas} = \frac{\phi_m}{\rho (1 + \text{Air Requirement})} = \frac{1.91\ 10^{-3}}{1.15 * 9.4303} = 1.76\ 10^{-4} \text{ [m}^3 \text{ s}^{-1}\text{]} \quad \text{(e.10)}$$

$$P_{natural\ gas} = \phi_{v,\,natural\ gas} * H_i = 1.76\ 10^{-4}\ 31.669\ 10^6 = 5580 \text{ [W]} \quad \text{(e.11)}$$

Summarizing a flow of 1.8 10^{-4} m^3/s natural gas is needed to compensate the heat losses. The burner achieves the temperature of 2273 K if the flue gas temperature achieves 2773 K. The heat content of the natural gas supplied is 5.6 kW.

The following step is to heat the TEC. An additional heat sink of 1500 W must be added. Then the radiant power needed to heat the TEC and furnace is 2720 W. Using equation (e.9) - (e.11) a flow of 3.93 10^{-4} m^3/s natural gas is needed. The heat content of the gas supplied is then 12.4 kW.

F Measurement Equipment

During the experiments, various measurements are carried out. First the measurement of the temperatures in the test-rig is discussed. To measure temperatures a pyrolaser unit, a ratiopyrometer and thermocouples are used. Second the three gas flows have to be measured and controlled. Here rotameters are used.

F.1 The Pyrolaser

The pyrolaser (unit# PL-124), The Pyrometer Instrument Co., is used to measure the surface temperature of the burner. The pyrolaser works as a standard one-wavelength pyrometer (865 nm) using Planck's law to correlate the measured radiative flux and the temperature:

$$E_\lambda = \varepsilon_\lambda \frac{C_1}{\lambda^5} \frac{1}{e^{C_2/\lambda T} - 1} \qquad \text{(f.1)}$$

E_λ is calibrated versus a black body.

The special feature of the pyrolaser is that it measures the emissivity of a material at the same time. It fires a laser beam at the surface of the object and measures the reflected laser power. Using the assumption that the object reflects the laser beam diffusively, the emissivity can be derived through:

$$\varepsilon_\lambda + \rho_\lambda + \tau_\lambda = 1 \qquad \text{(f.2)}$$

In general the transmittance τ is zero. For more information on the pyrolaser the reader is referred to Gelten [1993] and Baustian & Matthews [1987].

Unfortunately life is not as simple as equations (f.1) and (f.2). Using the pyrolaser still major systematic errors can be made. The systematic errors identified for our situation are:

— influence by the media between pyrolaser and object,
— the object does not reflect the laser beam diffusively,
— the transmittance is not zero.

At 865 nm the pyrolaser measures through the windows of H_2O and CO_2. Because the combustion was mainly performed stochiometrically the first error is neglected.

Gelten [Figure 19, p. 36, 1993] measured the reflection as function of the angle of a 10 ppi foam. The reflection was not perfectly diffusive but the variation was only 3-6 %. Thus this effect is neglected.

The fact that the transmittance is not zero is accepted. This is only a problem with the 10 ppi foam, the 20 ppi foam has a transmittance of zero. In both cases an effective top temperature of the foam is measured.

Specifications of the pyrolaser #PL-124.

Temperature fields	600 — 1500 °C and 900 — 3000 °C
Resolution	1 °C
Accuracy	3 °C at 1500 °C with the emissivity > 0.8
Measurement distance	2 — 10 m and 0.8 — 1.2 m
Wave-length	865 nm ± 15 nm
Sight-angle	7°
Measurement angle	1/3 °
Measurement time	10 — 1000 ms adjustable
Measurement speed	1 — 35 per s.
Producer	The Pyrometer Instrument Co., Inc., New Jersy, USA.

F.2 The Ratiopyrometer

Due to operational problems with the pyrolaser (broken lens and filter) the measurements with the furnace are carried out with another pyrometer. This so-called ratiopyrometer was provided by the faculty of chemical engineering.

The ratiopyrometer makes direct use of Planck's law (equation (f.1)). But for simplification Wien's approximation is used (relative error is smaller than 1 ‰) [Leybold]:

$$E_\lambda = \varepsilon_\lambda \frac{C_1}{\lambda^5} e^{-C_2/\lambda T} \tag{f.3}$$

The emitted power E_λ is measured at two wavelengths and the ratio is taken. Together with the calibration of E_λ against a black body with temperature T_b the following expression is formed:

$$\frac{\varepsilon_1}{\varepsilon_2}\frac{\lambda_2^5}{\lambda_1^5}\exp\left(\frac{-C_2\left(\lambda_1^{-1}-\lambda_2^{-1}\right)}{T}\right) = \frac{\lambda_2^5}{\lambda_1^5}\exp\left(\frac{-C_2\left(\lambda_1^{-1}-\lambda_2^{-1}\right)}{T_b}\right) \tag{f.4}$$

Which can be rewritten as:

$$\frac{1}{T} = \frac{1}{T_b} + \frac{1}{C_2\left(\lambda_2^{-1}-\lambda_1^{-1}\right)} \ln\frac{\varepsilon_{\lambda_2}}{\varepsilon_{\lambda_1}} \tag{f.5}$$

When the ratio of emissivities equals one it follows that the temperature of the object is equal to the calibrated temperature.

The temperature of the foam is measured through a quartz window. The window became filthy when the top temperature was higher than 1600 °C.

To correct this systematic error the temperature is measured with and without window and the transmittance is calculated:

$$\tau_{window} = \frac{T^4_{with}}{T^4_{without}} = 0.9 — 1.0; \quad T_{correct} = \sqrt[4]{\frac{T^4_{measured}}{\tau_{window}}} \qquad (f.6)$$

With the calibrated transmittance the correct temperature is calculated.

Specifications of the ratiopyrometer QP 31.

Temperature fields	1000 — 3000 °C
Resolution	1 — 4 °C at maximum and minimum radiation intensity
Accuracy	± 12 °C at 1200 °C ± 17 °C at 2600 °C
Wave-lengths of the filters	500 nm (green) 580 nm (yellow)
Time constant	ca. 400 ms
Contact	P.J. Broers, Faculty of Chemical Engineering, SH-5.17, tel. (040-47)3058, EUT.
Producer	Leybold-Heraeus GmbH, Werk Hanau, Germany.

F.3 Thermocouples

The thermocouples in the test-rig measure the following temperatures:

1. The supplied gas mixture, chromel - alumel (K-type).
2. The flue gasses in the chimney, chromel - alumel (K-type).
3. Top of the sieveplate, wolfram 5% rhenium - wolfram 26 % rhenium.
4. Side of the foam, wolfram 5% rhenium - wolfram 26 % rhenium.
5. Side of the foam, wolfram 5% rhenium - wolfram 26 % rhenium.
6. Wall of the furnace, platina - platina 13% rhodium.
7. Wall of the furnace, platina - platina 13% rhodium.
8. Flue gasses in the furnace, platina - platina 13% rhodium.
9. Top of the additional foam in the chimney, platina - platina 13% rhodium.
10. Outside insulation of the furnace, chromel - alumel (K-type).
11. Outside insulation of the furnace, chromel - alumel (K-type).
12. Water inlet, chromel - alumel (K-type).
13. Water outlet side channels, chromel - alumel (K-type).
14. Water outlet inner channels, chromel - alumel (K-type).
15. Outside insulation burner-head, chromel - alumel (K-type).
16. Reference junctions Pt-PtRh13% and WRe5%-WRe26%, chromel - alumel (K-type).

Figure 4.1 shows the locations of the different thermocouples in the furnace. The WRe5%-WRe26% and the Pt-PtRh13% are shielded from the

combustion atmosphere by placing a glassfiber cover around the wires. Then the glassfiber is impregnated with high-temperature glue based on zirconia. The WRe-couples are mounted in the burner-head touching the foam. They lasted for one to two hours. When PtRh-couples were mounted on the same place, they lasted for 10 seconds or less.

Two further chromel-alumel couples are used to monitor the temperatures of the reference junction of the other couples. The reference junction consists of a aluminium bar on which the thermocouples are connected to copper wire.

The K-type couples are measured with a Fluke 2190A Digital Thermometer. The other thermocouples are measured by a HP 3497A datalogger and saved by a Macintosh Classic using the software package Workbench and the GPIB protocol.

Voltage U [mV]	Temperature T [°C]	Voltage U [mV]	Temperature T [°C]
0	0.0	22	1210.5
2	134.8	24	1329.4
4	252.2	26	1453.7
6	361.2	28	1584.2
8	466.2	30	1721.8
10	569.1	32	1868.7
12	671.3	34	2028.6
14	774.3	36	2208.0
16	878.9	38	2418.0
18	986.1	39.95	2703.2
20	1096.3		

Table F.1 Thermovoltage versus temperature for WRe5%-WRe26% thermocouples (reference junction at 0 °C).

For the Pt-PtRh13% the following fit is used for the temperature (data from Mcgee [1988]):

$$T\,[°C] = -5.346242\ 10^{-3}\ U^4 + 2.948217\ 10^{-1}\ U^3 - 6.141085\ U^2 + 1.312916\ 10^2\ U + 14.50409 \qquad (f.7)$$

with U in mV !!

The reference junctions are not at 0 °C so the reading has to be corrected. This can be done easily. The temperature of the reference junction is measured using a chromel-alumel thermocouple. From this temperature the thermovoltage of a Pt-PtRh13% or a WRe5%-WRe26% can be found in the tables. The thermovoltage based on the reference temperature 0 °C is now:

$$U_m\ (T_r=0°C) = U_m(T_r>0°C) + U_r(T_r=0°C) \qquad (f.8)$$

The systematic errors made by thermocouples have two sources. The first source is distortion of the calibration. This error is neglected. The second source is that the thermocouple does not have the same temperature as the object to be measured. To identify this error the situation around the thermocouple has to analyzed.

For the Pt-PtRh13% and WRe5%-WRe26% thermocouples in the test-rig installation effects will cause large errors. The WRe5%-WRe26% couples are mounted against the foam. The thermocouple conducts heat from the foam to the surroundings much better than the insulation. So the measurement junction is colder than the foam. Numerical analysis is the only way to evaluate the difference between the reading of the thermocouple and the temperature of the foam. But for all three couples the systematic error can be expected to be of the same order because the heat transfer situation is the same for the three couples: same foam, same insulation, same lengths, same diameters.

The WRe-couples are used to determine the location of the flame zone in the foam. The accuracy wished is of the order: under in the foam, in the middle of the foam, or at the top of the foam. Therefore the thermocouples are compared relatively and the systematic error is neglected.

The Pt-PtRh13% couples are mounted in the furnace. Two couples measure the wall temperature of the inner side of the cylinder. One couple measures the flue gas temperature. One couple measures the temperature of the foam in the chimney.

Starting with the couples mounted in the cylinder. The heat conductivity of the thermocouple wires is 10 to 100 times higher than the heat conductivity of the insulation. Thus the hot junction of the couple will be colder than the insulation. This type of error has been modelled numerically by Smeets [1980]. Smeets calculated the isotherms of a thermocouple mounted in saffil insulation. Saffil resembles the ZAL 45 board, used in our experiments. The resultant error is 300 K [chart B.5, Smeets, 1980].

The couple in the gas flow has to measure the gas temperature. The heat transfer situation is very complex. The couple is heated by the gas flow and the burner and is cooled by radiation from the couple to the furnace walls and conduction to the furnace walls. The whole situation can only be solved numerically.

But an analytical estimation of the error can be made. The influence of the burner is neglected and the whole furnace wall is assumed to have a constant temperature. Further the heat conduction through the couple is neglected compared to radiation and convection. The heat balance of the thermocouple yields:

$$\frac{A_{tc}\,\sigma\,(T_{tc}^4 - T_{in}^4)}{\frac{1}{\varepsilon_{tc}} + \frac{A_{tc}}{A_{in}}\left(\frac{1}{\varepsilon_{in}} - 1\right)} = A_{tc}\,h\,(T_{flue} - T_{tc}) \qquad (f.9)$$

for the heat transfer coefficient Kramer's rule [Hinze, 1959] can be used:

$$Nu = \frac{h\, D_{couple}}{k_{flue}} = 0.42\, Pr^{0.2} + 0.57\, Pr^{0.33}\, Re^{0.5} \qquad (f.10)$$

The material properties are evaluated at the film temperature $(T_{flue}+T_{tc})/2$. To evaluate the material properties the fits in appendix D are used. Expression (f.10) can be solved for the gas temperature T_{flue}.

In figure F.1 the gas temperature is solved as function of the total emissivity of the thermocouple. The temperature of the couple is 1644 K and of the furnace 1273 K, based on the experiment in figure 4.12b. The emissivity of the furnace ε_w is 0.3. The diameter of the couple is 2 mm, its length in the furnace 20 mm.

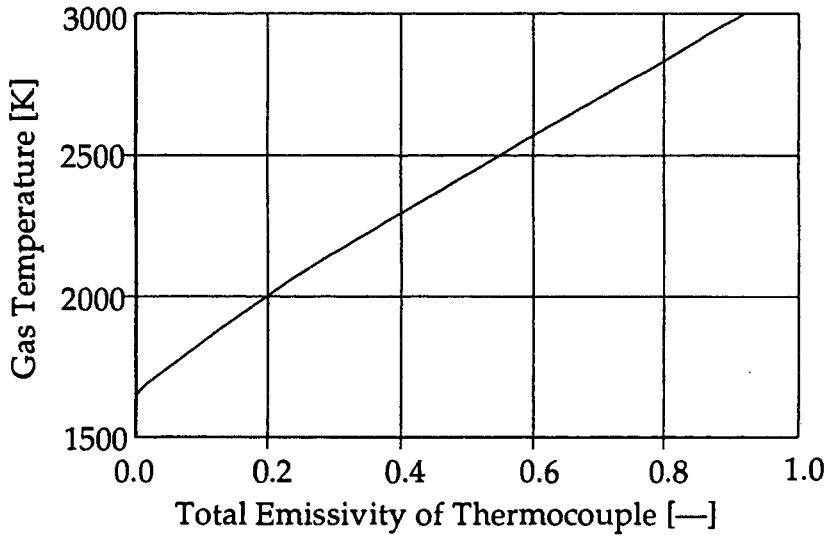

Figure F.1 The flue gas temperature as function of the thermocouple emissivity.

The problem left is the emissivity of the couple. The outer layer of the couple is high-temperature glue as stated at the beginning of this section. This glue is based on zirconia, but the exact composition is not known. Underneath the glue, a glassfiber sheet is placed over the wires. Concluding the emissivity is not well known. An approximation is for the emissivity is 0.15 based on the data of Bramson [1968] presented in figure C.2.

The estimated flue gas temperature is 1920 K, based on 0.15 for the thermocouple emissivity. Thus the reading of the thermocouple is 276 K too low. As stated in the previous paragraph, the emissivity is not well known. A variation of the emissivity of 0.1 around 0.15 gives a variation in the gas temperature of 180 K. This strong dependence of the error on the emissivity makes it hard to draw conclusions on the exact value of the error.

Figure F.2 shows the same situation as figure F.1, but now with constant emissivities. This time the thermocouple temperature is varied. The furnace wall temperature is 1273 K. The emissivity of the furnace wall is 0.3. The emissivity of the couple is varied. The burner power is 9.5 kW.

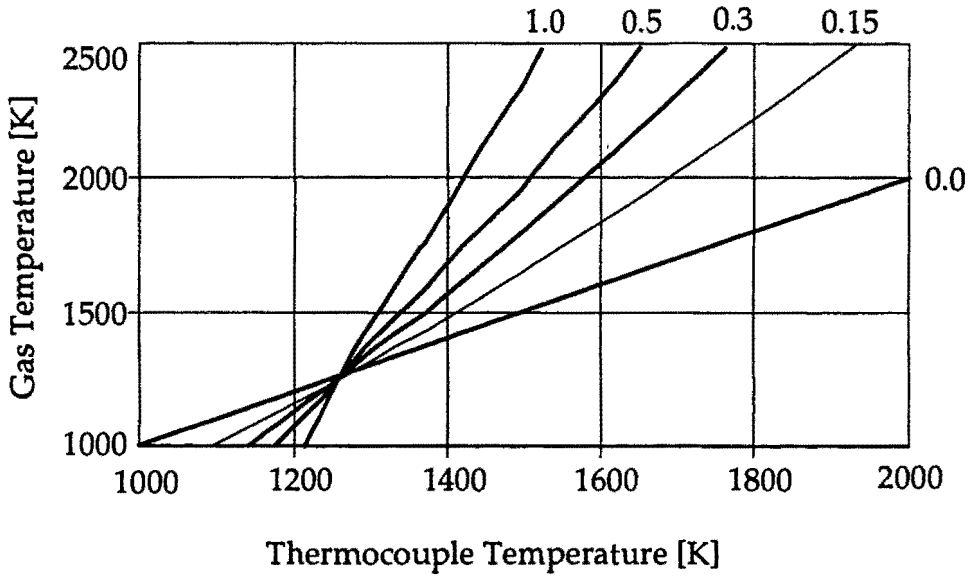

Figure F.2 The gas temperature as function of the thermocouple temperature. The parameter is the emissivity of the thermocouple.

F.4 Rotameters

Three rotameters are used. Two are used parallel for natural gas, the third is used for air. The calibrations can be found in tables F.2 to F.4. The real flow through the rotameter is found by dividing the flow according to calibration with the sizing-factor. The sizing-factor is defined as:

$$\phi_v = \frac{\phi_{v,\ \text{calibration}}}{S_f} \quad ; \qquad S_f = \sqrt{\frac{\rho_2\ T_2\ p_1}{\rho_1\ T_1\ p_2}} \tag{f.11}$$

The subscript "2" means at measurement conditions and "1" at calibration conditions. The pressure is the absolute pressure !

Calibration Tables

Used for natural gas:

Rota Oeflingen 690521/SI/14, tube Rota 10/400 no. 6082.
Reference number calibration report: 921004
Random error 0.3 % according to calibration

Reading [scalenumber]	ϕ_v air T=20°C, p=1 bar [l/min]	Reading [scalenumber]	ϕ_v air T=20°C, p=1 bar [l/min]
10	0.380	120	3.662
20	0.624	130	3.974
30	0.963	140	4.137
40	1.250	150	4.627
50	1.549	160	4.966
60	1.838	170	5.272
70	2.131	180	5.591
80	2.418	190	5.870
90	2.727	200	6.113
100	3.037	210	6.280
110	3.341	220	6.465

Table F.2 Calibration rotameter reference 921004.

Rota Oeflingen 690521/SI/16, tube Rota 10/400 no. 6088.
Reference number calibration report: 921005
Random error 0.3 % according to calibration

Reading [scalenumber]	ϕ_v air T=20°C, p=1 bar [l/min]	Reading [scalenumber]	ϕ_v air T=20°C, p=1 bar [l/min]
20	0.670	120	3.923
30	1.009	130	4.266
40	1.320	140	4.626
50	1.640	150	4.984
60	1.959	160	5.333
70	2.265	170	5.676
80	2.576	180	6.026
90	2.910	190	6.347
100	3.247	200	6.572
110	3.583	210	6.756

Table F.3 Calibration rotameter reference 921005.

Used for air:

Fisher & Porter TF 0346, tube D 045, float 13044 U 06.
Reference number calibration report: 921003
Random error 0.5 % according to calibration

Reading [scalenumber]	ϕ_v air T=20°C, p=1 bar [l/min]
16	25.4
20	32.9
30	51.3
40	69.4
50	86.7
60	103.6
70	119.8
80	137.2

Table F.4 Calibration rotameter reference 921003.

F.5 Pressure Measurement

Before each flowmeter and over the burner-head pressure (differences) are measured. For the static pressure before the flowmeters Bourbon-tube pressure gages are used. The accuracy of the gage used for air is 0.05 bar. The accuracy of the gage used for natural gas is 2.5 mbar.

To measure the pressure difference over the burner-head a Betz manometer is used. Its accuracy is 0.5 Pa.

F.6 Error Analysis

In this section the random errors made are discussed. The systematic errors are discussed in the section concerning the measurement method. For the following parameters the error must be estimated:

— the natural gas flow,
— the air flow,
— the airfactor a,
— the burner power,
— the temperature measured by the pyrolaser,
— the temperature measured by the ratiopyrometer,
— the radiant output power,
— the radiant efficiency.

F.6.1 Random Errors of the Flows

The flows are calculated as,

$$\phi_v = \frac{\phi_{v,\,calibration}}{\sqrt{C\,\frac{T_2}{p_2}}} \; ; \qquad C = \frac{\rho_2\, p_1}{\rho_1\, T_1} \tag{f.12}$$

C is constant without error. For the absolute error of flow $\Delta\phi_v$ the following expression yields:

$$\Delta\phi_v^2 = \left(\frac{\partial\phi_v}{\partial\phi_{v,\,cal}}\right)^2 \Delta\phi_{v,\,cal}^2 + \left(\frac{\partial\phi_v}{\partial T_2}\right)^2 \Delta T_2^2 + \left(\frac{\partial\phi_v}{\partial p_2}\right)^2 \Delta p_2^2 \tag{f.13}$$

$$\Delta\phi_v^2 = \frac{p_2}{C\,T_2}\,\Delta\phi_{v,\,cal}^2 + \frac{1}{4}\,\frac{\phi_{v,\,cal}^2}{C\,T_2\,p_2}\,\Delta p_2^2 + \frac{1}{4}\,\frac{\phi_{v,\,cal}^2\,p_2}{C\,T_2^3}\,\Delta T_2^2 \tag{f.14}$$

For different workpoints the errors are calculated and summarized in table F.5 for natural gas and in table F.6 for air. The error of the flow according to the calibration $\Delta\phi_{v,cal}$ is based on a reading error of 1 scale-part. The constant C is 2.261 10^{-3} Pa K^{-1} for natural gas and 3.457 10^{-3} Pa K^{-1} for air.

ϕ_v [$m^3\,s^{-1}$]	$\phi_{v,cal}$ [$m^3\,s^{-1}$]	$\Delta\phi_{v,cal}$ [$m^3\,s^{-1}$]	p [bar]	Δp [mbar]	T [K]	ΔT [K]	$\Delta\phi_v$ [$m^3\,s^{-1}$]	$\Delta\phi_v/\phi_v$ [%]
$2.9\,10^{-4}$	$2.2\,10^{-4}$	$6.7\,10^{-7}$	1.078	2.5	298.15	1	$1.0\,10^{-6}$	0.35
$1.4\,10^{-4}$	$1.1\,10^{-4}$	$6.7\,10^{-7}$	1.085	2.5	298.15	1	$8.9\,10^{-7}$	0.65

Table F.5 Error of the natural gas flow.

ϕ_v [$m^3\,s^{-1}$]	$\phi_{v,cal}$ [$m^3\,s^{-1}$]	$\Delta\phi_{v,cal}$ [$m^3\,s^{-1}$]	p [bar]	Δp [bar]	T [K]	ΔT [K]	$\Delta\phi_v$ [$m^3\,s^{-1}$]	$\Delta\phi_v/\phi_v$ [%]
$1.0\,10^{-3}$	$3\,10^{-5}$	$8.6\,10^{-4}$	1.5	0.05	298.15	1	$4.0\,10^{-5}$	3.9
$2.4\,10^{-3}$	$3\,10^{-5}$	$1.6\,10^{-3}$	2.42	0.05	298.15	1	$5.3\,10^{-5}$	2.2

Table F.6 Error of the air flow.

F.6.2 Random Error of the Airfactor

The airfactor is calculated according to:

$$a = \frac{\phi_{v,\ air\ supplied}}{\phi_{v,\ air\ stochiometric}} = \frac{\phi_{v,\ air\ supplied}}{\phi_{v,\ gas} * 8.4303} \frac{[m^3\ s^{-1}]}{[m^3\ s^{-1}]} \qquad (f.15)$$

The error of the airfactor is caused by the propagation of the errors of the gas and air flows.

$$\Delta a^2 = \left(\frac{\partial a}{\partial \phi_{v,\ air}}\right)^2 \Delta\phi^2_{v,\ air} + \left(\frac{\partial a}{\partial \phi_{v,\ gas}}\right)^2 \Delta\phi^2_{v,\ gas} \qquad (f.16)$$

$$\Delta a^2 = \left(\frac{1}{8.4303\ \phi_{v,\ gas}}\right)^2 \Delta\phi^2_{v,\ air} + \left(\frac{-\phi_{v,\ air}}{8.4303\ \phi^2_{v,\ gas}}\right)^2 \Delta\phi^2_{v,\ gas} \qquad (f.17)$$

a [—]	$\phi_{v,gas}$ [$m^3\ s^{-1}$]	$\Delta\phi_{v,gas}$ [$m^3\ s^{-1}$]	$\phi_{v,air}$ [$m^3\ s^{-1}$]	$\Delta\phi_{v,air}$ [$m^3\ s^{-1}$]	Δa [—]	$\Delta a/a$ [%]
0.983	$2.9\ 10^{-4}$	$1.1\ 10^{-6}$	$2.4\ 10^{-3}$	$5.3\ 10^{-5}$	$2.2\ 10^{-2}$	2.2
0.90	$1.4\ 10^{-4}$	$8.9\ 10^{-7}$	$1.0\ 10^{-3}$	$4.0\ 10^{-5}$	$3.6\ 10^{-2}$	3.9
0.42	$2.9\ 10^{-4}$	$1.1\ 10^{-6}$	$1.0\ 10^{-3}$	$4.0\ 10^{-5}$	$1.6\ 10^{-2}$	3.9

Table F.7 Error of the air factor for some workpoints.

F.6.3 Random Error of the Burner Power

The error of the burner power is also dependent on the flow of natural gas (H_i=31.669 MJ m^{-3}):

$$P_{burner} = H_i\ \phi_{v,\ gas}$$
$$\Delta P_{burner} = H_i\ \Delta\phi_{v,\ gas} \qquad (f.18)$$

P [W]	$\phi_{v,gas}$ [$m^3\ s^{-1}$]	$\Delta\phi_{v,gas}$ [$m^3\ s^{-1}$]	ΔP [W]	$\Delta P/P$ [%]
9500	$3.0\ 10^{-4}$	$1.1\ 10^{-6}$	32.2	0.34
4600	$1.5\ 10^{-4}$	$8.9\ 10^{-7}$	28.1	0.61

Table F.8 Error of the burner power for some workpoints.

F.6.4 Random Error of the Temperature Measured by the Pyrolaser

The top temperature of the foam is measured by two pyrometers: the pyrolaser and the ratiopyrometer. The pyrolaser is used during the measurements without furnace. Its error is partially influenced by the error in the spectral emissivity at 865 nm.

In figure F.3 the emissivity is shown as function of the black body temperature of a 10 ppi foam. The black body temperature is the temperature the object would have if it were a black body. For the same black body temperature the emissivity can vary up to 16 %.

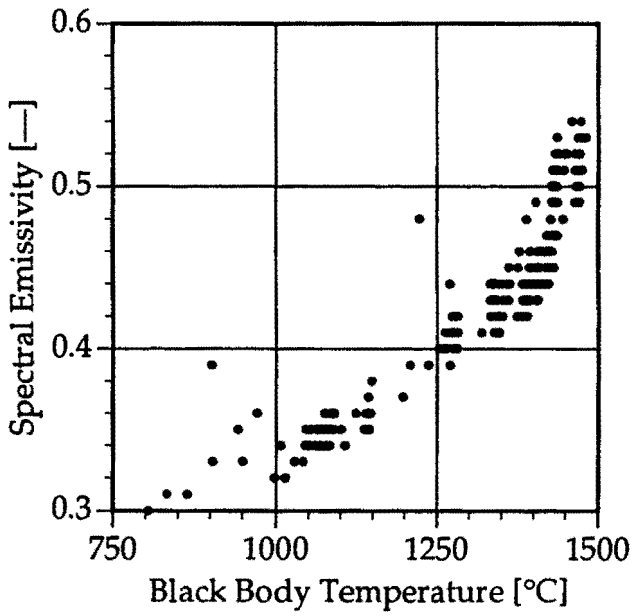

Figure F.3 The spectral emissivity at 865 nm of the foam as function of the black body temperature according to the pyrolaser.

To determine the error, expression (f.1) is rewritten by substituting Planck's law for E_λ based on the black body temperature T_b. The expression is rearranged to:

$$T = \frac{C_2}{\lambda \ln\left(\exp\left(\frac{C_2}{\lambda T_b}\right)\varepsilon_\lambda - \varepsilon_\lambda + 1\right)} \qquad \text{(f.19)}$$

The error ΔT is caused by the error of the emissivity $\Delta\varepsilon_\lambda$ and of the black body temperature ΔT_b.

$$\Delta T^2 = \Delta\varepsilon_\lambda{}^2 \left(\frac{C_2 \lambda \left[\exp\left(\frac{C_2}{\lambda T_b}\right) - 1 \right]}{\exp\left(\frac{C_2}{\lambda T_b}\right) \varepsilon_\lambda - \varepsilon_\lambda + 1} \frac{1}{\left[\lambda \ln\left\{ \exp\left(\frac{C_2}{\lambda T_b}\right) \varepsilon_\lambda - \varepsilon_\lambda + 1 \right\} \right]^2} \right)^2 +$$

$$+ \left(\frac{C_2^2 \exp\left(\frac{C_2}{\lambda T_b}\right) \varepsilon_\lambda}{\lambda^2 T_b^2 \left[\exp\left(\frac{C_2}{\lambda T_b}\right) \varepsilon_\lambda - \varepsilon_\lambda + 1 \right] \left[\ln\left\{ \exp\left(\frac{C_2}{\lambda T_b}\right) \varepsilon_\lambda - \varepsilon_\lambda + 1 \right\} \right]^2} \right)^2 \Delta T_b^2 \qquad \text{(f.20)}$$

The wavelength λ is 865 nm. The error ΔT_b is taken 3 K according to the specifications of the pyrolaser. The error $\Delta\varepsilon_\lambda$ is estimated from figure F.3.

T [K]	T_b [K]	ΔT_b [K]	ε_λ [—]	$\Delta\varepsilon_\lambda$ [—]	ΔT [K]	$\Delta T/T$ [%]
1503.4	1373.15	3	0.35	0.02	8.56	0.57
1535.6	1423.15	3	0.425	0.03	10.6	0.69
1843.2	1708.15	3	0.49	0.08	33.5	1.8
1879.2	1748.15	3	0.515	0.05	20.9	1.1

Table F.9 Error of the temperature measured by the pyrolaser.

F.6.5 Random Error of the Temperature Measured by the Ratiopyrometer

During the measurements with the furnace, the temperature of the foam is measured through a window. Therefore the ratiopyrometer is used. The reading of the ratiopyrometer is corrected for the influence of the window. First the transmittance of the window is calculated from a calibration measurement. Second the reading is corrected with the transmittance. To estimate the errors the following values are used: temperature with window T_{with}=1773 K, without window $T_{without}$=1823 K. The measurement error ΔT = 25 K (section F.2). Thus

$$\tau_{window} = \frac{T_{with}^4}{T_{without}^4} = 0.9; \quad T_{correct} = \sqrt[4]{\frac{T_{measured}^4}{\tau_{window}}} \qquad \text{(f.21)}$$

The absolute error of the transmittance is found according to

$$\Delta\tau_{window}^2 = \left(\frac{\partial\tau}{\partial T_{with}} \right)^2 \Delta T_{with}{}^2 + \left(\frac{\partial\tau}{\partial T_{without}} \right)^2 \Delta T_{without}{}^2 \qquad \text{(f.22)}$$

$$\Delta\tau = \sqrt{\Delta T_{without}^2\left(4\frac{T_{with}^4}{T_{without}^5}\right)^2 + \Delta T_{with}^2\left(4\frac{T_{with}^3}{T_{without}^4}\right)^2} = 0.07 \qquad \text{(f.23)}$$

Now the absolute error in the correct temperature can be calculated. The absolute error in temperature is still 25 K.

$$\Delta T_{correct}^2 = \left(\frac{\partial T_{correct}}{\partial T_{measured}}\right)^2 \Delta T_{measured}^2 + \left(\frac{\partial T_{correct}}{\partial \tau}\right)^2 \Delta\tau^2 \qquad \text{(f.24)}$$

$$\Delta T_{correct} = \sqrt{\Delta\tau^2\left(\frac{1}{4}\frac{T_{measured}}{\tau^{0.8}}\right)^2 + \tau^{-0.5}\Delta T_{measured}^2} = 44\ K \qquad \text{(f.25)}$$

$$\text{relative error } \frac{\Delta T_{correct}}{T_{correct}} = \frac{44}{1823} * 100 = 2.5\ \% \qquad \text{(f.26)}$$

F.6.6 Random Error of the Radiant Power

During the measurements without furnace, the radiant power is easily determined. To calculate the radiant power the black body temperature measured by the pyrolaser is used:

$$P_{rad} = \sigma A_{foam} (T_{b,\,foam}^4 - \varepsilon_{foam} T_{surr}^4) \qquad \text{(f.27)}$$

$$\Delta P_{rad}^2 = \Delta T_{b,foam}^2 (4 A_{foam} \sigma T_{b,foam}^3)^2 + \Delta\varepsilon_{foam}^2 (A_{foam} \sigma T_{surr}^4)^2 + \Delta T_{surr}^2 (4 A_{foam} \sigma \varepsilon_{foam} T_{surr}^3)^2 \qquad \text{(f.28)}$$

The temperature of the surroundings is 293.15 K with an error of 1 K and the error of the black temperature is 3 K (see specifications pyrolaser in section F.1. Remains the error of the total emissivity. The total emissivity is the quotient of the black and the emissivity corrected temperature:

$$\varepsilon_{foam} = \frac{T_{b,\,foam}^4}{T_{\varepsilon,\,foam}^4}$$

$$\Delta\varepsilon_{foam}^2 = \Delta T_{\varepsilon,\,foam}^2\left(4\frac{T_{b,\,foam}^4}{T_{\varepsilon,\,foam}^5}\right)^2 + \Delta T_{b,\,foam}^2\left(4\frac{T_{b,\,foam}^3}{T_{\varepsilon,\,foam}^4}\right)^2 \qquad \text{(f.29)}$$

Table F.10 is constructed based on the values of table F.9.

ε [—]	T_b [K]	ΔT_b [K]	T_ε [K]	ΔT_ε [K]	$\Delta\varepsilon$ [—]	$\Delta\varepsilon/\varepsilon$ [%]
0.70	1373.15	3	1503.4	8.56	0.017	2.4
0.74	1423.15	3	1535.6	10.6	0.021	2.9
0.74	1708.15	3	1843.2	33.5	0.054	7.3
0.75	1748.15	3	1879.2	20.9	0.034	4.5

Table F.10 Error of the total emissivity of the foam.

Now the error of the radiant power can be calculated, using table F.10.

P_{rad} [kW]	T_b [K]	ΔT_b [K]	T_{surr} [K]	ΔT_{surr} [K]	ε [—]	$\Delta\varepsilon$ [—]	ΔP_{rad} [W]	$\Delta P/P$ [%]
0.9	1373.15	3	293.15	1	0.70	0.017	7.8	0.9
1.0	1423.15	3	293.15	1	0.74	0.021	8.7	0.8
2.1	1708.15	3	293.15	1	0.74	0.054	15	0.7
2.3	1748.15	3	293.15	1	0.75	0.034	16	0.7

Table F.11 Error of the radiant power for some workpoints.

F.6.7 Random Error of the Radiant Efficiency

The radiant power divided by the burner power gives the radiant efficiency of the burner:

$$\eta_{rad} = \frac{P_{rad}}{P_{burner}}$$

$$\Delta\eta_{rad} = \sqrt{\frac{\Delta P_{rad}^2}{P_{burner}^2} + \frac{P_{rad}^2\,\Delta P_{burner}^2}{P_{burner}^4}} \qquad \text{(f.30)}$$

η_{rad} [—]	P_{rad} [kW]	ΔP_{rad} [W]	P_{burner} [kW]	ΔP_{burner} [W]	$\Delta\eta_{rad}$ [—]	$\Delta\eta/\eta$ [%]
0.11	1.0	7.8	9.6	32.2	0.0008	0.7
0.24	2.3	16	9.6	32.2	0.0017	0.7

Table F.12 Error of the radiant efficiency for some workpoints.

G Thermal Shock

The most important failmode of the cellular ceramic material mounted in the burner is thermal shock. Therefore its mechanism will be explained in this appendix and the critical temperature difference in our case will be calculated.

When a body is cooled or heated, its temperature distribution is ruled by Fourier's law:

$$k \nabla^2 T + \frac{Q}{\rho c_p} = \frac{\partial T}{\partial t} \qquad (g.1)$$

where Q is the heat supplied. In the most cases of thermal shock, the convective boundary condition applies,

$$k \frac{\partial T}{\partial n} = h (T_0 - T_s) \qquad (g.2)$$

where n the normal to the surface is and T_0 the temperature of the surrounding medium. This supplies the base for the Biot number: the quotient of convective and conductive heat transfer,

$$\beta = \frac{h L}{k} \qquad (g.3)$$

The product of the heat transfer coefficient and the characteristic length determines the rate at which heat is transferred to the surface. This affects the rate of rise or fall of surface temperature. The thermal conductivity determines the rate at which heat is distributed throughout the body.

A high transient flux at the surface of a body, causes a temperature difference between the centre and the surface of the body. The temperature difference induces thermal stress, which is at maximum at the surface. The thermal stress will be tensile, if the body is cooled and compressive, if heated. If the stress exceeds the failure stress of the material, cracks can develop.

The triaxial stress-strain relations in an orthogonal coordinate system x, y, z are,

$$\begin{aligned} \varepsilon_x &= \frac{1}{E} [\sigma_x - \nu (\sigma_y + \sigma_z)] \\ \varepsilon_y &= \frac{1}{E} [\sigma_y - \nu (\sigma_x + \sigma_z)] \\ \varepsilon_z &= \frac{1}{E} [\sigma_z - \nu (\sigma_x + \sigma_y)] \end{aligned} \qquad (g.4)$$

Considering an infinite plate in the x, y plane uniformly cooled, expression (g.4) can be solved at the surface, where the peak stress appears. With,

$$\varepsilon_x = \alpha\,\Delta T$$
$$\varepsilon_y = \alpha\,\Delta T$$
$$\varepsilon_z = \sigma_z = 0 \qquad \text{(g.5)}$$

the stress at the surface is,

$$\sigma_m = \sigma_x = \sigma_y = \frac{E\,\alpha\,\Delta T}{1 - \nu} \qquad \text{(g.6)}$$

For the uniaxial stress state the numerator is equal to unity and is equal to (1-2ν) for a triaxial stress state. Expression (g.6) presents the maximum stress, which would appear at the surface of the plate by cooling down the surface to T_s, whereas the core is maintaining its initial temperature. This is a limit case, never reached. The actual stress σ is only a fraction of σ_m;

$$\sigma = \frac{E\,\alpha\,\Delta T}{1 - \nu}\, f(\beta) \qquad \text{(g.7)}$$

where f(β) presents a dimensionless function, inferior to one, which characterizes the shock severity:

$$f(\beta) \to 1, \text{ if } \beta \to \infty \quad \text{very fast thermal exchange}$$
$$f(\beta) \to 0, \text{ if } \beta \to 0 \quad \text{very low thermal exchange} \qquad \text{(g.8)}$$

Figure G.1 shows the variation of f(β): the non-dimensional surface stress with the dimensionless time: the Fourier number $(k\,t)/(\rho\,c_p\,L^2)$.

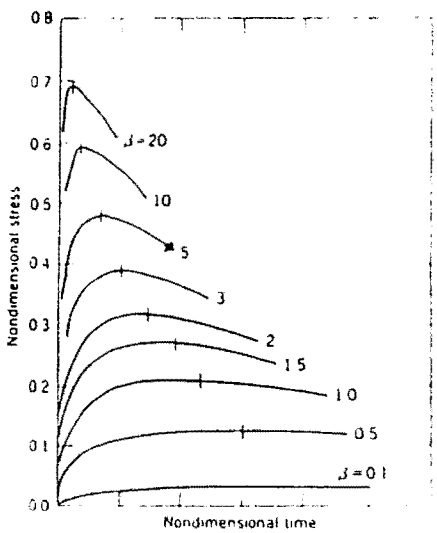

Figure G.1 Variation of non-dimensional surface stress f(β) with dimensionless time for an infinite flat plate. Parameter is the Biot number. [Boch, 1987].

Local fracture will develop when the stress σ reaches the local strength σ_f corresponding to a critical temperature gradient:

$$\Delta T_{crit} = \frac{\sigma_f (1 - \nu)}{E \alpha f(\beta)} \text{ [K]} \qquad \text{(g.9)}$$

The first thermal shock parameter R is thus defined as:

$$R = \frac{\sigma_f (1 - \nu)}{E \alpha} \text{ [K]} \qquad \text{(g.10)}$$

R is in generally considered for fast thermal shocks. For mild thermal shocks, $f(\beta)$ appears to be roughly proportional to β:

$$f(\beta) = A \beta \qquad \text{(g.11)}$$

$$\Delta T_{crit} = \frac{\sigma_f (1 - \nu)}{E \alpha} \frac{k}{A h L} \text{ [K]} \qquad \text{(g.12)}$$

$$\Delta T_{crit} = R' \frac{C}{h} \text{ [K]} \qquad \text{(g.13)}$$

where the second thermal shock parameter R'=R k and the shapefactor C=1/AL.
For our zirconia foam, data are summarized in table 3.2.

$$R = \frac{\sigma_f (1-\nu)}{\alpha E} = \frac{1000\ 10^6\ (1-0.23)}{10\ 10^{-6}\ 200\ 10^9} = 385 \text{ [K]}$$
$$R' = \frac{\sigma_f (1-\nu)\ k}{\alpha E} = 385 * 1.8 = 693 \text{ [W m}^{-1}\text{]} \qquad \text{(g.13)}$$

The heat transfer coefficient h consists of two parts, a convective, and a radiative part: $h=h_c+h_{rad}$. In case of burner turn-off, the convective part of the heat transfer coefficient will be due to natural convection. To estimate this, a correlation for a horizontal plate, topside heated, is taken [Kreith & Bohn, 1986]. The burner is cooled by air of 293 K.

For the characteristic length the foam diameter is used. The Nusselt-relation for natural convection is valid for $7\ 10^6 < Gr*Pr < 2\ 10^8$. The temperature difference in the Grashof number is 1980 K, the foam being on 2273 K and the surroundings on 293 K. Thus

$$h_c = \frac{0.16\,(Gr\,Pr)^{1/3}\,k_{air}}{D_{foam}} = \frac{0.16\,(2.1\,10^8\,0.74)^{1/3}\,76.8\,10^{-3}}{0.075} = 88.1\,\frac{W}{m^2\,K}$$

$$h_{rad} = \frac{\varepsilon_{foam}\,\sigma\,(T_{foam}^4 - T_{surr}^4)}{T_{foam} - T_{surr}} = \frac{0.6\,\sigma\,(2273^4 - 293^4)}{2273 - 293} = 459\,\frac{W}{m^2\,K}$$

$$\beta = \frac{h\,D_{foam}}{k_{foam}} = \frac{547.1 * 0.075}{1.8} = 22.8 \qquad \text{(g.14)}$$

The fluid properties must be evaluated at the mean of the solid temperature and the fluid bulk temperature. The Biot number is high, thus the first thermal shock parameter is used to estimate the critical temperature difference. From figure G.1, $f(\beta)$ is estimated to be 0.65, thus $\Delta T_{crit} = 592$ [K]. Fracture will follow, when the thermal shock applied to the foam is larger than ΔT_{crit}.